NUREG/CR-6724

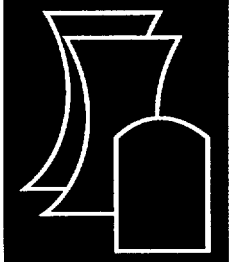

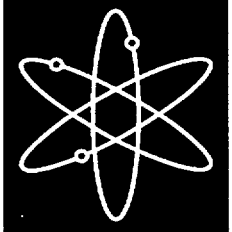

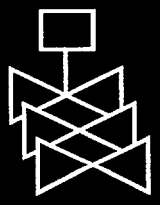

TRAC-M/FORTRAN 90 (Version 3.0) Theory Manual

Los Alamos National Laboratory

U.S. Nuclear Regulatory Commission
Office of Nuclear Regulatory Research
Washington, DC 20555-0001

NUREG/CR-6724

TRAC-M/FORTRAN 90 (Version 3.0) Theory Manual

Manuscript Completed: April 2001
Date Published: July 2001

Prepared by
J.W. Spore, J.S. Elson, S.J. Jolly-Woodruff, T.D. Knight
J.-C. Lin, R.A. Nelson, K.O. Pasamehmetoglu, LANL

J.H. Mahaffy, C. Murray, PSU

Los Alamos National Laboratory
Los Alamos, New Mexico 87545

Pennsylvania State University
University Park, PA 16802

F. Odar, NRC Project Manager

Prepared for
Division of Systems Analysis and Regulatory Effectiveness
Office of Nuclear Regulatory Research
U.S. Nuclear Regulatory Commission
Washington, DC 20555-0001
NRC Job Code W6245

AVAILABILITY OF REFERENCE MATERIALS IN NRC PUBLICATIONS

NRC Reference Material

As of November 1999, you may electronically access NUREG-series publications and other NRC records at NRC's Public Electronic Reading Room at www.nrc.gov/NRC/ADAMS/index.html.
Publicly released records include, to name a few, NUREG-series publications; *Federal Register* notices; applicant, licensee, and vendor documents and correspondence; NRC correspondence and internal memoranda; bulletins and information notices; inspection and investigative reports; licensee event reports; and Commission papers and their attachments.

NRC publications in the NUREG series, NRC regulations, and *Title 10, Energy*, in the Code of *Federal Regulations* may also be purchased from one of these two sources.

1. The Superintendent of Documents
   U.S. Government Printing Office
   Mail Stop SSOP
   Washington, DC 20402–0001
   Internet: bookstore.gpo.gov
   Telephone: 202-512-1800
   Fax: 202-512-2250
2. The National Technical Information Service
   Springfield, VA 22161–0002
   www.ntis.gov
   1–800–553–6847 or, locally, 703–605–6000

A single copy of each NRC draft report for comment is available free, to the extent of supply, upon written request as follows:
Address: Office of the Chief Information Officer,
Reproduction and Distribution
Services Section
U.S. Nuclear Regulatory Commission
Washington, DC 20555-0001
E-mail: DISTRIBUTION@nrc.gov
Facsimile: 301–415–2289

Some publications in the NUREG series that are posted at NRC's Web site address www.nrc.gov/NRC/NUREGS/indexnum.html are updated periodically and may differ from the last printed version. Although references to material found on a Web site bear the date the material was accessed, the material available on the date cited may subsequently be removed from the site.

Non-NRC Reference Material

Documents available from public and special technical libraries include all open literature items, such as books, journal articles, and transactions, *Federal Register* notices, Federal and State legislation, and congressional reports. Such documents as theses, dissertations, foreign reports and translations, and non-NRC conference proceedings may be purchased from their sponsoring organization.

Copies of industry codes and standards used in a substantive manner in the NRC regulatory process are maintained at—

The NRC Technical Library
Two White Flint North
11545 Rockville Pike
Rockville, MD 20852–2738

These standards are available in the library for reference use by the public. Codes and standards are usually copyrighted and may be purchased from the originating organization or, if they are American National Standards, from—

American National Standards Institute
11 West 42nd Street
New York, NY 10036–8002
www.ansi.org
212–642–4900

Legally binding regulatory requirements are stated only in laws; NRC regulations; licenses, including technical specifications; or orders, not in NUREG-series publications. The views expressed in contractor-prepared publications in this series are not necessarily those of the NRC.

The NUREG series comprises (1) technical and administrative reports and books prepared by the staff (NUREG–XXXX) or agency contractors (NUREG/CR–XXXX), (2) proceedings of conferences (NUREG/CP–XXXX), (3) reports resulting from international agreements (NUREG/IA–XXXX), (4) brochures (NUREG/BR–XXXX), and (5) compilations of legal decisions and orders of the Commission and Atomic and Safety Licensing Boards and of Directors' decisions under Section 2.206 of NRC's regulations (NUREG–0750).

TRAC-M/FORTRAN 90 (VERSION 3.0)
THEORY MANUAL

by

**J. W. Spore, J. S. Elson, S. J. Jolly-Woodruff, T. D. Knight,
J.-C. Lin, R. A. Nelson, K. O. Pasamehmetoglu,
R. G. Steinke, C. Unal, J. H. Mahaffy and C. Murray**

ABSTRACT

The United States Nuclear Regulatory Commission (USNRC) is developing the modernized versions of the Transient Reactor Analysis Code (TRAC-M) to provide advanced best-estimate simulations of real and postulated transients in pressurized and boiling water reactors (PWRs and BWRs) and for many related thermal-hydraulic facilities. The TRAC-M/ Fortran 90 (TRAC-M/F90) program, the latest released version, is written for TRAC-M/F90 Version 3.0. In addition, we indicate areas where TRAC-M/F90 differs from the TRAC-M Fortran 77 (TRAC-M/F77) code (Version 5.5.2). Both codes feature a one- and/or three-dimensional, two-fluid treatment for the thermal hydraulics, together with other necessary modeling capabilities to describe a reactor system. Currently both codes are intended for analysis of pressurized water reactors (PWRs), but future versions of TRAC-M/F90 will include a capability to model BWRs. Both codes produce graphics output that is compatible with the TRAC visualization and plotting tool XTV. In addition, TRAC-M/F90's graphics file can be used with the XMGR code. TRAC-M/F77 is written in standard Fortran 77 and includes a newly enhanced reflood model. TRAC-M/F90 is written in standard Fortran 90 and includes a derived-type database and improved data interfaces.

This report is one of four describing various features of TRAC-M/F90. Two of the other documents are the TRAC-M/F90 User's and Programmer's Manuals. The fourth document is the TRAC-M/F77 Developmental Assessment Manual. This Theory Manual provides a detailed description of the field equations, solution procedure, numerics, and closure correlations and models of the code. This report also provides the basis for each model, correlation, or solution strategy through references to original literature and/or a description of the development process. Additionally, it lists the assumptions made in the implementation, including the definitions of required parameters not normally calculated by the code, and it describes other details of the implementation. We have provided a partial assessment of some of the models and correlations against other pertinent models and correlations or separate-effects data. However, a true measure of the overall accuracy of the code must include

assessment of the code against integral experimental data because of synergistic effects. Such assessment results are provided in the TRAC-M/F77 Developmental Assessment Manual.

In the process of reviewing the details for the code and writing this report, we found that the numerics and the models and correlations used in the code are a good representation of the state of the art. However, simplified models are used in some areas where either a relevant model was not found in the literature or the literature model could not be implemented easily into the code's logic. From the assessment against integral tests, we believe that TRAC-M/F90 is a viable calculational tool for analyzing pressurized light-water reactors (LWRs) during a loss-of-coolant accident and operational transients. (Future releases of the TRAC-M/F90 documentation will address boiling water reactor (BWR) analysis.) In addition, the developmental assessment calculations for TRAC-M/F77 indicate that TRAC-M/F90 will be applicable to a wide range of test facilities.

CONTENTS

FIGURES

FIGURES (cont)

FIGURES (cont)

FIGURES (cont)

FIGURES (cont)

FIGURES (cont)

FIGURES (cont)

FIGURES (cont)

FIGURES (cont)

TABLES

TABLES (cont)

EXECUTIVE SUMMARY

The United States (US) Nuclear Regulatory Commission (NRC) is developing the modernized versions of the Transient Reactor Analysis Code (TRAC-M) to provide advanced best-estimate simulations of real and postulated transients in pressurized water reactors (PWRs) and boiling water reactors (BWRs) for many related thermal-hydraulic facilities. The TRAC-M/Fortran 90 (TRAC-M/F90) program is the latest released version. This document is written for Version 3.0 of TRAC-M/F90. In addition, we indicate areas where TRAC-M/F90 differs from TRAC-M/Fortran 77 (TRAC-M/F77). The code features a one- and/or three-dimensional, two-fluid treatment for the thermal hydraulics, together with other necessary modeling capabilities to describe a PWR system. BWR capabilities will be added to future code releases of TRAC-M/F90.

This report is one of four documents describing various features of TRAC-M/F90. The remaining documents are the TRAC-M/F77 Developmental Assessment Manual and the TRAC-M/F90 User's and Programmer's Manuals. This Theory Manual provides a detailed description of the code's field equations, solution procedure, numerics, and closure correlations and models.

The Theory Manual is structured along the same lines as the code. Section 2.0. describes the field equations, finite-difference formulations, solution strategy, numerical methods, and control procedures. Also described in Section 2.0. are the heat-conduction and reactor kinetics equations and their solution.

Section 3.0. discusses TRAC's closure models and includes a "roadmap" that relates the various closure relations to the field equations. The inherent quasi-steady assumption and its implications also are discussed in Section 3.0.. Section 3.1. gives an overview of the code's closure relations. Section 3.2. describes the basic flow-regime map that is at the heart of the logic for selecting interfacial-shear and heat-transfer correlations for appropriate flow patterns. Section 3.3. summarizes the code's correlations and logic for the calculation of interfacial area. Section 3.4. describes the interfacial mass transfer. The correlations and logic describing the interfacial and wall drag are found in Sections 3.5. and 3.6., respectively, and Sections 3.7. and 3.8. cover the correlations and logic for interfacial heat transfer and wall heat transfer, respectively.

Section 4.0. provides the descriptions of special flow models, such as critical flow, offtake model, vent valves, and countercurrent flow limitation, that impact the calculation of velocities and interfacial drag. Section 4.0. also includes other special models, such as fuel-cladding gap conductance. Section 5.0. covers special function components, including pumps, boundary-condition components (fills and breaks), plenums, pressurizers, and valves. Finally, Section 6.0. provides a summary of the overall conclusions.

Much of the material in the main sections is described in greater detail in supporting appendices. Three appendices describe the water and material properties, the necessary thermodynamic and transport properties for the noncondensable-gas field, and the

solubility model for the liquid-solute field. Other appendices discuss the quasi-steady assumption and averaging operators, basic flow-regime maps, fluid closure (energy, mass, and momentum), flow process models, special component models, fuel-rod models, core power, and control procedure. We have structured the document to aid in understanding calculated results.

The audit nature of this report results in the descriptions of the individual correlation/models being relatively independent of most of the other descriptions. Because of this audit nature and the generality of TRAC, the individual results are difficult to synthesize into a global observation. Also, the process of looking closely at individual correlations makes it difficult to account for synergistic effects.

We believe that the models and correlations used in TRAC are a good representation of the state of the art in thermal-hydraulic literature. They are consistent with the literature, among themselves, and with the code numerics. The results are limited by the general assumptions, such as the quasi-steady approach, and by the time- and area-averaged field equations, which are the current state of the art in our understanding of two-phase thermal hydraulics. We believe TRAC is a viable tool for best-estimate, thermal-hydraulic analysis during various real or postulated transients in PWRs.

ACKNOWLEDGMENTS

Many people have contributed to the development of the TRAC series. The direct antecedent of TRAC-M is TRAC-PF1/MOD2 ("MOD2", otherwise known as "TRAC-P"). Most of the development of TRAC-M/F90 has involved a massive restructuring of the code's databases, data interfaces, and network solution. The database and data interface improvements are described elsewhere in the code's documentation set (mainly in the Programmer's Manual). The main impact on the Theory Manual involves the solution of the field equations, as acknowledged below. The following acknowledgments carry over mainly from a similar list compiled earlier for MOD2. However, it would be impossible to write such an acknowledgment section for TRAC-M without recognizing the enormous contributions of James F. Dearing in restructuring the code databases in Fortran 90.

Because of the long development history and because of the many people involved, we will not attempt to list everyone who worked on the code. So, with a general acknowledgment to these people, we intend to acknowledge specifically those people who developed the major new features of MOD2 and who contributed to the actual writing of the current document. Because TRAC-PF1/MOD2 is built upon TRAC-PF1/MOD1, certain parts required minor modifications only. Likewise, parts of the current document are similar to TRAC-PF1/MOD1 documents and are derived from these earlier documents with necessary modifications. We have not listed the names of the authors of these documents; however, we would like to fully acknowledge their indirect contribution to the current manual. We are especially appreciative of the effort put into the TRAC-PF1/MOD1 Correlations and Models document coordinated by Thad D. Knight, et al.

The following individuals contributed to the composing and writing of the various sections in the current manual. They are not necessarily the people who did the coding for the corresponding parts of TRAC-PF1/MOD2 or TRAC-M/F90.

Document Coordination	Ju-Chuan Lin, Jay W. Spore
Introduction	Kemal O. Pasamehmetoglu, Paul T. Giguere
Field Equations and Numerical Methods	Robert G. Steinke, Jay W. Spore, Susan J. Jolly-Woodruff, Kemal O. Pasamehmetoglu, Norman M. Schnurr, Laura A. Guffee, Ju-Chuan Lin, Stephen A. Birdsell, John H. Mahaffy, Chris Murray
Closure Relation Section	Jay S. Elson

Basic Flow-Regime Maps	Kemal O. Pasamehmetoglu
Fluid Energy Closure	Kemal O. Pasamehmetoglu, Ralph A. Nelson, Cetin Unal
Fluid Mass Closure	Kemal O. Pasamehmetoglu, Ralph A. Nelson, James R. White
Fluid Momentum Closure	Jay W. Spore, Michael W. Cappiello, Cetin Unal, Ju-Chuan Lin
Flow Process Models	Laura A. Guffee, Robert G. Steinke, Stephen A. Birdsell, James F. Lime
Special Component Models	Robert G. Steinke, Jay W. Spore, Kemal O. Pasamehmetoglu
Additional Mass-Field Closure	Robert G. Steinke, Eric Haytcher, Kemal O. Pasamehmetoglu
Summary and Conclusions	Jay W. Spore
Thermodynamic and Transport Fluid Properties	Eric Haytcher
Material Properties	Eric Haytcher, Kemal O. Pasamehmetoglu
Report Compilation	Kemal O. Pasamehmetoglu, Denise B. Pelowitz, Karyn R. Ames, Wendy M. Burditt, E. Katherine Valdez
Report Editing	Karyn R. Ames, Virginia Buchner, Lisa G. Rothrock, Lori S. Tamura

The following individuals provided the major improvements to the TRAC-PF1/MOD2 code:

Momentum Closure	Jay W. Spore, Robert G. Steinke
Capacitance Method	Robert G. Steinke, James F. Dearing

3D Two-Step Numerics	Susan B. Woodruff, John H. Mahaffy James F. Dearing
Generalized Heat Structures	John H. Mahaffy
Reflood Package	Ralph A. Nelson, Kemal O. Pasamehmetoglu, Cetin Unal
Interfacial Constitutive Package	Jay W. Spore, Michael W. Cappiello, Kemal O. Pasamehmetoglu
Improved Wall Shear	Jay W. Spore
Improved Treatment of Noncondensables	John H. Mahaffy, Ju-Chuan Lin
Special Models	
CCFL	Jay W. Spore, Paul Dotson
Decay Heat	Jay W. Spore
Offtake Model	Laura A. Guffee
Subcooled Boiling Model	Paul Dotson, Jay W. Spore
Valve Model	Jay W. Spore

In addition, we wish to acknowledge personnel at the Japan Atomic Energy Research Institute who provided the fully implicit axial-conduction solution for the TRAC-PF1/MOD2 code. These personnel are Y. Murao, H. Akimoto, Y. Abe, and A. Ohnuki. We would also like to acknowledge the United Kingdom Atomic Energy Authority for providing the external thermocouple model, and the following Los Alamos National Laboratory staff: Dennis R. Liles, for the thermal-hydraulics modeling; and Manjit S. Sahota, for the critical-flow model.

In the development of TRAC-M/F90 from MOD2, James F. Dearing restructured the code databases into Fortran 90 derived types. This has far-reaching importance for all aspects of TRAC development. John H. Mahaffy and Chris Murray significantly improved the data interfaces with two related efforts: (1) full separation of the evaluation of terms in the flow equations from the solution of the resulting system of linear equations, resulting in an improved network solution; and (2) improved inter-component communication, implemented as a system service.

ACRONYMS AND ABBREVIATIONS

1D	one-dimensional
2D	two-dimensional
3D	three-dimensional
4D	four-dimensional
ANS	American Nuclear Society
ASME	American Society of Mechanical Engineers
B&W	Babcock and Wilcox
BWR	boiling water reactor
CCFL	countercurrent flow limitation
CCTF	Cylindrical-Core Test Facility
cgs	centimeter-gram-second units
CHF	critical heat flux
CPU	central processing unit
CSO	Chen, Sundaram, and Ozkaynak
CSS	constrained steady-state
CTSS	Cray Timesharing System
ECC	emergency core-coolant
ECCS	emergency core-coolant system
EPRI	Electric Power Research Institute
FSAR	final safety analysis report
GE	General Electric
GSS	generalized steady-state
HEM	homogeneous equilibrium model
HTC	heat-transfer coefficient
HTFS	heat-transfer fluid flow service
HS	heat-structure component
IAF	inverted annular flow
ICE	implicit continuous eulerian
ID	identification
IFDC	interfacial drag-coefficient selection
INEEL	Idaho National Engineering and Environmental Laboratory
JAERI	Japan Atomic Energy Research Institute
L-U	lower-upper (matrix decomposition)
LANL	Los Alamos National Laboratory
LBLOCA	large-break LOCA
LOCA	loss-of-coolant accident
LOFT	Loss-of-Fluid Test
LU	Lehigh University
LWR	light water reactor

NBS	National Bureau of Standards (now known as NIST)
NESC	National Energy Software Center
NIST	National Institute of Standards and Technology (formerly NBS)
NPP	nuclear-power-plant
NRC	United States Nuclear Regulatory Commission
OSV	onset of significant voiding
pdf	probability density function
PI	proportional plus integral
PID	proportional plus integral plus derivative
PORV	power-operated relief valve
ppm	parts per million
PWR	pressurized water reactor
RMS	root mean square
rps	revolutions per second
SBLOCA	small-break LOCA
SCTF	Slab Core Test Facility
SETS	stability-enhancing two-step
SI	International System of Units
SLOR	successive line over-relaxation
TRAC	Transient Reactor Analysis Code
UCSP	upper-core-support-plate
UPTF	Upper-Plenum Test Facility
USNRC	United States Nuclear Regulatory Commission

1.0. INTRODUCTION

The Transient Reactor Analysis Code (TRAC) is an advanced, best-estimate computer program designed to calculate the transient reactor behavior of a pressurized water reactor (PWR). As such, TRAC incorporates four-component (liquid water, liquid solute, water vapor, and noncondensable gas), two-fluid (liquid and gas) modeling of thermal-hydraulic processes involved in such transients. The complexity of the thermal-hydraulic modeling requires many additional models and correlations to provide closure for the equation set. As used here, a model consists of a set of correlations with logic imposed into a coherent description of a phenomenon. This document describes for TRAC-M Fortran 90 (TRAC-M/F90) the general equation sets solved by the code, the numerical solution techniques employed, and the code's closure models and correlations. A best-estimate code continues to evolve and to incorporate new capabilities from the development process; we have written the current document for Version 3.0. In addition, we indicate areas where TRAC-M/F90 differs from TRAC-M Fortran 77 (TRAC-M/F77), Version 5.5.2.

TRAC-M/F90 and TRAC-M/F77 are the latest in a series of TRAC codes, including TRAC-PF1/MOD2 (also known as "TRAC-P"), TRAC-PF1/MOD1, TRAC-PF1, TRAC-PD2, TRAC-P1A, and TRAC-P1, the earliest publicly released version. (The main development path for TRAC now comprises the versions of TRAC-M/F90. As discussed below, TRAC-M/F77 is an important "side-branch" with an enhanced PWR reflood model.) The development history represented by these earlier code versions begins with a very fundamental and important enhancement in the analysis of the behavior of light-water reactors (LWRs). This improvement is the decision to track separately the liquid and vapor fields in the reactor-coolant system. These codes required the greatly improved computer systems that were becoming available during the 1970s and they pushed advances in numerical techniques to solve the complex equation set and to permit the large number of nodes required for the best-estimate analysis of some transients of interest.

A preliminary version of TRAC consisting of only one-dimensional (1D) components was completed in December 1976. Although this version was not released publicly nor documented formally, it was used in TRAC-P1 development and formed the basis for the 1D loop-component modules. The first publicly released version, TRAC-P1, was completed in December 1977; it is described in Ref. 1-1.

The TRAC-P1 program was designed primarily for the analysis of large-break loss-of-coolant accidents (LOCAs) in PWRs. However, because of its versatility, it could be applied directly to many analyses ranging from blowdowns in simple pipes to integral LOCA tests in multiloop facilities. A refined version, TRAC-P1A, was released to the National Energy Software Center (NESC) in March 1979. It is described in Refs. 1-1. and 1-2. Although it still treats the same class of problems, TRAC-P1A not only is more efficient than TRAC-P1 and incorporates improved hydrodynamic and heat-transfer models, but also is easier to implement on various computers. TRAC-PD2 (Ref. 1-3.) contains improvements in reflood, heat-transfer models, and numerical solution

methods. Although it is a large-break LOCA (LBLOCA) code, it has been applied successfully to small-break problems and to the Three Mile Island incident.

TRAC-PF1 (Ref. 1-4.) was designed to improve the ability of TRAC-PD2 to handle small-break LOCAs (SBLOCAs) and other transients. TRAC-PF1 has all of the major improvements of TRAC-PD2. In addition, it used a two-fluid model with stability-enhancing two-step (SETS) numerics (Ref. 1-5.) in the 1D components. The two-fluid model, in conjunction with a stratified-flow regime, models countercurrent flow better than the drift-flux model used previously. The two-step numerics allow large time steps for slow transients. A 1D core component permits calculations with reduced dimensionality although the three-dimensional (3D) VESSEL option has been retained. A noncondensable gas field has been added to the 1D and the 3D hydrodynamics. Significant improvements also have been made to the trip logic and the input. TRAC-PF1 was released publicly in July 1981.

The development of TRAC-PF1/MOD1 maintained the models necessary for applying the code to LBLOCAs and added or modified models as necessary to enhance the application of the code to SBLOCAs and operational transients (Refs. 1-6. and 1-7.). In particular, we added or enhanced many user-convenience features to promote the application of the code to transients involving more complex control of the nuclear plant. TRAC-PF1/MOD1 contains generalized reactivity-feedback models (subject to point-kinetics assumptions), generalized trip and control-system modeling, and necessary components to model the rest of the plant. The code is applicable to most transients for which large asymmetries in the power generation do not exist, the 1D fluid modeling in the pipe is valid, and thermal stratification in the liquid in the 1D components is not important. (The 3D VESSEL component can model thermal stratification in a coarse manner.) The code maintains the capability to run in either a 1D or a mixed 1D and 3D mode, with SETS numerics in the 1D components.

TRAC-PF1/MOD2 ("MOD2," otherwise known as "TRAC-P") was superior to all earlier versions of TRAC, both in its numerics and its closure relationships. Among many improvements in MOD2, the SETS numerics were extended to the 3D VESSEL component, the interfacial closure relations were completely rewritten, and a new core reflood model was introduced. The 1D and 3D SETS numerics, MOD2 closure relations, and most of MOD2's modeling capabilities have been brought directly over to TRAC-M. These still provide new and state-of-the-art features for LWR safety analysis.

MOD2 is the direct antecedent of TRAC-M/F90 (and of TRAC-M/F77, as described below in Section 1.4.). Most of the development of TRAC-M/F90, Version 3.0, has involved a massive restructuring of TRAC's databases and data interfaces. (The "M" in the code's name stands for "modernized".) Almost everything else in MOD2 that affects thermal-hydraulic modeling (including closure relations, flow process models, most special component models, fluid and material properties, reactor-power logic, heat conduction, control system, and SETS numerics) was carried over to TRAC-M/F90 (and to TRAC-M/F77). In fact, an important aspect of the development of TRAC-M/F90 (and of TRAC-M/F77) was null, or almost null, testing against an extensive set of MOD2

results. TRAC-M/F90's databases are restructured into standard, portable, Fortran 90-derived types, and almost all arrays are dynamically allocated at runtime using standard Fortran 90 calls. This had, and will continue to have, far-reaching importance for all aspects of TRAC development. Also, the code's data interfaces were significantly improved with two related efforts: (1) full separation of the evaluation of terms in the flow equations from the solution of the resulting system of linear equations, resulting in an improved network solution for the field equations; and (2) improved inter-component communication, implemented as a system service. The main impact of TRAC-M/F90 development, from its MOD2 base, on the TRAC Theory Manual involves the solution of the field equations, as described in Section 2.0. The rest of this document is based on a draft Theory Manual that was prepared earlier for MOD2. Full details on the database and data-interface improvements in the code are given in the TRAC-M/F90 Programmer's Manual (Ref. 1-4.).

In Section 1.1. a brief summary and the general features of the computer program are given. Section 1.2. lists the code's essential distinguishing characteristics. The code's modeling capabilities are summarized in Section 1.3. Section 1.4. gives the current status of TRAC development. The status includes a summary of modeling features in this newest version of TRAC that were not available in earlier versions (before MOD2), a comparison of the TRAC-M/F77 and TRAC-M/F90 codes, and an indication of future areas of TRAC development. Section 1.5. describes the value of the current code as compared to its predecessors. Section 1.6. covers the scope of this document, including subsections on its structure, its targeted interest groups, and its basic assumptions.

1.1. Computer Program Summary

The official name of the code is TRAC-M/F90 (Version 3.0). Throughout this document, the term "TRAC" will indicate both TRAC-M/F90 and TRAC-M/F77 (Version 5.5.2). Where confusion could exist with earlier versions, or where TRAC-M/F90 and TRAC-M/F77 differ, we will explicitly identify the applicable code.

The programming language of TRAC-M/F90 is standard Fortran 90; the programming language of TRAC-M/F77 is standard Fortran 77. Portability was a key goal in the development of both TRAC-M/F90 and TRAC-M/F77. Unlike MOD2, there are no conditional preprocessor directives (platform-specific "IF DEFs") embedded in the Fortran source code. Both codes use a few low-level routines written in American National Standards Institute (ANSI) standard C and use the ANSI-standard C preprocessor.

TRAC performs best-estimate analyses of LOCA and other transients in PWRs. The code also models a wide variety of thermal-hydraulic experiments in reduced-scale facilities. Models used include reflood, multidimensional two-phase flow, nonequilibrium thermodynamics, generalized heat transfer, and reactor kinetics. Automatic steady-state and dump/restart capabilities also are provided. The partial differential equations that describe the two-phase flow and the heat transfer are solved by finite differences. The heat-transfer equations are treated using a semi-implicit differencing technique.

The fluid dynamic equations in both one and three dimensions use a multistep procedure (SETS numerics) that allows the material Courant limit to be violated. The highly versatile TRAC describes most thermal-hydraulic experiments in addition to a wide variety of LWR system designs. The code modularity allows better geometric problem description, more detailed models of physical processes, and reduced maintenance cost.

The only limit on the problem size is the amount of computer memory. The number of reactor components in a problem and the manner in which they are coupled are arbitrary. Reactor components that are built into TRAC are breaks and fills (boundary conditions), generalized heat structures (rods and slabs), pipes, pressurizers, pumps, tees, valves, and vessels with associated internals. Accumulators can be modeled with a special option in the pipe component, and steam generators can be modeled with a combination of pipes, tees, and heat structures. Running time is highly problem-dependent and is a function, among other things, of the total number of mesh cells, the nature of the transient, the maximum allowable time-step size, and the selection of 1D or 3D vessel modeling. The introduction of SETS numerics to the 3D vessel component will improve runtime when the overall time step would be Courant-limited by a 3D vessel component. Some important characteristics of TRAC pertinent to LWR safety are summarized in the next section.

1.2. TRAC Characteristics

Some distinguishing characteristics of TRAC are summarized below. Within restrictions imposed by computer running times, we are incorporating state-of-the-art technology in two-phase thermal hydraulics into the code.

1.2.1. Variable-Dimensional Fluid Dynamics

A 3D (r, θ, z) flow calculation can be used within the reactor vessel to allow an accurate calculation of the complex multidimensional flow patterns inside the reactor vessel that are important in determining accident behavior. For example, phenomena such as emergency core-coolant (ECC) downcomer penetration during blowdown, multidimensional plenum and core flow effects, and upper-plenum pool formation and core penetration during reflood can be treated directly. The flow within the loop components is treated one-dimensionally.

1.2.2. Nonhomogeneous, Nonequilibrium Modeling

A full two-fluid (six-equation) hydrodynamics model describes the steam-water flow, thereby allowing important phenomena, such as a countercurrent flow, to be treated explicitly. A seventh field equation (mass balance) describes a noncondensable gas field, and an eighth field equation tracks the solutes in the liquid.

1.2.3. Flow-Regime-Dependent Constitutive Equation Package

The thermal-hydraulic equations describe the transfer of mass, energy, and momentum between the steam-water phases and the interaction of these phases with the heat flow from the system structures. Because these interactions are dependent on the flow

topology, a flow-regime-dependent constitutive equation package has been incorporated into the code. Assessment calculations performed to date with MOD2 and TRAC-M/F77 indicate that many flow conditions can be handled adequately with the current package. This continues to be an active area of research in modeling two-phase flow. Therefore, it is an area in the code that will possibly continue to improve.

1.2.4. Comprehensive Heat-Transfer Capability

TRAC incorporates detailed heat-transfer analyses of the vessel and the loop components. Included is a two-dimensional (2D) (r, z) treatment of fuel-rod heat conduction with dynamic fine-mesh rezoning to resolve both bottom-flood and falling-film quench fronts. The heat transfer from the fuel rods and other system structures is calculated using flow-regime-dependent heat-transfer coefficients (HTCs) obtained from a generalized boiling surface based on local conditions.

1.2.5. Consistent Analysis of Entire Accident Sequences

An important TRAC feature is its ability to address entire accident sequences, including computation of initial conditions, with a consistent and continuous calculation. For example, the code models the blowdown, refill, and reflood phases of a LOCA. This modeling eliminates the need to perform calculations using different codes to analyze a given accident. In addition, a steady-state solution capability provides self-consistent initial conditions for subsequent transient calculations. Both a steady-state and a transient calculation can be performed in the same run, if desired.

1.2.6. Component, Functional, and Computational Mesh Modularity

The TRAC program is completely modular by component. The components in a calculation are specified through input data. The available components allow the user to model virtually any PWR design or experimental configuration. Thus, TRAC has great versatility in its range of applications. This feature also allows component modules to be improved, modified, or added without disturbing the remainder of the code. TRAC component modules currently include breaks and fills to model pressure and flow boundary conditions, generalized heat structures (rods and slabs), pipes, pressurizers, pumps, tees, valves, and vessels with associated internals (downcomer, lower plenum, core, upper plenum, etc.).

The TRAC program also is modular by function; that is, the major aspects of the calculations are performed in separate modules. For example, the basic 1D hydrodynamics solution algorithm, the wall-temperature-field solution algorithm, HTC selection, and other functions are performed in separate sets of routines that are accessed by all component modules. This modularity allows the code to be upgraded readily as improved correlations and test information become available.

An important part of TRAC-M/F90 development, related to the functional modularity, is the strengthening of the code's existing organization by computational mesh. A new data structure, developed as part of the improved data-interface effort, views components as collections of mesh segments and contains data describing the relationships between these mesh segments. Capabilities of mesh-specific subroutines

have been made more general to meet the needs of the range of physical components. Where possible, direct references to component types have been removed from mesh-specific subroutines, and the necessary features are driven by the components in a more general way. The effect is to bring component-specific operations to a higher level of the code.

1.3. TRAC Capabilities

Most physical phenomena that are important in large- and small-break LOCA and non-LOCA analyses can be treated by TRAC. The phenomena include the following:

1. ECC downcomer penetration and bypass, including the effects of countercurrent-flow hot walls;
2. lower-plenum refill with entrainment and phase separation effects;
3. bottom-reflood and falling-film quench fronts;
4. multidimensional flow patterns in the core, downcomer, and plenum regions;
5. pool formation and countercurrent flow at the upper-core-support-plate (UCSP) region;
6. pool formation in the upper plenum;
7. steam binding;
8. average-rod and hot-rod cladding temperature histories;
9. alternate ECC-injection systems, including hot-leg and upper-head injection;
10. direct injection of subcooled ECC water, without the requirement for artificial mixing zones;
11. critical flow (choking) using the improved critical-flow model (the detailed noding technique of TRAC-PD2 can still be used, although we generally do not recommend it);
12. liquid carryover during reflood;
13. metal/water reaction;
14. water-hammer effects;
15. wall friction losses;
16. natural-circulation flows;
17. horizontally stratified flows, including horizontal countercurrent flow driven by void-fraction gradients down the pipe;
18. vertical-stratification modeling in the vessel component and in the interphase mass transfer (condensation) to better calculate pressurizer refill and the general refilling of any vertically-oriented component;

19. increased range in the water properties to permit the code to calculate fluid conditions beyond the critical point (pressures in excess of 22.12 MPa) and closer to the freezing point;

20. noncondensable-gas tracking, including the injection of the noncondensable gas from the accumulators and the effects of the noncondensable gas on the interfacial condensation;

21. liquid-solute (boron) tracking, which can be coupled to the reactivity-feedback calculation;

22. point-reactor kinetics with a generalized representation of the reactivity feedback associated with the core-average fuel temperature, the core-average coolant temperature, the core-average void fraction, and the core-average boron concentration;

23. balance-of-plant modeling capability;

24. a PLENUM component consisting of a single hydraulic cell with an essentially unlimited number of connections to simplify 1D connections;

25. mixed 1D and 3D calculations or fully 1D calculations;

26. fast computational speed for 1D and 3D problems when the transient is reasonably slow, such as SBLOCA and some non-LOCA transients;

27. very general trip, control-system, and component-action (such as feedwater-pump flow characteristics) modeling capability;

28. the ability to use trips and controls in the steady-state calculation to drive the steady-state conditions towards desired values and thus to eliminate unnecessary iterations on the steady-state calculation;

29. user-convenience features, including free-format input with capability to use comment cards or fields, forward and reverse additive-friction factors for the hydraulics, capability to choose to input Darcy K-factors for the additive friction, capability to choose to input cell-centered elevations instead of the old gravity parameters at cell interfaces, and sophisticated input checking;

30. consistent generation of steady-state conditions for initializing transients so that the same thermal-hydraulic models and numerics are used in both the steady state and the transient;

31. general orientation and magnitude of the VESSEL component for the gravitational acceleration vector; and

32. a generalized heat-structure component to allow the user to connect two hydro cells, resulting in greatly increased flexibility in heat-conduction modeling.

1.4. TRAC Significant Changes

In this section we first summarize the improvements in TRAC-PF1/MOD2 that were brought over to TRAC-M/F90 and TRAC-M/F77. We then describe the development of TRAC-M/F90 and TRAC-M/F77 from their MOD2 base (indicating the differences between the two codes), and briefly discuss planned future development of the two codes.

TRAC has the following improvements that were "inherited" from MOD2:

1. SETS numerics are applied to the 3D hydro solution. This change allows the VESSEL component to take large time-step sizes during a relatively slow transient, thus allowing faster running time. The implementation of SETS numerics is described in Section 2.1.8.
2. The development of a generalized heat-structure component allows the user to connect any hydro cell with any other hydro cell. This component allows increased flexibility for heat-conduction modeling.
3. An improved reflood model is implemented in the code. The new model is described in Appendix F, Section F.2.. (Note that, as described later in this section, this reflood model is available in both TRAC-M/F90 and TRAC-M/F77, and that TRAC-M/F77 has, in addition to this model, a newer enhanced reflood model.)
4. The wall-shear model is changed and made consistent between 1D and 3D components. The new wall-shear model is described in Appendix H, Section H.2.
5. A new valve model is developed based upon experimental data for partially closed globe valves. The new model is described in Appendix J, Section J.9.
6. The Gauss-Seidel numerical solution for the 3D VESSEL pressure matrix equation was observed to be inaccurate for small breaks and operational transients. This inaccuracy would typically be observed as a mass error in the VESSEL component. This problem is solved in TRAC by the elimination of the Gauss-Seidel method and by the development and implementation of a capacitance method for solving the VESSEL pressure matrix equations. TRAC's capacitance method is described in Section 2.0.
7. The VESSEL component is allowed general orientation with respect to the gravitational acceleration vector.
8. The ANS'79 decay-heat standard, described in Appendix M, is included in TRAC as the default model.
9. An offtake model, described in Sections 2.1.8.6.3. and 4.3. as well as Appendix I, Section I.4., is implemented in TRAC.

10. Interfacial heat-transfer and interfacial shear correlations, described in Appendix F, Section F.1., and Appendix H, Section H.1., are considerably different than those in TRAC-PF1/MOD1. The interfacial shear and heat-transfer packages are made consistent with each other. The consistency is also assured between 1D and 3D components.

11. The 60-, 120-, and 180-degree rotational symmetry in cylindrical geometry allows significantly reduced noding if loop and vessel behavior is symmetric.

12. Momentum flux terms were modified so that momentum was conserved while the stable donor-cell differencing was maintained.

13. An improved subcooled-boiling model was implemented. The new model is described in Appendix G, Section G.1. and includes a mechanistic model for partitioning the wall heat transfer between flashing water to steam and heating up the subcooled liquid. The new model also includes an empirical correlation model for determination of the liquid enthalpy at bubble departure.

14. A thermal-radiation-enclosure heat-transfer model was added to the HTSTR (heat-structure) component. (This capability currently is only available in TRAC-M/F77.)

15. An option for improved time-step-size diagnostic edits was added. (This capability currently is only available in TRAC-M/F77.)

The base code for the TRAC-M development effort was TRAC-PF1/MOD2 Version 5.4.25. (In the course of TRAC-PF1/MOD2 development, the code's name was officially shortened to TRAC-P.) TRAC-M was first developed as a series of Fortran 77 (F77) versions (TRAC-M/F77), with the main goals of increased portability and providing a good base for subsequent Fortran 90 (F90) development (TRAC-M/F90).

TRAC-M/F77 Version 1.10 is an important branch point. It is the base code for all TRAC-M/F90 versions, and it is the base code for a new reflood model in TRAC-M/F77 that analyzes simultaneous top-down and bottom-up quenching.

We summarize here the main features that distinguish the F77 and F90 versions of TRAC-M, and indicate future areas of development. (Note that essentially all future development of TRAC-M is now planned for the F90 series.)

TRAC-M/F77 is currently at Version 5.5.2. It has the following characteristics:

- Portable Fortran 77.

- Same numerics, models, and correlations as MOD2 (TRAC-P) Version 5.4.25, except for the addition of a new core-reflood model that has the capability to analyze simultaneous top-down and bottom-up quenching (Ref. 1-12. and

1-13.), and an optimization methodology for development of closure relations (Ref. 1-12.).

Note that use of the SEPD (Separator) component model, which was brought over from MOD2, is not recommended. Also, the TURB (Turbine) component model, also inherited from MOD2, had received minimal support over its years in MOD2. Both the SEPD and TURB components are to be replaced in future TRAC-M/F90 versions (post-Version 3.0).

- Removal of the graphics output file TRCGRF, which was used in older code versions for graphics post-processing. All graphics output is written to files XTVGR.T and XTVGR.B; this graphics output is compatible with the TRAC-M visualization and plotting tool XTV.

TRAC-M/F90 (Version 3.0), the base F90 code version for this document, has the following characteristics:

- Portable Fortran 90, with a complete rewrite of the databases, using F90-derived types and standard Fortran 90 dynamic memory allocation.

- Improved data interfaces, including
  - full separation of the evaluation of terms in the flow equations from the solution of the resulting system of linear equations. This provides a well-defined location for equation terms, eliminates the need for generation of this data for 1D components before evaluation of the equations in 3D components, and results in a rewrite of the network solution procedure for the fluid field equations. (The underlying SETS numerics remain unchanged.)
  - improved inter-component communication, implemented as a system service.

- Removal of the MOD2 TURB (turbine) component. The turbine capability is to be re-introduced in future TRAC-M/F90 versions (post-Version 3.0).

- Removal of the thermal-radiation-enclosure heat-transfer model from the HTSTR (heat-structure) component. The "hooks" that call the radiation model are retained in commented-out form. The associated data-access logic was also removed. (The enhanced time-step-size diagnostics, which use the same data-access logic as the radiation model, were also removed.)

- Removal of the graphics output file TRCGRF, which was used in older code versions for graphics post-processing. All graphics output is written to file TRCXTV (which combines the information in TRAC-M/F77 files XTVGR.T and XTVGR.B). Both codes produce graphics output that is compatible with

the TRAC visualization and plotting tool XTV. In addition, TRAC-M/F90's graphics file can be used with the XMGR code.

Note that Version 3.0 of TRAC-M/F90 has the same outdated SEPD (Separator) Component as MOD2 and TRAC-M/F77.

The new field-equation solution scheme in TRAC-M/F90 is described in Section 2.0.

Currently the only identified future improvement to TRAC-M/F77 is the addition of improved graphics output for the point-kinetics model (and a minor error correction for that model). The main path for future TRAC-M development is in the TRAC-M/F90 series. Major aspects of ongoing TRAC-M development include the following:

- Incorporation of boiling-water-reactor (BWR) modeling capabilities similar to those of TRAC-B. This includes addition of the following:
  - Vessel-channel (CHAN) component with leak paths,
  - Jet-pump (JETP) component,
  - Heater component,
  - Turbine (TURB) component, replacing the MOD2 TURB, and
  - Separator (SEPD) component, replacing the MOD2 SEPD.
- Separation of TRAC-M/F90 into an input engine (TracInp) and a computational engine (TracCmp). This logic is described in the TRAC-M/F90 User's Manual (Ref. 1-15.).
- Development of a new single-junction component (SJC), which will be used by the forthcoming leak-path logic for the CHAN component, and will facilitate RELAP-5-style modeling.
- Addition of improved graphics output for the point-kinetics model (and a minor error correction for that model).

1.5. TRAC Value to the United States Nuclear Regulatory Commission (USNRC)

The TRAC-M codes extend the capabilities of TRAC-PF1/MOD1 in the areas described in the previous section. We have addressed many of the areas for improvement identified in the assessment of TRAC-PF1/MOD1. Also, the TRAC-M codes continue to prove the value and applicability of the SETS numerics and provide fast-running calculational tools for many reactor transients. TRAC is a very advanced thermal-hydraulic computer code capable of predicting large-, intermediate-, and small-break LOCA transients as well as most non-LOCA transients. In most cases, TRAC-M is easier to apply than the earlier versions. Because of the added generality in the models and closure relations, the enhanced user-convenience features, and the added capabilities in

many areas, we recommend the TRAC-M code over previous versions for general use in addressing licensing problems and questions relating to PWRs.

The portability of the TRAC-M codes will assist both the user and developer communities. The database and data-interface restructuring of TRAC-M/F90 provide a very sound base for future code development and maintenance.

1.6. Scope of the TRAC -M/F90 Theory Manual

This document is one of four documents released with TRAC-M/F90. The other three documents are the Developmental Assessment Manual (to be published), the User's Manual (Ref. 1-15.), and the Programmer's Manual (Ref. 1-14.). These are equally as important as the Theory Manual to obtain a complete understanding of the TRAC-M/F90 code. In addition, there is a Developmental Assessment Manual (Ref. 1-16. and 1-17.) and a Programmer's Guide for TRAC-M/F77 (Ref. 1-18.).

In the current document, the field equations that are solved by the code and the solution strategy and numerical techniques employed are described in addition to the closure relationships. In this respect, it is more involved than the models and correlations document published for TRAC-PF1/MOD1 (Ref. 1-6.), which concentrated on the closure relationships only. We believe it is important for the reader to be exposed to the solution strategy and numerical methods employed while considering the closure relationships. Quite often, the numerical theory limits the choice and the implementation of the closure relationships. As described in Section 1.6.1., the closure relations themselves are discussed at two levels of detail. There is a complete summary in the main text that includes an explicit linkage of the closure relations to terms in the field equations, and there are appendices that provide full details on the closure relations.

In documenting the closure relationships in the appendices to this Theory Manual, we followed an identical format to the TRAC-PF1/MOD1 models and correlations document. The licensing compendium (Ref. 1-8., Section 4.4) describes a process for evaluating code scaling, applicability, and uncertainty. To support this process, the USNRC requires documentation concerning the code. Specifically, compendium Section 4.4.3.1 prescribes the objectives and requirements for the models and correlations document. The document has the following three objectives:

1. "To provide detailed information on (the quality of) closure equations, that is, on correlation models and/or criteria used in the code;"
2. "To describe how these closure relations are coded in the program and [to] assure that what is listed in the code manual is indeed what the code uses;" [and]
3. "To provide a technical rationale and justification for using these closure relations (as coded in the program) in the range of interest to NPP [nuclear-power-plant] safety evaluation."

To meet these three objectives, the licensing compendium specifies that the models and correlations document should provide the following information for each model/correlation:

1. the original model/correlation
   a. source or reference,
   b. database,
   c. accuracy, and
   d. applicability to NPP conditions;
2. assessment of effects if the model/correlation is applied outside its database;
3. implementation of the model/correlation in the code;
4. description of modifications required to overcome computational difficulties; and
5. assessment of effects of implementation and/or modification on code overall applicability and accuracy.

In terms of closure relationships, this document will attempt to address items 1-5 for the TRAC models and correlations. However, we generally limited the assessment prescribed in items 2 and 5 and concentrated the assessment in those areas we consider most important. In particular, one can interpret item 5 to require sensitivity calculations on integral plant-transient simulations. These types of sensitivity calculations are beyond the scope of this document. We performed most of the assessment of those models/correlations for which the original reference is inadequate (significant modifications have been made) or the application is far outside the database. In many cases we performed this assessment in isolation; that is, we calculated the model/correlation separately from the main code. This isolation of the model/correlation saved time and effort but may have exaggerated the importance of the assumptions used to obtain the experiment data. In particular, this procedure neglects any synergistic effects of the model/correlation coupling with the rest of the code.

The TRAC-M/F77 Developmental Assessment Manual (Ref. 1-16. and 1-17.) includes many test problems and separate-effects experiments against which TRAC is assessed (as will the Developmental Assessment document for TRAC-M/F90). These problems individually concentrate on a single or a few models, while testing the overall code performance. The contents of the TRAC-M/F77 Developmental Assessment Manual (Ref. 1-16. and 1-17.) are not repeated in this manual. Also, in describing the implementation of the model/correlation, we derive from the original reference the equation that we have incorporated into the code. We specify the location of the model/correlation by subroutine(s). We consider the documentation of specific variables and mnemonics used in the code to be a large task beyond the scope and schedule of this document. Instead, their location by subroutine and equation as coded makes the code quite readable.

We also document the transitions between related models/correlations, as appropriate. These transitions are in some cases more important than the actual models/correlations themselves and are necessary to prevent nonphysical discontinuities that can result in instabilities in the solution scheme and in unrealistic calculated results.

Finally, this document is a description of just those models and correlations used in TRAC. It is not meant to be a comprehensive survey of all available, similar models, or, for that matter, of all models that one might consider to be important to all aspects of PWR features and transients. Nor does the report survey all available data pertinent to the various models/correlations. Rather, we have used data from readily available sources to pursue the assessment activities. This document also does not fill the requirements for a textbook on thermal-hydraulic phenomena and/or modeling.

This document describes the TRAC solution strategy, numerical techniques, models, and correlations, and makes statements about them related to applicability, scaleability, adequacy, and accuracy. Through a description of the database for a model/correlation and any additional assessment for that model/correlation, we provide a basis for judging quality, although we do not provide assurance that the "best" model/correlation has been selected. While the assessment of individual correlations and models is important, we believe that one should judge the overall quality of the code based on the developmental and independent assessment results.

1.6.1. Document Structure

For much of the material in the Theory Manual we introduce a topic in an appropriate main section and provide more detail in an appendix. The main exceptions are the treatments of the hydrodynamic field equations and the heat-conduction logic, which are covered entirely in the main text. The treatment of the closure relations is "top-down" in the main text, going from the general to the specific. The appendices treat the same closure relations in more detail, and in generally a "bottom-up" fashion. This allows the reader to obtain first an overall grasp of the code's logic, and then to easily find additional detail if desired.

This document is structured along the same lines as TRAC. We have structured the document to aid in understanding the calculated results. Aside from the parts of the code that handle the details of input and output, the code basically solves a set of field equations that describe the fluid, the transport of energy in solid structures (conduction), and in certain applications, the reactor kinetics. Section 2.0. summarizes the field equations used in the code. We have not included the derivation of the field equations because that is beyond the scope of this document. However, Section 2.0. also includes the description of the solution strategy and the numerical techniques. For TRAC, the fluid field equations are by far the most complete; the solutions of the conduction equation and the reactor kinetics are more like boundary conditions applied to the fluid equations. Therefore, the document concentrates on and highlights those models and correlations required by the fluid equations while documenting the models and correlations pertaining to the conduction and kinetics at the appropriate level of detail. The heat-conduction models are described in Section 2.0., and the kinetics are introduced

in Section 2.0. and described in more detail in Appendix M. TRAC's control procedure is introduced in Section 2.0. and described in detail in Appendix N.

The document relies on the presence of the field equations in Section 2.0. to provide cohesion and structure; the terms in the field equations indicate that the closure relations are required and show how the closure relations are incorporated. To reinforce this linkage between the field equations and the closure relations, Section 3.0. provides an introduction to TRAC's closure relations that includes a "roadmap" that explicitly links the individual closure relations to the individual terms in the hydrodynamic field equations. The closure relations are described in further detail in the appendices to this document (Appendices D through H). The inherent quasi-steady assumption and its implications also are introduced in Section 3.0. and described in detail in an appendix (Appendix D). Section 3.1. gives an overview of TRAC's closure relations. Section 3.2. describes the basic flow-regime map that is at the heart of the logic for selecting interfacial shear and heat-transfer correlations for appropriate flow patterns. The description of the flow-regime map follows the field equations in Section 2.0. because the map provides the basis in the code for selecting, according to the appropriate flow pattern, many of the closure relations used to describe the two-phase fluid. The basic flow-regime map forms the basis for linking correlations into models spanning a wide variety of flow conditions. Each collection of related correlations and models, whether they describe interfacial shear or interfacial heat transfer or wall heat transfer, etc., modifies the basic map to account for the amount of knowledge available about a given phenomenon. Generally, the more detailed the knowledge is concerning a particular phenomenon, the more detailed the flow regimes must be. Additional detail on the flow regimes is given in Appendix E. Section 3.3. summarizes the code's correlations and logic for calculation of interfacial area, which is dependent on the flow regime. Section 3.4. describes the interfacial mass transfer. The correlations and logic describing the interfacial and wall drag are in Sections 3.5. and 3.6., respectively. Sections 3.7. and 3.8. cover the correlations and logic for interfacial heat transfer and wall heat transfer, respectively. Appendices F, G, and H expand the treatment of interfacial and wall heat transfer, fluid mass closure, and interfacial and wall drag, respectively. Because the logic for selecting various models and correlations is an item to be documented and because this logic tends to be localized in the code, we have grouped the models and correlations in Appendices F, G, and H by field equation. Section 3.0., and related appendices, clarify the modifications required to the basic flow-regime map for each process. The next two sections describe process and boundary models for the fluid equations. These models provide details beyond the scope of the field equations that are required to model complete reactor systems. Section 4.0. and Appendix I describe those models that are not component-oriented (in the TRAC sense of components) and that generally have an impact on the momentum equation and/or interfacial drag. Three main examples of these models are critical flow, CCFL, and form loss. Section 4.0. also includes other special models, such as fuel-cladding gap conductance. Section 5.0. and Appendix J cover special function components, including pumps, boundary condition components (fills and breaks), plenums, pressurizers, and valves. Finally, Section 6.0. provides a summary of the overall conclusions of this Theory Manual.

Appendices A and B cover the code's thermodynamic and transport fluid properties, and material properties, respectively. Appendix D discusses the quasi-steady assumption that underlies TRAC's closure logic. Appendix E gives an expanded treatment of TRAC's basic flow regime logic.

For Appendix F through K we have generally assumed that the fluid is liquid water and water vapor. We have, however, described as appropriate the effects of the noncondensable gas and the liquid solute. Appendix F describes the closure relations required by the fluid energy-field equations. These relations include both the interfacial heat transfer and the wall-to-fluid heat transfer, which includes the discussion of the heat-transfer coefficients. Appendix G provides the closure relations required by the fluid mass-conservation equations and builds on interfacial heat transfer presented in Appendix F. Appendix H provides the closure relations required by the fluid momentum equations, including both the interfacial drag and the wall drag. This appendix also describes all of those models that affect the interfacial drag, which includes the entrainment model invoked during reflood.

Appendix I describes the flow process models, including the abrupt area-change model, critical flow, countercurrent flow limitation (CCFL), and vent valves in the VESSEL component. Appendix J describes the special component models that interact specifically with the momentum equations: PUMP, steam/water separator (SEPD), FILL, BREAK, PLENUM, turbine (TURB), accumulator, pressurizer, and valve.

Appendix K provides the closure relations required by the extra mass-conservation fields: noncondensable gas and liquid solute. It provides the thermodynamic and transport properties for the noncondensable-gas field and the solubility model for the liquid-solute (boron) field. These fields are calculated by the extra fluid mass-conservation field equations. The discussion of the noncondensable-gas and liquid-solute effects on other models is provided as appropriate with each model. The code assumes that these two components move with the gas and liquid fields as appropriate and that the interactions are minimal. Other sections and appendices have described how the presence of the noncondensable gas and liquid solute have affected the interfacial and wall heat transfer, the interfacial mass transfer, and the interfacial and wall drag. For the most part, the effect of the liquid solute is limited to a feedback effect in the reactor kinetics.

Appendix L describes fuel-cladding gap conductance and the metal-water reaction model. Appendix M describes in detail the reactor-core power model. Finally, Appendix N gives details on the code's control procedure, including signal variables, control blocks, and trips.

The general structure of this document lends itself well to the writing process because it follows the code structure and does not require that descriptions of a related set of closure relations be distributed throughout the document. The localization of related models and correlations permits a more logical, clearer description of the logic linking them and minimizes the opportunities for omissions and duplications. Indeed, one of

the most important questions to be addressed concerns the transitions/couplings of various models. To the extent that the code does this, the document structure lends itself very well to describing the logic and transitions among the various models. The selected structure is also more in tune with targeted interest groups that are described in the next subsection.

The code sorts the problem of single-phase versus two-phase fluid at a very high level in determining the equation set to be solved. If the fluid is single-phase liquid or vapor, all of the interfacial processes are eliminated and the code considers only the interactions with the walls and the transport of a single-phase fluid. For the case of single-phase liquid, the code sets the vapor velocity to that of a bubble, and for the case of single-phase vapor, sets the liquid velocity to that of a droplet. The code used this prescription to prevent accelerating the appearing phase from zero velocity when the fluid first becomes two-phase. For the single-phase case, large sections of the document dealing with flow regimes, interfacial heat and mass transfer, drag, and most of the correlations for wall heat-transfer coefficients are not pertinent.

For the two-phase case, the code has to evaluate the terms dealing with the interfacial interactions plus determine two-phase effects on wall drag and wall heat transfer. The document is structured to discuss the flow-regime map in Section 3.0. because the map is important to many of the choices made in sorting the correct correlations for the interfacial phenomena. For the case of single-phase liquid or vapor, the code does not distinguish flow regimes because there is only a single velocity to describe the single-phase fluid. The only single-phase flow structures recognized by the code are laminar or turbulent flow. The code makes the choice of laminar versus turbulent at the lowest level in the correlation sets. An interesting note is that for single-phase liquid at normal PWR operating pressure and temperature in a 0.762-m-i.d. pipe (typical for a PWR), the laminar transition point occurs at ~3.5 mm/s, which is essentially loop stagnation; any significant flow results in turbulent flow conditions.

Future versions of this TRAC-M/F90 Theory Manual will address TRAC-M/F90's capabilities, which are now under development, for analysis of BWRs.

1.6.2. Targeted Interest Groups

We have structured the document to follow the code calculation. We have written this document for the code user who attempts to understand the reasons behind the qualitative and quantitative nature of the comparisons between calculated results and data; to determine the applicability of the code to particular facilities and/or transients; or to determine the appropriateness of calculated results, with or without data to support the calculations. The definition of code user includes anyone who is involved in running the code or in analyzing the calculated results.

People involved in the development of TRAC or similarly based codes should find the information contained in this document interesting. The document provides insight into the smoothness requirements of codes to maintain computational efficiency and to obtain closure and into the constraints of physical phenomena. It provides one solution

to the many problems associated with closure and demonstrates methodologies for obtaining continuity at the boundaries among correlation sets that, because of their mathematical forms and different databases, are inherently discontinuous.

A third group of individuals who may be interested in this document includes managers who are involved in funding/directing work involving TRAC or experiments producing data that could be used to develop correlations or models. While we do not wish to understate the importance of the numerical techniques incorporated in TRAC, we believe that the current schemes demonstrate exceptional stability and robustness that will serve adequately in codes like TRAC for years to come. However, the models and correlations in the code can have a significant impact on the speed of a calculation; they can and frequently do affect adversely the time-step size and the number of iterations used. Because of the impact on the speed of the calculation and because the models and correlations greatly affect the accuracy of the results, the area of model/correlation development may result in significant improvements in the overall code performance. This document provides a baseline against which to measure the adequacy of the current models and correlations and a tool to help prioritize future experiment and development activities.

As indicated before, this document is not intended to substitute for a textbook on thermal-hydraulic phenomena or modeling, but rather to provide one example of how one could select correlations and models and define logic to link them into a coherent system to describe, in conjunction with the field equations, a large variety of thermal-hydraulic conditions and transients. Even within the field of reactor safety in the United States other, similar calculational tools exist (for examples, see Ref. 1-9. through 1-11.) in which different objectives, constraints, and histories have led to different choices for solution strategies, models, and correlations.

1.6.3. Basic Assumptions Within the Document

We have attempted to state clearly that certain models do not exist in the code; however, it is difficult to be complete in listing all things not included. Because we have been thorough in writing the description of the models and correlations, one should assume that if the document does not describe a model for a given phenomenon or process, the code does not contain such a model. We have described the standard closure relationships used in the code and, where appropriate, any special cases that alter the standard prescriptions. Basically, if we have not described a special case, the code does not consider it and uses the standard relations.

In the appendices, items like interfacial areas and bubble/droplet sizes are documented in those appendix subsections that require the information. This organization of detailed information leads to some duplication but forces the documentation to be complete, both in a model/correlation description sense and in the overall sense. We have documented in a similar fashion any kind of old-time/new-time averaging, void-fraction weighting of correlation results, and any limits placed on the magnitude of the result or the rate at which the result is permitted to change. We have used a standard, detailed outline for writing the descriptions of individual correlations and models in an effort to maintain a

uniform level of detail and format in the contributions from the many authors. However, on a model-by-model basis, some variations occur because of the history of the development process. Also, as indicated in Section 1.6., the level of assessment varies based on the available references pertaining to a given model/correlation and on the need to support a given model/correlation.

The term fluid in general refers to any combination of liquid water, steam, and non-condensable gas (the liquid solute is a part of liquid water), although in specific cases the term may be restricted to a subset. For clarity, we have avoided such constructions as "fluid temperature" and refer instead to "liquid temperature" or "vapor (gas) temperature."

REFERENCES

1-1. Safety Code Development Group, "TRAC-P1: An Advanced Best Estimate Computer Program for PWR LOCA Analysis," Los Alamos Scientific Laboratory report LA-7279-MS (NUREG/CR-0063) (June 1978).

1-2. Safety Code Development Group, "TRAC-P1A: An Advanced Best Estimate Computer Program for PWR LOCA Analysis," Los Alamos Scientific Laboratory report LA-7777-MS (NUREG/CR-0665) (May 1979).

1-3. Safety Code Development Group, "TRAC-PD2: Advanced Best Estimate Computer Program for Pressurized Water Reactor Loss-of-Coolant Accident Analysis," Los Alamos Scientific Laboratory report LA-8709-MS (NUREG/CR-2054) (April 1981).

1-4. Safety Code Development Group, "TRAC-PF1: An Advanced Best Estimate Computer Program for Pressurized Water Reactor Analysis," Los Alamos National Laboratory report LA-9944-MS (NUREG/CR-3567) (February 1984).

1-5. J. H. Mahaffy, "A Stability-Enhancing Two-Step Method for Fluid Flow Calculations," *Journal of Computational Physics* **46**, 329-341 (1982).

1-6. Safety Code Development Group, "TRAC-PF1/MOD1 Correlations and Models," Los Alamos National Laboratory report LA-11208-MS (NUREG/CR-5069) (December 1988).

1-7. Safety Code Development Group, "TRAC-PF1/MOD1: An Advanced Best Estimate Computer Program for Pressurized Water Reactor Thermal-Hydraulic Analysis," Los Alamos National Laboratory report LA-10157-MS (NUREG/CR-3858) (July 1986).

1-8. "Compendium of ECCS Research for Realistic LOCA Analysis: Draft Report for Comment," US NRC report (NUREG-1230) (April 1987).

1-9. M. J. Thurgood, J. M. Kelly, T. E. Guidotti, R. J. Kohrt, and K. W. Crowell, "COBRA/TRAC—A Thermal-Hydraulics Code for Transient Analysis of Nuclear Reactor Vessels and Primary Coolant Systems," Pacific Northwest Laboratories report PNL-4385 (NUREG/CR-3046) (March 1983).

1-10. D. D. Taylor, R. W. Shumway, and G. L. Singer, "TRAC-BD1/MOD1: An Advanced Best Estimate Computer Program for Boiling Water Reactor Transient Analysis," Vols. 1-4, EG&G Idaho, Inc., report EGG-2294 (NUREG/CR-3633) (April 1984).

1-11. V. H. Ransom, R. J. Wagner, J. H. Trapp, L. R. Feinauer, G. W. Johnson, D. M. Kiser, and R. A. Riemke, "RELAP5/MOD2 Code Manual, Volume 1: Code Structure, Systems Models and Solution Methods," EG&G Idaho, Inc., report EGG-2396 (NUREG/CR-4312) (August 1985).

1-12. R. A. Nelson, Jr., D. A. Pimentel, S. J. Jolly-Woodruff, and J. W. Spore, "Reflood Completion Report, Volume I: A Phenomenological Thermal-Hydraulic Model of Hot Rod Bundles Experiencing Simultaneous Bottom and Top Quenching and an Optimization Methodology for Closure Development," Los Alamos National Laboratory report LA-UR-98-3043 (April 1998).

1-13. B. E. Boyack, J. F. Lime, D. A. Pimentel, J. W. Spore, and T. D. Knight, "Reflood Completion Report, Volume II: Developmental Assessment of a New Reflood Model for the TRAC-M/F77 Code," Los Alamos National Laboratory report LA-UR-98-3043 (April 1998).

1-14. B. T. Adams, J. F. Dearing, P. T. Giguere, R C. Johns, S. J. Jolly-Woodruff, J. Mahaffy, C. Murray, J. W. Spore, and R. G. Steinke, "TRAC-M/FORTRAN 90 (Version 3.0) Programmer's Manual," Los Alamos National Laboratory document LA-UR-00-803 (February 2000).

1-15. R. G. Steinke, V. Martinez, N. M. Schnurr, J. W. Spore, and J. V. Valdez, "TRAC-M Fortran 90 (Version 3.0) User's Manual," Los Alamos National Laboratory document LA-UR-00-835 (February 2000).

1-16. B. E. Boyack, J. F. Lime, D. A. Pimental, J. W. Spore, and J. L. Steiner, "TRAC-M/F77, Version 5.5, Developmental Assessment Manual, Volume I: Nonproprietary Assessment Sections," Los Alamos National Laboratory document LA-UR-99-6480 (December 1999).

1-17. B. E. Boyack, J. F. Lime, D. A. Pimental, J. W. Spore, and J. L. Steiner, "TRAC-M/F77, Version 5.5, Developmental Assessment Manual, Volume II: Proprietary Assessment Sections," Los Alamos National Laboratory document LA-CP-99-345 (December 1999).

1-18. R. G. Steinke, S. J. Jolly-Woodruff, and J. W. Spore, "TRAC-M: Fortran 77, Version 5.5, Programmer's Guide, Volume III," Los Alamos National Laboratory document LA-UR-99-2312 (NUREG/CR-6658) (October 1999).

2.0. FIELD EQUATIONS AND NUMERICAL METHODS

The following subsections briefly describe the field equations (fluid and structures). The most difficult part of the solution is to solve the thermal-hydraulic behavior of the fluid and the coupling to the fuel/structural heat transfer through the heat-transfer coefficients (HTCs). The code devotes most of the programming and most of the computer time to solving this part of the problem. This area is more complex because there are more coupled field equations associated with describing the fluid (more independent variables), more phenomena to be considered, and the HTCs are very dependent on the fluid properties and velocities. On the other hand, the field equations describing the energy field in the solid structures and the nuclear reaction are much simpler and involve fewer variables. Although less complicated, these fields are as important as the thermal-hydraulic model to the overall solution of the problem.

The TRAC code, as well as most other similar codes, invokes a quasi-steady approach to the heat-transfer coupling between the wall and the fluid as well as the closure relations for interfacial and wall-to-fluid heat transfer and drag. This quasi-steady approach assumes detailed knowledge of the local fluid parameters and ignores time dependencies so that the time rate of change in the closure relationships becomes infinite and the time constants are zero. The quasi-steady approach has the advantages of being reasonably simple and generally applicable to a wide range of problems and of not requiring previous knowledge of the given transient. Where appropriate, we will integrate the effects of the quasi-steady approach; however, the descriptions of the methodology by necessity will be somewhat limited. Appendix D discusses the quasi-steady assumption and the averaging operators used in the code.

In Section 2.1. the field equations are described, including the finite-difference methods. In the same section, the overall solution strategy and the numerical solution methods are also described. Heat-conduction calculations and the reactor kinetics are discussed in Section 2.2. and Appendix M, respectively. Brief discussions of the Reactor-Core Power Model and Control Procedures are provided in Sections 2.3. and 2.4., respectively, whereas detailed discussions on these topics appear respectively in Appendices M and N.

Section 2.0. contains many equations and symbols. As a result, we have provided separate nomenclatures for Sections 2.1. and 2.2.

2.1. Fluid Field Equations

TRAC uses a two-phase, two-fluid model for fluid flow in both the 1D and 3D components. Kocamustafaogullari (Ref. 2-1.), Ishii (Ref. 2-2.), and Bergles et al. (Ref. 2-3., pp. 40-122) have provided detailed derivations of the equations similar to those used in TRAC, and a more concise derivation related to the TRAC equations is available in a report by Addessio (Ref. 2-4.). That this model is formally ill-posed was the subject of considerable debate several years ago and is discussed by Stewart and Wendroff (Ref. 2-5., pp. 388-389). Our experience, however, has always been that this is a moot

point, since the numerical solution procedures effectively introduce minor modifications to the field equations, making them well posed. A paper by Stewart (Ref. 2-6.) confirms these observations and demonstrates clearly that with normal models for interfacial drag and reasonable finite-difference nodalizations, the problem solved numerically is well posed.

Before presenting the fluid field equations, we need to define certain terminology. In our nomenclature, the term *gas* implies a general mixture of water vapor and the noncondensable gas. The subscript g will denote a property or parameter applying to the gas mixture; the subscript v indicates a quantity applying specifically to water vapor (referred to as simply *vapor*); and the subscript a (for *air*) signifies a noncondensable-gas quantity. The term *liquid* implies pure liquid water, and the subscript ℓ denotes a quantity applying specifically to liquid water. For convenience, we define the following terms that will be used in the subsequent equations and list them alphabetically with the Greek symbols at the end. In the subsections where the numerical methods are discussed, various dummy variables are used. Although the dummy variables are not listed in the following nomenclature, their significance becomes obvious to the reader by reading the text. The following notation applies to the discussion of numerical methods. A caret ($\hat{}$) above a variable denotes an explicit predictor value. A tilde ($\tilde{}$) above a variable denotes an intermediate result, and a line ($\bar{}$) above denotes an arithmetic average of values at adjacent cells. A double line underneath a symbol refers to a matrix, whereas a single line underneath means a vector (1D array).

NOMENCLATURE

A: flow area between mesh cells

A_i: interfacial area between the liquid and gas phases

c: speed of sound or shear coefficient

e: internal energy

$\vec{g}$: gravity vector

g: magnitude of the gravity vector

h: heat-transfer coefficient (HTC)

h_{sg}: gas saturation enthalpy

h_{wg}: $(1-f_1)\ h'_{wg}$, the effective wall HTC to gas

$h_{w\ell}$: $f_\ell h'_{w\ell}$, the effective wall HTC to liquid

h'_ℓ: liquid enthalpy of the bulk liquid if the liquid is vaporizing or the liquid saturation enthalpy if vapor is condensing

h'_v: vapor enthalpy of the bulk vapor if the vapor is condensing or the vapor saturation enthalpy if liquid is vaporizing

K: form-loss coefficient or wall friction coefficient

m: solute concentration in the liquid (mass of solute per unit mass of liquid)

P: fluid pressure or total pressure

q: heat-transfer rate per unit volume

q_d: power deposited directly (without heat-conduction process)

q_{gl}: liquid-to-gas sensible heat transfer

q': heat flux

r: radius

S: factor applied to the 1D component so that its positive flow direction becomes the positive flow direction of the vessel

S_c: plated-out solute density (mass of plated solute divided by cell volume)

SC: product of an orifice factor

S_m: source term in the solute-mass differential equation

t: time

T: temperature

T_{sv}: saturation temperature corresponding to the vapor partial pressure

$\vec{V}$: velocity vector

V: magnitude of the velocity

vol: hydrodynamic-cell volume

w: weighting factor

x: distance

Y: dummy variable

z: axial coordinate

α: gas volume fraction

β: momentum-convection temporal expansion flags

γ: weighting factor

Γ: interfacial mass-transfer rate

Γ^+: maximum of Γ and 0

Γ^-: minimum of Γ and 0

ρ: density

ΔP: pressure difference

Δr: radial ring increment for 3D components

Δt: time-step size

ΔV: velocity change

Δx: cell length for 1D components

Δz: axial level increment for 3D components

$\Delta\theta$: azimuthal segment increment for 3D components

δP: linear Taylor series expansion term for pressure

δT: linear Taylor series expansion term for temperature

$\delta\alpha$: linear Taylor series expansion term for void fraction

θ: inclination angle from vertical or the azimuthal coordinate

ϕ: angle between the main and side tubes in TEE component

Subscripts

1D: one dimensional

3D: three dimensional

donor: donor cell

T: the first cell in the side leg of the TEE or the interface between the j^{th} cell of the primary and the first cell in the side leg

a: noncondensable gas

d: generic for r, θ, or z or for i, j, or k

g: gas mixture

i: interfacial

ℓ or l: liquid

max: maximum

min: minimum

r: radial

sat: saturation

v: water vapor

w: wall

z: axial

θ: azimuthal

Superscripts

n: current-time quantity

$n + 1$: new-time quantity

$'$: last estimate

In the discussion of the finite-difference equations, all quantities except for the velocities are centered in the hydrodynamic cell (cell-centered), and the velocities are cell-edge quantities.

2.1.1. Gas/Liquid Equations

The basic volume- and time-averaged, two-phase, two-fluid model consists of six partial differential equations.

Combined Internal Energy Equation

$$\frac{\partial\left[(1-\alpha)\,\rho_\ell\, e_\ell + \alpha\rho_g e_g\right]}{\partial t} + \nabla\cdot\left[(1-\alpha)\,\rho_\ell\, e_\ell \vec{V}_\ell + \alpha\,\rho_g\, e_g \vec{V}_g\right]$$

$$= -P\nabla\cdot\left[(1-\alpha)\vec{V}_\ell + \alpha\vec{V}_g\right] + q_{w\ell} + q_{wg} + q_{d\ell} + q_{dg} \ . \qquad (2\text{-}1)$$

Combined-Gas Energy Equation

$$\frac{\partial\left(\alpha\rho_g e_g\right)}{\partial t} + \nabla\cdot\left(\alpha\rho_g e_g \vec{V}_g\right) = -P\frac{\partial\alpha}{\partial t} - P\nabla\cdot\left(\alpha\vec{V}_g\right) + q_{wg} + q_{dg} + q_{ig} + q_{g\ell} + \Gamma\, h'_v \ . \qquad (2\text{-}2)$$

Liquid Mass Equation

$$\frac{\partial\left[(1-\alpha)\rho_\ell\right]}{\partial t} + \nabla\cdot\left[(1-\alpha)\rho_\ell\vec{V}_\ell\right] = -\Gamma \ . \qquad (2\text{-}3)$$

Combined-Gas Mass Equation

$$\frac{\partial\left(\alpha\rho_g\right)}{\partial t} + \nabla\cdot\left(\alpha\,\rho_g\vec{V}_g\right) = \Gamma \ . \qquad (2\text{-}4)$$

Liquid Equation of Motion

$$\frac{\partial\vec{V}_\ell}{\partial t} + \vec{V}_\ell\cdot\nabla\vec{V}_\ell = -\frac{1}{\rho_\ell}\nabla P + \frac{c_i}{(1-\alpha)\rho_\ell}\left(\vec{V}_g - \vec{V}_\ell\right)\left|\vec{V}_g - \vec{V}_\ell\right|$$

$$-\frac{\Gamma^-}{(1-\alpha)\rho_\ell}\left(\vec{V}_g - \vec{V}_\ell\right) - \frac{c_{w\ell}}{(1-\alpha)\rho_\ell}\vec{V}_\ell\left|\vec{V}_\ell\right| + \vec{g} \ . \qquad (2\text{-}5)$$

Combined-Gas Equation of Motion

$$\frac{\partial \vec{V}_g}{\partial t} + \vec{V}_g \cdot \nabla \vec{V}_g = -\frac{1}{\rho_g}\nabla P - \frac{c_i}{\alpha \rho_g}(\vec{V}_g - \vec{V}_\ell)\left|\vec{V}_g - \vec{V}_\ell\right|$$

$$-\frac{\Gamma^+}{\alpha \rho_g}(\vec{V}_g - \vec{V}_1) - \frac{c_{wg}}{\alpha \rho_g}\vec{V}_g\left|\vec{V}_g\right| + \vec{g} \ . \qquad (2\text{-}6)$$

An alternative to solving one of the phasic mass equations is to solve the total mass equation, which is obtained by summing Eqs. (2-3) and (2-4). This yields the following result:

Total Mass Equation

$$\frac{\partial\left[(1-\alpha)\rho_\ell + \alpha \rho_g\right]}{\partial t} + \nabla \cdot \left[(1-\alpha)\rho_\ell \vec{V}_\ell + \alpha \rho_g \vec{V}_g\right] = 0 \ . \qquad (2\text{-}7)$$

Solving either Eq. (2-3) or (2-4) together with Eq. (2-7) is equivalent to solving both Eqs. (2-3) and (2-4).

Closure is obtained for these equations using normal thermodynamic relations and specifications for the interfacial drag coefficients (c_i), the interfacial heat transfer (q_{ig} and q_{i1}), the phase-change rate (Γ), the wall-shear coefficients (c_{wg} and c_{w1}), and the wall heat flows (q_{wg} and q_{w1}). These equations do not require directly the quasi-steady assumption as long as the correct closure relations for the given transient exist. A real difficulty arises because, depending on how the closure relations were developed, a different set of closure relations may be required for each transient, and each set must comply with the assumptions associated with the definition of the time and volume averaging used in the field equations. If a steady- or quasi-steady-state database or a relationship derived from such a database is used to represent a closure relation, the code necessarily applies the quasi-steady assumption stated in Section 2.0. This latter case applies for the closure relations within TRAC. Further discussion of this assumption is presented in Appendix D. Cross-references between TRAC'S closure relations and the field relations are provided in Section 3.0.

The phase-change rate required by the equation set is evaluated from a simple thermal-energy-jump relation

$$\Gamma = \frac{-\left(q_{ig} + q_{i\ell}\right)}{\left(h'_v - h'_\ell\right)} \ , \qquad (2\text{-}8)$$

where

$$q_{ig} = \frac{P_v}{P} h_{ig} A_i \frac{(T_{sv} - T_g)}{\text{vol}} \tag{2-9}$$

and

$$q_{i\ell} = h_{i\ell} A_i \frac{(T_{sv} - T_\ell)}{\text{vol}} \ . \tag{2-10}$$

Here A_i is the interfacial area, h_{ig} and $h_{i\ell}$ are HTCs, and T_{sv} is the saturation temperature corresponding to the partial steam pressure. Appendix F, Section F.1. discusses the closure relationships used to define A_i, h_{ig}, and $h_{i\ell}$. The term Γ^+ is equal to Γ for positive Γ and zero for negative Γ; Γ^- is equal to Γ for negative Γ and zero for positive Γ. The quantities h'_v and h'_ℓ are the appropriate enthalpies of the vapor and liquid, respectively. These enthalpies are the bulk fluid enthalpy for the phase moving to the interface and the saturation enthalpy for the product of the phase change.

Using Newton's law of cooling extended to a thermal nonequilibrium situation, the wall heat-transfer terms assume the form

$$q_{wg} = h_{wg} A_w \frac{(T_w - T_g)}{\text{vol}} = q'_{wg} A_w / \text{vol} \tag{2-11}$$

and

$$q_{w\ell} = h_{w\ell} A_w \frac{(T_w - T_\ell)}{\text{vol}} = q'_{w\ell} A_w / \text{vol} \ , \tag{2-12}$$

where A_w is the actual heated surface area. The h_{wg} and $h_{w\ell}$ of the cell include the information regarding the portion of the wall having gas and liquid contact. Appendix F, Section F.2. discusses the closure relationships used to define h_{wg} and $h_{w\ell}$.

The mass equations are written in fully conservative form to permit the construction of a numerical scheme that rigorously conserves some measure of the system fluid mass. The energy equations are written in a partially conservative form to make numerical solution simpler than would be possible if the fully conservative form (bulk kinetic-energy terms included) were used. The nonconservative form of the momentum equations, defined as motion equations, also permits simpler numerical solution strategies and can generally be justified because the presence of wall friction makes the fully conservative form of the momentum equation far less useful. When sharp flow-area changes exist, however, numerical solution of the nonconservative motion equations can produce significant errors. The motion equations have been modified in the MOD2 code to force momentum conservation (see Section 2.1.7.).

2.1.2. Noncondensable Gas

A single noncondensable-gas field may be modeled with TRAC. It is assumed to be in thermal equilibrium with any steam that is present and to move with the same velocity as the steam (mechanical equilibrium). Hence, only a single mass-continuity equation is needed to track the noncondensable gas.

Noncondensable-Gas Mass Equation

$$\frac{\partial(\alpha\rho_a)}{\partial t} + \nabla\cdot\left(\alpha\rho_a\vec{V}_g\right) = 0 \ . \tag{2-13}$$

With this field present, the total gas density and energy are sums of the vapor and the noncondensable components,

$$\rho_g = \rho_v + \rho_a \tag{2-14}$$

and

$$\rho_g e_g = \rho_v e_v + \rho_a e_a \ . \tag{2-15}$$

We assume Dalton's law applies; therefore,

$$P = P_v + P_a \ . \tag{2-16}$$

The subscripts v and a indicate, respectively, the steam and air properties; the code normally applies the thermodynamic properties for air to the noncondensable gas. The code user may, however, select hydrogen or helium as an alternative.

2.1.3. Liquid Solute

TRAC includes a mass-continuity equation for a solute moving with the liquid field.

Liquid-Solute Concentration Equation

$$\frac{\partial\left[(1-\alpha)m\rho_\ell\right]}{\partial t} + \nabla\cdot\left[(1-\alpha)m\,\rho_\ell\,\vec{V}_\ell\right] = S_m \ , \tag{2-17}$$

where m is the solute concentration (mass of solute/unit mass of liquid water) in the liquid phase.

The solute does not affect the hydrodynamics directly. If we assume that the solute represents orthoboric acid, the amount of the dissolved and the plated-out orthoboric acid in the core may affect the hydrodynamics indirectly through neutronic-reactivity feedback corresponding to user-specified input values obtained from a boron-mass reactivity-coefficient table (see Appendix M, Section M.2.5.). If the solute concentration exceeds the orthoboric-acid solubility at the liquid temperature in a specific

hydrodynamic cell, we assume that the excess solute in that cell plates out. Plating on structures can occur if the cell fluid flashes or boils and thus increases the concentration beyond the solubility limit. We also assume that any plated-out solute instantaneously redissolves to the maximum allowable concentration if more liquid enters the cell. Because the solute does not affect the hydrodynamics directly, the solute variable may be used as a tag to track the movement of fluid from a specific source through the system.

2.1.4. Basic Finite-Volume Approximations to the Flow Equations

TRAC-M/F90 contains the option to select one of two related numerical methods for solution of the two-phase-flow equations. The default Stability Enhancing Two-Step (SETS) method has the advantage of avoiding Courant stability limits on time-step size but the disadvantage of relatively high numerical diffusion. When the variable NOSETS is given a value of one in the namelist input, the default will be replaced by a semi-implicit method that usually has substantially less numerical diffusion but has time-step sizes restricted by a material Courant limit. Currently, the NOSETS option forces selection of a single method for the entire system. It is not possible, for example to use a semi-implicit vessel and SETS for the 1-D loops.

Both basic finite-volume models are descendents of the Implicit Continuous Eulerian technique (ICE) (Ref. 2-7.). The key improvement introduced by Liles and Reed (Ref. 2-8.) in their semi-implicit method was a tighter coupling of the energy equation to the mass and momentum equations than that used in ICE. This coupling is crucial to stable modeling of two-phase flows with substantial boiling or condensation. The SETS method (Refs. 2-9. and 2-10.) includes the semi-implicit method at its core and increases stability with an additional evaluation of each field equation during each time step.

In the following subsections, the semi-implicit and SETS methods will be described at three levels of detail. The basic aspects of each method are illustrated for simple 1D single-phase-flow equations as follows:

$$\frac{\partial \rho}{\partial t} + \frac{\partial}{\partial x}(\rho V) = 0 \,, \tag{2-18}$$

$$\frac{\partial (\rho e)}{\partial t} + \frac{\partial}{\partial x}(\rho e V) = -P\frac{\partial V}{\partial x} + h_w A_w \frac{(T_w - T)}{\mathrm{vol}} \,, \tag{2-19}$$

and

$$\frac{\partial V}{\partial t} + V\frac{\partial V}{\partial x} = -\frac{1}{\rho}\frac{\partial P}{\partial x} - KV|V| \,, \tag{2-20}$$

where K is a wall friction coefficient that may be a function of velocity and fluid properties and T_w is a pipe wall temperature. More detail is then provided through explanation of special adaptations to improve robust simulation of single- and/or two-phase flow. Finally, the full two-phase-flow equations are presented.

Fairly standard notation is used in presenting the finite-volume equations. A superscript "n" indicates known values at the beginning of a step in the time integration (old-time value). A superscript "n+1" labels a variable value at the end of the current time step (new-time value), which must be obtained as part of the solution of the equations. Subscripts provide information on spatial location. Integer subscripts such as "j" or "j+1" label volume center information (e.g., P_j^{n+1} is the new-time pressure in volume "j"). A half-integer subscript indicates a value obtained at the surface separating two volumes (e.g., $V^n_{j+1/2}$ is the old-time velocity at the surface separating volume "j" from volume "j+1").

When values of cell-centered variables are needed at cell edges, an average of some form is required. The methods discussed here use values only from the volumes immediately adjacent to the given edge, so the averages are always in the following form:

$$\langle Y \rangle_{j+1/2} = w_{j+1/2} Y_j + (1 - w_{j+1/2}) Y_{j+1} \ . \tag{2-21}$$

For simple 1D flow, terms expressing mass and energy flow for the j^{th} finite volume then have the following form:

$$\frac{\partial}{\partial x_j}(YV) = \frac{[w_{j+1/2}Y_j + (1 - w_{j+1/2})Y_{j+1}]V_{j+1/2} - [w_{j-1/2}Y_{j-1} + (1 - w_{j-1/2})Y_j]V_{j-1/2}}{\Delta x}$$

$$= \frac{\langle Y \rangle_{j+1/2} V_{j+1/2} - \langle Y \rangle_{j-1/2} V_{j-1/2}}{\Delta x} \ . \tag{2-22}$$

The form is more complex for 1D flow with a spatially varying cross-sectional flow area. In this case the mass flux term is abbreviated as

$$\nabla_j \cdot (YV) = \tag{2-23}$$

$$\frac{[w_{j+1/2}Y_j + (1 - w_{j+1/2})Y_{j+1}](A_{j+1/2}V_{j+1/2}) - [w_{j-1/2}Y_{j-1} + (1 - w_{j-1/2})Y_j](A_{j-1/2}V_{j-1/2})}{vol_j} \ , \tag{2-24}$$

where $A_{j+1/2}$ is the flow area between cells j and j+1 and vol_j is the volume of the j^{th} cell.

The related derivative used in the finite-difference momentum flux involves the use of a more complicated averaging method. This is driven by a need to model Bernoulli flows when appropriate and to conserve momentum properly when a side-junction flow is present. Details of this methodology are presented in Section 2.1.7. To aid in understanding the basic numerical methods, it is worth noting that with no area changes or side junctions, the numerical form of the velocity gradient is

$$\left.\frac{\partial V}{\partial x}\right|_{j+1/2} = \frac{(1 - w_{j+1/2})V_{j+3/2} + (2w_{j+1/2} - 1)V_{j+1/2} - w_{j+1/2}V_{j-1/2}}{\Delta x} \ . \tag{2-25}$$

For flows in 1D channels with variable cross-sectional area, the momentum-transfer term is abbreviated as $V_{j+1/2}\nabla_{j+1/2}V$.

Discussions of some details of the finite-volume approximations are provided in later sections of this document. Section 2.1.5. presents a generalization of the methods to 3D geometry. Special treatment of transition to single-phase flow and conditions beyond the critical point is described in Section 2.1.6. Section 2.1.7. describes details of special treatment used for momentum-flux terms. The actual solution of these equations is described in Section 2.1.8.

2.1.4.1. Basics of the Semi-Implicit Method. When fluid flow is modeled with a fully explicit method, time-step sizes are restricted by the Courant limit as

$$\Delta t \le k \cdot \frac{\Delta x}{|V| + c}\ , \tag{2-26}$$

where Δx is a characteristic mesh length, V is the flow velocity, c is the speed of sound, and parameter k varies in value depending on the details of the method, but here can be taken to be 1.0. This simple class of methods is appropriate when it is important to track the details of pressure wave propagation (e.g., shock waves). However, in most reactor transients, this level of detail is not important. At most, continuity waves (moving liquid levels or froth fronts) must be followed. Frequently the transient is simply an evolution between quasi-steady states.

Both the ICE and semi-implicit methods relax the explicit restrictions on time-step size by evaluating terms involved in pressure wave propagation at the new (n+1) time level. For a simple form of the momentum equation, this requires new-time values in the pressure gradient term as given by

$$\frac{(V^{n+1}_{j+1/2} - V^{n}_{j+1/2})}{\Delta t} + V^{n}_{j+1/2}\left.\frac{\partial V^{n}}{\partial x}\right|_{j+1/2}$$

$$+ \frac{1}{\langle\rho\rangle^{n}_{j+1/2}}\frac{(P^{n+1}_{j+1} - P^{n+1}_{j})}{\Delta x} + K^{n}_{j+1/2}V^{n+1}_{j+1/2}\left|V^{n}_{j+1/2}\right| = 0\ . \tag{2-27}$$

Similarly, relaxation of the restrictions on time-step size also requires that velocities involved in flux of mass and energy be evaluated at the new-time level. The equations then become

$$\frac{(\rho^{n+1}_{j} - \rho^{n}_{j})}{\Delta t} + \frac{\partial}{\partial x_j}(\rho^{n}V^{n+1}) = 0 \text{ and} \tag{2-28}$$

$$\frac{(\rho_j^{n+1}e_j^{n+1}-\rho_j^n e_j^n)}{\Delta t}+\frac{\partial}{\partial x_j}(\rho^n e^n V^{n+1})+P_j^{n+1}\frac{(V_{j+1/2}^{n+1}-V_{j-1/2}^{n+1})}{\Delta x}$$

$$+ \textit{heat sources or sinks} = 0 \qquad (2\text{-}29)$$

By using the above equation structure, information on a pressure disturbance in any cell is available to any other cell during the same time step. This eliminates the sound speed from the Courant stability limit, leaving what is commonly referred to as the "material Courant" stability limit ($\Delta t < (\Delta x)/|V|$). The absolute value of flow velocity remains in the denominator of the expression because information relevant to continuity waves is still propagated only one cell per time step by the semi-implicit method.

Completion of the problem definition requires a choice of two independent variables from the four thermodynamic variables: pressure, temperature, density, and specific internal energy. Density is not a good choice because of the need to model liquid solid regions. Given the low compressibility of liquid, a small error in a solution for density can translate to a significant error in pressure. When pressure is designated as an independent variable, a small error in the solution for pressure results in an even smaller fractional error in density. The choice of the second independent variable is driven by considerations beyond the simple equations presented above. Multiphase and multicomponent systems tend toward an equilibrium in which the phases and/or components are all at the same temperature. This behavior is reflected in constitutive relations for interphase (or wall-to-fluid) heat transfer that depend on differences of temperatures and that must be evaluated implicitly with respect to these temperature differences in the numerical equations. When the gas phase contains a mixture of species, all species are assumed to be at the same temperature. Selecting temperature as an independent variable in these situations can significantly simplify final solution of the equations.

Equations of state provide density and internal energy as functions of pressure and temperature. The relationships are generally nonlinear; therefore, the combination of discretized flow equations and state equations yields a coupled set of nonlinear equations. A key feature of this program is that an iterative method (see Section 2.1.8.) is used to obtain a solution to the nonlinear equations. The nonlinear equations are not simply replaced by a linearized approximation, as is done in RELAP5 (Ref. 2-21.).

A stability analysis of these semi-implicit equations introduces limitations on weighting factors used for cell-edge averages. The equations are unconditionally unstable unless

$$w_{j+1/2} \geq (1/2)\left(1+\frac{\Delta t|V_{j+1/2}|}{\Delta x_{j+1/2}}\right) \quad \text{for} \quad V_{j+1/2} \geq 0 \text{ and}$$

$$w_{j+1/2} \leq (1/2)\left(1-\frac{\Delta t|V_{j+1/2}|}{\Delta x_{j+1/2}}\right) \quad \text{for} \quad V_{j+1/2} < 0 \ . \qquad (2\text{-}30)$$

When the inequalities are replaced with equalities in the above expression, a difference scheme with the minimal permitted numerical diffusion results. However, experience with a range of two-phase-flow problems has resulted in the final adoption of the following more robust choice of weighting factors:

$$w_{j+1/2} = 1 \quad \text{for} \quad V_{j+1/2} \geq 0 \text{ and}$$
$$w_{j+1/2} = 0 \quad \text{for} \quad V_{j+1/2} < 0 \, . \tag{2-31}$$

This is the standard donor-cell difference method.

2.1.4.2. Enhancements to the Semi-Implicit Method. The finite-volume equations given above reflect the semi-implicit method as implemented in early versions of TRAC and to some extent in RELAP5 (Ref. 2-21.). However, the discovery of instabilities in bubbly flow (Mahaffy, Ref. 2-11.) resulted in improvements to the wall friction term in Eq. (2-27) and, more importantly, to the interfacial friction term in the two-phase momentum equations. Optimal stability would be obtained by evaluating the friction terms fully implicitly. Unfortunately, this would result in serious complications for the solution procedure outlined in Section 2.1.8. The existing solution procedure relies on the finite-difference motion equations containing no more than the first power of the new-time velocity. This permits a direct solution for V^{n+1} as a linear function of adjacent new-time pressures.

More stable force terms can be obtained from linearization of a fully implicit force term. First, assume that the new-time velocity is not very different from the old-time velocity, or

$$V^{n+1}_{j+1/2} = V^{n}_{j+1/2} + \delta V_{j+1/2} \, . \tag{2-32}$$

Now, substitute this expression into the fully implicit wall friction term as follows:

$$K^{n}_{j+1/2} V^{n+1}_{j+1/2} \left| V^{n+1}_{j+1/2} \right| = K^{n}_{j+1/2} (V^{n}_{j+1/2} + \delta V_{j+1/2}) \left| V^{n}_{j+1/2} + \delta V_{j+1/2} \right|$$
$$= 2K^{n}_{j+1/2} \left| V^{n}_{j+1/2} \right| \delta V_{j+1/2} + K^{n}_{j+1/2} V^{n}_{j+1/2} \left| V^{n}_{j+1/2} \right| + 0(\delta V^2) \, . \tag{2-33}$$

Finally, drop terms containing δV^2 and replace δV with the difference between the new- and old-time velocity to give

$$K^{n}_{j+1/2} V^{n+1}_{j+1/2} \left| V^{n+1}_{j+1/2} \right| \approx 2K^{n}_{j+1/2} V^{n+1}_{j+1/2} \left| V^{n}_{j+1/2} \right| - K^{n}_{j+1/2} V^{n}_{j+1/2} \left| V^{n}_{j+1/2} \right| \, . \tag{2-34}$$

In the two-phase-flow equations, the same linearized implicit approximation is applied to the interfacial drag term.

The history of use of the semi-implicit equations within TRAC has resulted in a related approximation in the current semi-implicit method. When using the semi-implicit equations as part of the SETS method, it was found that a linearization of the implicit momentum-flux term can improve the stability of the motion equation. Details of this linearization are presented in the next subsection. The direct impact on the semi-implicit equations is reflected in the following equation:

$$V_{j+1/2}\left.\frac{\partial V}{\partial x}\right|_{j+1/2} = [\beta V^{n+1}_{j+1/2} + (1-\beta)V^{n}_{j+1/2}]\left.\frac{\partial V^n}{\partial x}\right|_{j+1/2}, \tag{2-35}$$

where

$$\beta = \begin{bmatrix} 1 \quad for \quad \left.\dfrac{\partial V^n}{\partial x}\right|_{j+1/2} \geq 0 \\ 0 \quad for \quad \left.\dfrac{\partial V^n}{\partial x}\right|_{j+1/2} < 0 \end{bmatrix}.$$

With the special modifications to momentum-flux and friction terms, the finite-difference form of the motion equation becomes

$$\frac{(V^{n+1}_{j+1/2} - V^{n}_{j+1/2})}{\Delta t} + [\beta V^{n+1}_{j+1/2} + (1-\beta)V^{n}_{j+1/2}]\left(\left.\frac{\partial V^n}{\partial x}\right)\right|_{j+1/2} + \frac{1}{\langle\rho\rangle^{n}_{j+1/2}}\frac{(P^{n+1}_{j+1} - P^{n+1}_{j})}{\Delta x}$$

$$+ 2K^{n}_{j+1/2}V^{n+1}_{j+1/2}\left|V^{n}_{j+1/2}\right| - K^{n}_{j+1/2}V^{n}_{j+1/2}\left|V^{n}_{j+1/2}\right| = 0\,. \tag{2-36}$$

2.1.4.3. Semi-Implicit Method Adapted to Two-Phase Flow. Extension of the numerical method to the two-phase, two-fluid model is relatively straightforward. Special modifications to the method are necessary to treat changes from two-phase to single-phase flow and are described below. Source terms are present to model phase change and heat transfer. These are generally implicit in any driving temperature difference and explicit in any coefficient. The importance of gravitationally driven liquid flow requires an accurate model of gravitational force along the direction of motion. This uses an input angle (θ) between a vector from the center of cell j to the center of cell j+1 and a vector directed against gravity. In the application of the code, θ is more generally the inverse cosine ($\cos^{-1}$) of the change in elevation between cell centers divided by the flow length between cell centers.

To shorten notation in the following difference equations, some subscripts associated with location have been eliminated. For velocities not contained in spatial differences, the subscript denoting spatial location is assumed to be j+1/2. For cell-centered variables, the assumed subscript is j. The phrase "combined gas" refers to the mixture of noncondensable gas and steam, which is assumed to move with no interspecies diffusion.

Semi-Implicit Equations of Motion

Combined Gas

$$\frac{(V_g^{n+1}-V_g^n)}{\Delta t}+[\beta_g V_g^{n+1}+(1-\beta_g)V_g^n]\nabla_{j+1/2}V_g^n$$

$$+\frac{c_i^n|V_g^n-V_l^n|}{\langle\alpha\rho_g\rangle_{j+1/2}^n}[2(V_g^{n+1}-V_l^{n+1})-(V_g^n-V_l^n)]$$

$$+\frac{1}{\langle\rho_g\rangle_{j+1/2}^n}\frac{(P_{j+1}^{n+1}-P_j^{n+1})}{\Delta x_{j+1/2}}+\frac{\Gamma_{j+1/2}^{+n}}{\langle\alpha\rho_g\rangle_{j+1/2}^n}(V_g^{n+1}-V_l^{n+1})$$

$$+\frac{c_{wg}}{\langle\alpha\rho_g\rangle_{j+1/2}^n}(2V_g^{n+1}-V_g^n)|V_g^n|+g\cos\theta=0. \qquad (2\text{-}37)$$

Liquid

$$\frac{V_l^{n+1}-V_l^n}{\Delta t}+[\beta_l V_l^{n+1}+(1-\beta_l)V_l^n]\nabla_{j+1/2}V_l^n$$

$$+\frac{c_i^n|V_l^n-V_g^n|}{\langle(1-\alpha)\rho_l\rangle_{j+1/2}^n}[2(V_l^{n+1}-V_g^{n+1})-(V_l^n-V_g^n)]$$

$$+\frac{1}{\langle\rho_l\rangle_{j+1/2}^n}\frac{(P_{j+1}^{n+1}-P_j^{n+1})}{\Delta x_{j+1/2}}-\frac{\Gamma_{j+1/2}^{-n}}{\langle(1-\alpha)\rho_l\rangle_{j+1/2}^n}(V_l^{n+1}-V_g^{n+1})$$

$$+\frac{c_{wl}}{\langle(1-\alpha)\rho_l\rangle_{j+1/2}^n}(2V_l^{n+1}-V_l^n)|V_l^n|+g\cos\theta=0. \qquad (2\text{-}38)$$

Semi-Implicit Mass Equations

Combined Gas

$$\frac{\alpha_j^{n+1}\rho_{gj}^{n+1}-\alpha_j^n\rho_{gj}^n}{\Delta t}+\nabla_j\cdot[\alpha^n\rho_g^n V_g^{n+1}]=\Gamma^{n+1}. \qquad (2\text{-}39)$$

Noncondensable Gas

$$\frac{[\alpha_j^{n+1}\rho_{aj}^{n+1}-\alpha_j^n\rho_{aj}^n]}{\Delta t}+\nabla_j\cdot[\alpha^n\rho_a^n V_g^{n+1}]=0. \qquad (2\text{-}40)$$

Liquid

$$\frac{[(1-\alpha_j^{n+1})\rho_{lj}^{n+1} - (1-\alpha_j^n)\rho_{lj}^n]}{\Delta t} + \nabla_j \cdot [(1-\alpha^n)\rho_l^n V_l^{n+1}] = -\Gamma^{n+1} \ . \tag{2-41}$$

Liquid Solute

$$\frac{[(1-\alpha)^{n+1}\tilde{m}^{n+1}\rho_l^{n+1} - (1-\alpha)^n m^n \rho_l^n]}{\Delta t} + \nabla_j \cdot [(1-\alpha)^n m^n \rho_l^n V_l^{n+1}] = 0 \ , \tag{2-42}$$

$$m^{n+1} = \min\left[\tilde{m}^{n+1} + \frac{S_c^n}{(1-\alpha)^{n+1}\rho_l^{n+1}}, m_{\max}\right] , \tag{2-43}$$

and

$$S_c^{n+1} = (\tilde{m}^{n+1} - m^{n+1})(1-\alpha)^{n+1}\rho_l^{n+1} + S_c^n \ . \tag{2-44}$$

Semi-Implicit Energy Equations

Combined Gas

$$\begin{aligned} &\frac{[\alpha_j^{n+1}\rho_{gj}^{n+1}e_{gj}^{n+1} - \alpha_j^n \rho_{gj}^n e_{gj}^n]}{\Delta t} + \nabla_j \cdot [\alpha^n \rho_g^n e_g^n V_g^{n+1}] \\ &\quad + P^{n+1}\left[\frac{(\alpha^{n+1}-\alpha^n)}{\Delta t} + \nabla_j \cdot (\alpha^n V_g^{n+1})\right] \\ &\quad = q_{wg}^{n+1} + q_{dg}^n + q_{ig}^{n+1} + \Gamma^{n+1} h_{sg}^{n+1} \ . \end{aligned} \tag{2-45}$$

Total Fluid (gas and liquid)

$$\begin{aligned} &\frac{[\alpha_j^{n+1}\rho_{gj}^{n+1}e_{gj}^{n+1} + (1-\alpha_j^{n+1})\rho_{lj}^{n+1}e_{lj}^{n+1}] - \alpha_j^n \rho_{gj}^n e_{gj}^n + (1-\alpha_j^n)(\rho_{lj}^n e_{lj}^n)}{\Delta t} \\ &\quad + \nabla_j \cdot [\alpha^n \rho_g^n e_g^n V_g^{n+1} + (1-\alpha^n)\rho_l^n e_l^n V_l^{n+1}] \\ &\quad + P^{n+1}\nabla_j \cdot [(1-\alpha)^n V_l^{n+1} + \alpha^n V_g^{n+1}] \\ &\quad = q_{wg}^{n+1} + q_{wl}^{n+1} + q_{di}^n + q_{dg}^n \ . \end{aligned} \tag{2-46}$$

The wall heat transfer to the gas and liquid, q_{wg} and q_{wl}, and the interfacial mass-transfer rate, Γ, also require further definition. Note the mixture of old- and new-time values in these terms. The choice of old-time heat-transfer coefficients was driven by the desire to simplify the implementation of the method, but can result in bounded instabilities during calculations. These terms are given by

$$q_{wl}^{n+1} = h_{wl}^{n} A_w (T_w^n - T_l^{n+1})/\text{vol} \ , \tag{2-47}$$

$$q_{wg}^{n+1} = h_{wg}^{n} A_w (T_w^n - T_g^{n+1})/\text{vol} \ , \tag{2-48}$$

and

$$\Gamma^{n+1} = \frac{-(q_{ig}^{n+1} + q_{il}^{n+1})}{(h_v')^{n+1} - (h_l')^{n+1}} \ , \tag{2-49}$$

where

$$q_{ig}^{n+1} = h_{ig}^{n} A_i^n \frac{(T_{\text{sat}}^{n+1} - T_g^{n+1})}{\text{vol}} \tag{2-50}$$

and

$$q_{il}^{n+1} = h_{il}^{n} A_i^n \frac{(T_{\text{sat}}^{n+1} - T_l^{n+1})}{\text{vol}} \ . \tag{2-51}$$

Further definition is also needed for a special set of density averages used in the momentum equations. Cell-edge densities used in the denominator of Eqs. (2-37) and (2-38) are defined to produce a good prediction of hydrostatic pressure heads. For example, the edge-average gas macroscopic density is defined as

$$\langle \alpha\rho \rangle_{j+1/2}^{n} = \frac{\Delta x_j (\alpha\rho)_j^n + \Delta x_{j+1} (\alpha\rho)_{j+1}^n}{\Delta x_j + \Delta x_{j+1}} \ . \tag{2-52}$$

A similar definition holds for the cell-edge liquid macroscopic density. The edge-average microscopic densities are somewhat more complex. For example,

$$\langle \rho_g \rangle_{j+1/2}^{n} = \langle \alpha\rho_g \rangle_{j+1/2}^{n} \left[\frac{\Delta x_j \alpha_j^n + \Delta x_{j+1} \alpha_{j+1}^n}{\Delta x_j + \Delta x_{j+1}} \right]^{-1} \ . \tag{2-53}$$

This particular average is necessary for consistency within the SETS equations (see Section 2.1.4.6.), where macroscopic densities have a more fundamental importance within the solution.

The above finite-volume-flow equations hold only when a two-phase mixture is present at both the old- and new-time levels. Modifications are necessary when the old- or new-time-level fluid state is single phase; these are described in Section 2.1.6.

The motion equations are evaluated in subroutine TF1DS1 for 1D flow (3D flow uses TF3DS1). This evaluation takes the solution form illustrated by Eqs. (2-37) and (2-38) for velocities as linear functions of the new-time pressure gradient (see Section 2.1.8.). Terms in the mass and energy equations are evaluated in subroutine TF1DS (TFPLN for a plenum and TF3DS for 3D). This includes terms for the Jacobian matrix needed to solve this nonlinear system with a Newton iteration. The iteration is driven by subroutine HOUT.

2.1.4.4. Basics of the SETS Method. The goal of the SETS method was to eliminate the material Courant stability limit with minimal alterations to the existing semi-implicit method. Given the success of the semi-implicit method in propagating information about sound waves, a correction step was devised to perform a similar propagation of information on continuity waves. As a very simple example, consider the single-phase mass equation. For each time step, the semi-implicit method is used to establish the new-time velocity field. Next, the following correction (or "stabilizer") step is used to obtain a final value of the new-time density:

$$\frac{(\rho_j^{n+1} - \rho_j^n)}{\Delta t} + \frac{\partial}{\partial x_j}(\rho^{n+1} V^{n+1}) = 0 \ . \tag{2-54}$$

On the surface, this appears to be a fully implicit finite-difference equation. It is not, however, because the new-time velocities (V^{n+1}) are all known numbers obtained from the semi-implicit step. New-time densities are the only unknowns in this system of equations. Information about a density change in any given computational cell is propagated to all other cells within the same time step. Formal stability analysis and direct testing confirm expectations based on information propagation. The material Courant stability limit actually is eliminated. This does not imply unconditional stability for the method. The only modifications to the semi-implicit method involve flux terms. The continued practice of evaluating heat-transfer and friction coefficients at the old time results in other poorly defined stability problems.

One unusual aspect of SETS as implemented in the code is that the pattern of evaluation of semi-implicit and stabilizer equations is not the same for the motion equations as it is for the mass and energy equations. All mass and energy equations follow the above pattern of a semi-implicit step followed by a stabilizer step. However, the analogous momentum-stabilizer equation is evaluated before the evaluation of the semi-implicit equations. This pattern was established during the original development of SETS through tests of the various combinations of equation ordering. In these tests, two-phase-flow problems ran smoothly at significantly higher time steps with the current equation ordering than with others. The physical explanation for this behavior is the importance of the pressure gradient term in problems of interest. A solution is better

behaved when the velocity used for transport of mass and energy is a direct result of a pressure-balanced solution.

For our special example of 1D single-phase flow, the SETS difference equations are

Stabilizer Motion Equation

$$\frac{(\tilde{V}^{n+1}_{j+1/2} - V^{n}_{j+1/2})}{\Delta t} + V^{n}_{j+1/2}\left.\frac{\partial \tilde{V}^{n+1}}{\partial x}\right|_{j+1/2}$$

$$+ \frac{1}{\langle\rho\rangle^{n}_{j+1/2}}\frac{P^{n}_{j+1} - P^{n}_{j}}{\Delta x} + K^{n}_{j+1/2}(2\tilde{V}^{n+1}_{j+1/2} - V^{n}_{j+1/2})\left|V^{n}_{j+1/2}\right| = 0 \ . \qquad (2\text{-}55)$$

Semi-Implicit Equation Step

$$\frac{(V^{n+1}_{j+1/2} - V^{n}_{j+1/2})}{\Delta t} + V^{n}_{j+1/2}\left.\frac{\partial \tilde{V}^{n+1}}{\partial x}\right|_{j+1/2}$$

$$+ \frac{1}{\langle\rho\rangle^{n}_{j+1/2}}\frac{(\tilde{P}^{n+1}_{j+1} - \tilde{P}^{n+1}_{j})}{\Delta x} + K^{n}_{j+1/2}V^{n+1}_{j+1/2}\left|V^{n}_{j+1/2}\right| = 0 \ , \qquad (2\text{-}56)$$

$$\frac{(\tilde{\rho}^{n+1}_{j} - \rho^{n}_{j})}{\Delta t} + \frac{\partial}{\partial x_j}\rho^{n}V^{n+1} = 0 \ , \text{and} \qquad (2\text{-}57)$$

$$\frac{(\tilde{\rho}^{n+1}_{j}\tilde{e}^{n+1}_{j} - (\rho e)^{n}_{j})}{\Delta t} + \frac{\partial}{\partial x_j}\rho^{n}e^{n}V^{n+1} + \tilde{P}^{n+1}_{j}\frac{V^{n+1}_{j+1/2} - V^{n+1}_{j-1/2}}{\Delta x} = 0 \ . \qquad (2\text{-}58)$$

Stabilizer Mass and Energy Equations

$$\frac{(\rho^{n+1}_{j} - \rho^{n}_{j})}{\Delta t} + \frac{\partial}{\partial x_j}\rho^{n}V^{n+1} = 0 \text{ and} \qquad (2\text{-}59)$$

$$\frac{(\rho e)^{n+1}_{j} - (\rho e)^{n}_{j}}{\Delta t} + \frac{\partial}{\partial x_j}(\rho e)^{n+1}V^{n+1} + \tilde{P}^{n+1}_{j}\frac{V^{n+1}_{j+1/2} - V^{n+1}_{j-1/2}}{\Delta x} = 0 \ . \qquad (2\text{-}60)$$

A tilde above a variable indicates that it is a first estimate of the new-time value. Actual new-time variables have a superscript "n+1" and no tilde. Note that the only result of the above semi-implicit step appears to be just a new-time velocity field. In practice the situation is more complex. To save computational time, temperatures and pressures that are fully consistent with the densities and energies obtained from solving the stabilizer mass and energy equations are never calculated. If the correlation used to obtain an old-time wall friction coefficient requires temperature or pressure, the values used would be those obtained during the solution of the semi-implicit equation step.

As will be clear in the discussion of the solution of the SETS equations, each of the above equations is solved once per time step. During development of the method, attempts were made to make repeated evaluations of a form of the SETS equations during each time step to produce an iterative solution to the fully implicit method. This approach was found to converge poorly or not at all, particularly at time steps in excess of the material Courant limit.

2.1.4.5. Enhancements to the SETS Method. As with the semi-implicit method, linearized implicit terms are introduced in the motion equation to improve the behavior of friction and momentum transfer. The improved friction terms are identical to those derived in Section 2.1.4.2. The momentum-transfer terms are somewhat more complex. First, the new-time velocity and velocity gradient are linearized in the following forms:

$$\tilde{V}^{n+1}_{j+1/2} = V^{n}_{j+1/2} + \delta V_{j+1/2} \text{ and} \tag{2-61}$$

$$\nabla\tilde{V}^{n+1}_{j+1/2} = \nabla\tilde{V}^{n}_{j+1/2} + \delta(\nabla V_{j+1/2}) \ . \tag{2-62}$$

Substitution of these relationships into the implicit form of the momentum-transfer term gives

$$V^{n+1}_{j+1/2}\nabla\tilde{V}^{n+1}_{j+1/2} = (V^{n}_{j+1/2} + \delta V_{j+1/2})(\nabla\tilde{V}^{n}_{j+1/2} + \delta(\nabla V_{j+1/2}))$$

$$= V^{n}_{j+1/2}\nabla\tilde{V}^{n}_{j+1/2} + \delta V^{n}_{j+1/2}\nabla\tilde{V}^{n}_{j+1/2} + V^{n}_{j+1/2}\delta(\nabla V_{j+1/2}) + \delta V^{n}_{j+1/2}\delta(\nabla V_{j+1/2}) . \tag{2-63}$$

Keeping only terms with no more than the first power of a variation and back-substituting the variations in terms of differences between old- and new-time variables gives

$$\tilde{V}^{n+1}_{j+1/2}\nabla\tilde{V}^{n+1}_{j+1/2} \approx V^{n}_{j+1/2}\nabla\tilde{V}^{n+1}_{j+1/2} + (\tilde{V}^{n}_{j+1/2} - V^{n}_{j+1/2})\nabla\tilde{V}^{n}_{j+1/2} \ . \tag{2-64}$$

The difference in base points for the linearizations of Eqs. (2-61) and (2-62) is not an error in the equations. It is the result of numerical experimentation with the three possible alternatives. The situation is further complicated by instabilities resulting from negative values of the gradient or sign discrepancies between final and intermediate (tilde) velocities. Numerical experimentation resulted in the following robust form of the linearized implicit momentum-transfer term:

$$\tilde{V}^{n+1}_{j+1/2}\nabla\tilde{V}^{n+1}_{j+1/2} \approx V^{n}_{j+1/2}\nabla_{j+1/2}\tilde{V}^{n+1}_{j+1/2} + \beta(\tilde{V}^{n+1}_{j+1/2} - V^{n}_{j+1/2})\nabla_{j+1/2}\tilde{V}^{n}_{j+1/2} \ ,$$

where

$$\beta = \begin{bmatrix} 1 \quad for \quad \left.\frac{\partial V^n}{\partial x}\right|_{j+1/2} \geq 0 \; and \; V^n_{j+1/2}\tilde{V}^n_{j+1/2} > 0 \\ 0 \quad for \quad \left.\frac{\partial V^n}{\partial x}\right|_{j+1/2} < 0 \; or \; V^n_{j+1/2}\tilde{V}^n_{j+1/2} \leq 0 \end{bmatrix} . \tag{2-65}$$

With these modifications, the final form of the stabilizer motion equation is

$$\frac{(\tilde{V}^{n+1}_{j+1/2} - V^n_{j+1/2})}{\Delta t} + V^n_{j+1/2}\nabla_{j+1/2}\tilde{V}^{n+1}_{j+1/2} + \beta(\tilde{V}^{n+1}_{j+1/2} - V^n_{j+1/2})\nabla_{j+1/2}\tilde{V}^n_{j+1/2}$$

$$+ \frac{1}{\langle\rho\rangle^n_{j+1/2}}\frac{(P^n_{j+1} - P^n_j)}{\Delta x} + K^n_{j+1/2}(2\tilde{V}^{n+1}_{j+1/2} - V^n_{j+1/2})\left|V^n_{j+1/2}\right| = 0 . \tag{2-66}$$

The following revised form of the motion equation in the semi-implicit step has a minor change in the flux term to increase the robustness of the method further:

$$\frac{(V^{n+1}_{j+1/2} - V^n_{j+1/2})}{\Delta t} + V^n_{j+1/2}\nabla_{j+1/2}\tilde{V}^{n+1}_{j+1/2} + \beta(V^{n+1}_{j+1/2} - V^n_{j+1/2})\nabla_{j+1/2}\tilde{V}^n_{j+1/2}$$

$$+ \frac{1}{\langle\rho\rangle^n_{j+1/2}}\frac{(P^{n+1}_{j+1} - P^{n+1}_j)}{\Delta x} + K^n_{j+1/2}(2V^{n+1}_{j+1/2} - V^n_{j+1/2})\left|V^n_{j+1/2}\right| = 0 . \tag{2-67}$$

One significant modification is introduced in the stabilizer mass and energy equations. To save computational effort and overhead associated with the communication of more variables, the stabilizer equations listed in the previous section are not directly solved. Instead, the actual equations solved are the result of subtracting the semi-implicit equations from the corresponding stabilizer equations.

Stabilizer Mass and Energy Equations as Solved

$$\frac{(\rho^{n+1}_j - \tilde{\rho}^{n+1}_j)}{\Delta t} + \frac{\partial}{\partial x_j}(\rho^{n+1}V^{n+1}) = \frac{\partial}{\partial x_j}(\rho^n V^{n+1}) \text{ and} \tag{2-68}$$

$$\frac{(\rho e)^{n+1}_j - \tilde{\rho}^{n+1}_j \tilde{e}^{n+1}_j}{\Delta t} + \frac{\partial}{\partial x_j}((\rho e)^{n+1}V^{n+1}) = \frac{\partial}{\partial x_j}((\rho e)^n V^{n+1}) . \tag{2-69}$$

The advantage of this approach is more apparent in the application of the method to the full two-phase-flow equations. In that case, all source terms (mass and energy transfer) are canceled out of the equations to be solved. The disadvantage of this approach is that the rigorous mass conservation of Eq. (2-59) is lost. Mass conservation associated with Eq. (2-68) depends on the level of convergence of the iterative solution for the semi-implicit equations.

2.1.4.6. The SETS Method Adapted to Two-Phase Flow. The two-phase forms of the SETS equations contain some significant modifications. The first, which improves code robustness, is an initial evaluation of the equations of motion that is used solely to provide an improved prediction of the interfacial force terms needed in the standard stabilizer motion equations.

Equations for Prediction of Interfacial Drag Force

Combined Gas

$$\frac{(\hat{V}_g^{n+1} - V_g^n)}{\Delta t} + V_g^n \nabla_{j+1/2} \tilde{V}_g^n + \beta(\hat{V}_g^{n+1} - V_g^n)\nabla_{j+1/2}\tilde{V}_g^n$$

$$+ \frac{c_i^n \left| V_g^n - V_l^n \right|}{\langle \alpha\rho_g \rangle_{j+1/2}^n} [2(\hat{V}_g^{n+1} - \hat{V}_l^{n+1}) - (V_g^n - V_l^n)]$$

$$+ \frac{1}{\langle \rho_g \rangle_{j+1/2}^n} \frac{(P_{j+1}^n - P_j^n)}{\Delta x_{j+1/2}} + \frac{\Gamma_{j+1/2}^n}{\langle \alpha\rho_g \rangle_{j+1/2}^n} (\hat{V}_g^{n+1} - \hat{V}_l^{n+1})$$

$$+ \frac{c_{wg}}{\langle \alpha\rho_g \rangle_{j+1/2}^n} (2\hat{V}_g^{n+1} - V_g^n) \left| V_g^n \right| + g\cos\theta = 0 , \qquad (2\text{-}70)$$

where

$$\beta = 0, \quad if \ \nabla_{j+1/2} V^n < 0 \ or \ V^n \tilde{V}^n < 0 ;$$

$$= 1, \quad if \ \nabla_{j+1/2} V^n \geq 0 \ and \ V^n \tilde{V}^n \geq 0 .$$

Liquid

$$\frac{(\hat{V}_l^{n+1} - V_l^n)}{\Delta t} + V_l^n \nabla_{j+1/2} \tilde{V}_l^n + \beta(\hat{V}_l^{n+1} - V_l^n)\nabla_{j+1/2}\tilde{V}_l^n$$

$$+ \frac{c_i^n \left| V_g^n + V_l^n \right|}{\langle (1-\alpha)\rho_l \rangle_{j+1/2}^n} [2(\hat{V}_l^{n+1} - \hat{V}_g^{n+1}) - (V_l^n - V_g^n)]$$

$$+ \frac{1}{\langle \rho_l \rangle_{j+1/2}^n} \frac{(P_{j+1}^n - P_j^n)}{\Delta x_{j+1/2}} - \frac{\Gamma^{-n}_{j+1/2}}{\langle (1-\alpha)\rho_l \rangle_{j+1/2}^n} (\hat{V}_l^{n+1} - \hat{V}_g^{n+1})$$

$$+ \frac{c_{wl}}{\langle (1-\alpha)\rho_l \rangle_{j+1/2}^n} (2\hat{V}_l^{n+1} - V_l^n) \left| V_l^n \right| + g\cos\theta = 0 \ . \qquad (2\text{-}71)$$

Edge-average densities follow the definitions provided in the discussion of the semi-implicit method [Eqs. (2-52) and (2-53)].

The velocities obtained from the above equations are used to decouple the vapor and liquid stabilizer motion equations. The prediction of the interfacial force term is good enough that the interfacial force term in the following stabilizer equations does not need to depend on the new-time stabilizer velocities. As a result, the liquid stabilizer motion equation contains only liquid stabilizer (tilde) velocities as unknowns. The liquid and gas equations are two completely independent systems of equations, which are solved separately.

Stabilizer Equations of Motion

Combined Gas

$$\frac{(\tilde{V}_g^{n+1} - V_g^n)}{\Delta t} + V_g^n \nabla_{j+1/2} \tilde{V}_g^{n+1} + \beta(\tilde{V}_g^{n+1} - V_g^n)\nabla_{j+1/2}\tilde{V}_g^n$$

$$+ \frac{c_i^n \left| V_g^n - V_l^n \right|}{\langle \alpha\rho_g \rangle_{j+1/2}^n} [2(\hat{V}_g^{n+1} - \hat{V}_l^{n+1}) - (V_g^n - V_l^n)]$$

$$+ \frac{1}{\langle \rho_g \rangle_{j+1/2}^n} \frac{(P_{j+1}^n - P_j^n)}{\Delta x_{j+1/2}} + \frac{\Gamma^{+n}_{j+1/2}}{\langle \alpha\rho_g \rangle_{j+1/2}^n} (\hat{V}_g^{n+1} - \hat{V}_l^{n+1})$$

$$+ \frac{c_{wg}}{\langle \alpha\rho_g \rangle_{j+1/2}^n} (2\tilde{V}_g^{n+1} - V_g^n) \left| V_g^n \right| + g\cos\theta = 0 \ . \qquad (2\text{-}72)$$

Liquid

$$\frac{(\tilde{V}_l^{n+1} - V_l^n)}{\Delta t} + V_l^n \nabla_{j+1/2} \tilde{V}_l^{n+1} + \beta(\tilde{V}_l^{n+1} - V_l^n)\nabla_{j+1/2}\tilde{V}_l^n$$

$$+ \frac{c_i^n \left| V_g^n - V_l^n \right|}{\langle (1-\alpha)\rho_l \rangle_{j+1/2}^n} [2(\hat{V}_l^{n+1} - \hat{V}_g^{n+1}) - (V_l^n - V_g^n)]$$

$$+ \frac{1}{\langle \rho_l \rangle_{j+1/2}^n} \frac{(P_{j+1}^n - P_j^n)}{\Delta x_{j+1/2}} - \frac{\Gamma^n_{j+1/2}}{\langle (1-\alpha)\rho_l \rangle_{j+1/2}^n} (\hat{V}_l^{n+1} - \hat{V}_g^{n+1})$$

$$+ \frac{c_{wl}}{\langle (1-\alpha)\rho_l \rangle_{j+1/2}^n} (2\tilde{V}_l^{n+1} - V_l^n)\left| V_l^n \right| + g\cos\theta = 0 \ . \qquad (2\text{-}73)$$

Equations of Motion for the SETS Semi-Implicit Step

The equations solved during the semi-implicit step are almost identical to those presented in Section 2.1.4.3. but are reproduced here in their entirety to avoid ambiguity in details of the implementation. The primary difference between the motion equation in a pure semi-implicit method and its corresponding form in the semi-implicit step of SETS is the use of stabilizer velocities for momentum transport.

Combined Gas

$$\frac{(V_g^{n+1} - V_g^n)}{\Delta t} + V_g^n \nabla_{j+1/2} \tilde{V}_g^{n+1} + \beta(V_g^{n+1} - V_g^n)\nabla_{j+1/2}\tilde{V}_g^n$$

$$+ \frac{c_i^n \left| V_g^n - V_l^n \right|}{\langle \alpha\rho_g \rangle_{j+1/2}^n} [2(V_g^{n+1} - V_l^{n+1}) - (V_g^n - V_l^n)]$$

$$+ \frac{1}{\langle \rho_g \rangle_{j+1/2}^n} \frac{(\tilde{P}_{j+1}^{n+1} - \tilde{P}_j^{n+1})}{\Delta x_{j+1/2}} + \frac{\tilde{\Gamma}^{+n}_{j+1/2}}{\langle \alpha\rho_g \rangle_{j+1/2}^n} (V_g^{n+1} - V_l^{n+1})$$

$$+ \frac{c_{wg}}{\langle \alpha\rho_g \rangle_{j+1/2}^n} (2V_g^{n+1} - V_g^n)\left| V_g^n \right| + g\cos\theta = 0 \ . \qquad (2\text{-}74)$$

Liquid

$$\frac{(V_l^{n+1}-V_l^n)}{\Delta t}+V_l^n\nabla_{j+1/2}\tilde{V}_l^{n+1}+\beta(V_l^{n+1}-V_l^n)\nabla_{j+1/2}\tilde{V}_l^n$$

$$+\frac{c_i^n\left|V_l^n-V_g^n\right|}{\langle(1-\alpha)\rho_l\rangle_{j+1/2}^n}[2(V_l^{n+1}-V_g^{n+1})-(V_l^n-V_g^n)]$$

$$+\frac{1}{\langle\rho_l\rangle_{j+1/2}^n}\frac{(\tilde{P}_{j+1}^{n+1}-\tilde{P}_j^{n+1})}{\Delta x_{j+1/2}}-\frac{\tilde{\Gamma}_{j+1/2}^n}{\langle(1-\alpha)\rho_l\rangle_{j+1/2}^n}(V_l^{n+1}-V_g^{n+1})$$

$$+\frac{c_{wl}}{\langle(1-\alpha)\rho_l\rangle_{j+1/2}^n}(2V_l^{n+1}-V_l^n)\left|V_l^n\right|+g\cos\theta=0\ . \qquad (2\text{-}75)$$

Basic Semi-Implicit Mass Equations

These equations differ from those in a pure semi-implicit method; the resulting void fraction and new-time thermodynamic variables are intermediate results. Final new-time values for these variables are formally set by the stabilizer mass and energy equations. Individual thermodynamic variables also are carefully distinguished from products that comprise macroscopic densities and energies. These macroscopic quantities [e.g., $(\alpha\rho_g)$] are a direct result of the solution of the stabilizer mass and energy equations at the end of the previous time step. Another key difference is found in the modified form of the divergence operator, which can involve an unusual mixture of new- and old-time values [see Eq. (2-81)].

Combined Gas

$$\frac{\left[\tilde{\alpha}_j^{n+1}\tilde{\rho}_{gj}^{n+1}-(\alpha\rho_g)_j^n\right]}{\Delta t}+\nabla_j\cdot[(\alpha\rho_g)^nV_g^{n+1}]=\tilde{\Gamma}^{n+1}\ . \qquad (2\text{-}76)$$

Noncondensable Gas

$$\frac{\left[\tilde{\alpha}_j^{n+1}\tilde{\rho}_{gj}^{n+1}-(\alpha\rho_g)_j^n\right]}{\Delta t}+\nabla_j\cdot[(\alpha\rho_a)^nV_g^{n+1}]=0\ . \qquad (2\text{-}77)$$

Liquid

$$\frac{\left|(1-\tilde{\alpha}_j^{n+1})\tilde{\rho}_{lj}^{n+1}-[(1-\alpha)\rho_l]_j^n\right|}{\Delta t}+\nabla_j\cdot[(1-\alpha)\rho_l]^n V_l^{n+1}=-\tilde{\Gamma}^{n+1}\ . \tag{2-78}$$

Basic Energy Equations

Combined Gas

$$\begin{aligned}&\frac{[\tilde{\alpha}_j^{n+1}\tilde{\rho}_{gj}^{n+1}\tilde{e}_{gj}^{n+1}-(\alpha\rho_g e_g)_j^n]}{\Delta t}+\nabla_j\cdot[(\alpha\rho_g e_g)^n V_g^{n+1}]\\&+\tilde{P}^{n+1}\left[\frac{(\tilde{\alpha}^{n+1}-\alpha^n)}{\Delta t}+\nabla_j\cdot(\alpha^n V_g^{n+1})\right]\\&=\tilde{q}_{wg}^{n+1}+q_{dg}^n+\tilde{q}_{ig}^{n+1}+\tilde{\Gamma}^{n+1}\tilde{h}_{sg}^{n+1}\ .\end{aligned} \tag{2-79}$$

Total Fluid (gas and liquid)

$$\begin{aligned}&\frac{\left\{\tilde{\alpha}_j^{n+1}\tilde{\rho}_{gj}^{n+1}\tilde{e}_{gj}^{n+1}+(1-\tilde{\alpha}_{gj}^{n+1})\tilde{\rho}_{gj}^{n+1}\tilde{e}_j^{n+1}-[(\alpha\rho_g e_g)_j^n+(1-\alpha)\rho_l e_l]_j^n\right\}}{\Delta t}\\&+\nabla_j\cdot\{(\alpha\rho_g e_g)^n V_g^{n+1}+[(1-\alpha)\rho_l e_l]^n V_l^{n+1}\}\\&+\tilde{P}^{n+1}\nabla_j\cdot[(1-\alpha)^n V_l^{n+1}+\alpha^n V_g^{n+1}]\\&=\tilde{q}_{wg}^{n+1}+\tilde{q}_{wl}^{n+1}+q_{dl}^n+q_{dg}^n\ .\end{aligned} \tag{2-80}$$

The divergence operator is revised during the semi-implicit step to improve modeling accuracy of situations in which flux can be predominately attributed to phase change in the cell for which the continuity equation is being evaluated. The idea is to use new-time information for that portion of the flux associated with the same cell as the equation (cell j). This makes the local solution more sensitive to variation in phase-change rates. In terms of the notation used for the basic definition of the divergence operator, the revised form is

$$\tilde{\nabla}_j\cdot(Y^n V_g^{n+1})=$$

$$\frac{[w_{j+1/2}Y_j'+(1-w_{j+1/2})Y_{j+1}^n]A_{j+1/2}V_{j+1/2}-\langle w_{j-1/2}Y_{j-1}^n+(1-w_{j-1/2})Y_j'\rangle A_{j-1/2}V_{j-1/2}}{\mathrm{vol}_j}\ . \tag{2-81}$$

The special feature of this operator is that all occurrences of Y_j^n in the normal finite-volume divergence operator are replaced by a mixed time average defined as

$$Y_j' = \gamma Y_j^{n+1} + (1-\gamma) Y_j^n \ . \tag{2-82}$$

The weighting factor γ is determined by several considerations. For flow that is single phase over the entire time step, γ is set to zero. When the net predicted flow out of a cell of either phase exceeds the current mass in that cell, the weight is set to one (new-time cell-centered quantities are fluxed). For less dramatic situations, three ratios are computed. The first ratio has as a numerator the sum of the change in cell vapor mass for the time step due to all mass fluxes plus twice the change due to boiling. The ratio's denominator is the cell's mass decrease due only to outwardly directed vapor mass flows (positive number). The second ratio is the analog of the first as applied to the liquid phase. For the third ratio, the numerator adds half the old-time cell liquid mass to the predicted change in cell liquid mass for the time step. The denominator is half of the mass change due to outwardly directed flows at the cell's edges (negative number). When other considerations are not in control, the maximum of the three ratios is limited to the range of zero through one and is used for γ.

The ratios used to compute the weighting factor were obtained after a long period of experimentation with two-phase-flow problems. The first two ratios force the use of a cell-centered implicit value when outflow of a phase is almost exclusively the result of phase-change terms. The factor will also force this implicit evaluation when phase change is not significant and inflow significantly exceeds the outflow. The third ratio becomes important when some liquid outflow is present and a prediction is made that over half of the existing liquid mass will flow or boil away during the time step.

The mixture of old- and new-time values of the quantity being fluxed results in a difference scheme for this step that is not rigorously conservative. However, the standard finite-volume divergence operator is applied in the stabilizer mass and energy equations, restoring conservation to the final fluxes of mass and energy.

To understand the stabilizer mass and energy equations, it is important to remember what is unknown and what quantities have fixed values. In this respect, the superscript "n+1" can be deceptive. New-time velocity values are fixed by the semi-implicit step, as are all new-time terms marked with a tilde. In the stabilizer combined-gas mass equation, the only unknown new-time variables are the macroscopic gas densities $(\alpha\rho_g)^{n+1}$. For the noncondensable mass equation, the only unknowns are the terms $(\alpha\rho_a)^{n+1}$, and for the liquid mass equation, the only unknowns are the terms $[(1-\alpha)\rho_l]^{n+1}$. In the stabilizer combined-gas energy equation, the only unknown new-time variables are the macroscopic gas energy densities $(\alpha\rho_g e_g)^{n+1}$. For the liquid energy equation, the only unknowns are the terms $[(1-\alpha)\rho_l e_l]^{n+1}$.

Stabilizer Mass Equations

Combined Gas

$$\frac{[(\alpha\rho_g)_j^{n+1} - (\alpha\rho_g)_j^n]}{\Delta t} + \nabla_j \cdot [(\alpha\rho_g)^{n+1} V_g^{n+1}] = \tilde{\Gamma}_j^{n+1} . \tag{2-83}$$

Noncondensable Gas

$$\frac{[(\alpha\rho_a)_j^{n+1} - (\alpha\rho_a)_j^n]}{\Delta t} + \nabla_j \cdot [(\alpha\rho_a)^{n+1} V_g^{n+1}] = 0 . \tag{2-84}$$

Liquid

$$\frac{[(1-\alpha)\rho_l]_j^{n+1} - [(1-\alpha)\rho_l]_j^n}{\Delta t} + \nabla_j \cdot \{[(1-\alpha)\rho_l]^{n+1} \cdot V_l^{n+1}\} = -\tilde{\Gamma}_j^{n+1} . \tag{2-85}$$

Liquid Solute

$$\frac{[(1-\alpha)_j^{n+1} \tilde{m}_j^{n+1} \rho_{lj}^{n+1} - (1-\alpha)_j^n m_j^n \rho_{lj}^n]}{\Delta t}$$

$$+ \nabla_j \cdot \left[(1-\alpha)^{n+1} \tilde{m}^{n+1} \rho_l^{n+1} V_l^{n+1}\right] = 0 , \tag{2-86}$$

$$m_j^{n+1} = \min\left[\tilde{m}_j^{n+1} + \frac{S_{cj}^n}{(1-\alpha)_j^{n+1} \rho_{lj}^{n+1}} , m_{\max}\right] , \tag{2-87}$$

and

$$S_{cj}^{n+1} = (\tilde{m}_j^{n+1} - m_j^{n+1})(1-\alpha)_j^{n+1} \rho_{lj}^{n+1} + S_{cj}^n . \tag{2-88}$$

Stabilizer Energy Equations

Combined Gas

$$\frac{[(\alpha\rho_g e_g)_j^{n+1} - (\alpha\rho_g e_g)_j^n]}{\Delta t} + \nabla_j \cdot [(\alpha\rho_g e_g)^{n+1} V_g^{n+1}]$$

$$+ \tilde{P}_j^{n+1}\left[\frac{(\tilde{\alpha}_j^{n+1} - \alpha_j^n)}{\Delta t} + \nabla_j \cdot (\alpha^n V_g^{n+1})\right]$$

$$= \tilde{q}_{wg}^{n+1} + q_{dg}^n + \tilde{q}_{ig}^{n+1} + \tilde{\Gamma}_j^{n+1}\tilde{h}_{sg}^{n+1} \quad . \tag{2-89}$$

Liquid

$$\frac{[(1-\alpha)\rho_l e_l]_j^{n+1} - [(1-\alpha)\rho_l e_l]_j^n}{\Delta t} + \nabla_j \cdot \{[(1-\alpha)\rho_l e_l]^{n+1} V_l^{n+1}\}$$

$$+ \tilde{P}_j^{n+1}\left\{\frac{(\alpha_j^n - \tilde{\alpha}_j^{n+1})}{\Delta t} + \nabla_j \cdot [(1-\alpha)^n V_l^{n+1}]\right\}$$

$$= \tilde{q}_{wl}^{n+1} + q_{dl}^n - \tilde{q}_{ig}^{n+1} - \tilde{\Gamma}_j^{n+1}\tilde{h}_{sg}^{n+1} \quad . \tag{2-90}$$

As indicated in Section 2.1.4.5., the code does not directly solve all of the above stabilizer equations. The actual equations solved are differences between these equations and their corresponding equations from the semi-implicit step. For the case of solute transport, no corresponding equation exists in the semi-implicit step. As a result, the stabilizer solute-transport equation, Eq. (2-86), is solved exactly as listed above. The final forms of the other equations as set in subroutine STBME follow:

Stabilizer Mass Equations

Combined Gas

$$\frac{[(\alpha\rho_g)_j^{n+1} - \tilde{\alpha}_j^{n+1}\tilde{\rho}_{gj}^{n+1}]}{\Delta t} + \nabla_j \cdot [(\alpha\rho_g)^{n+1} V_g^{n+1}] = \nabla_j \cdot [(\alpha\rho_g)^n V_g^{n+1}] \quad . \tag{2-91}$$

Noncondensable Gas

$$\frac{[(\alpha\rho_a)_j^{n+1} - \tilde{\alpha}_j^{n+1}\tilde{\rho}_{gj}^{n+1}]}{\Delta t} + \nabla_j \cdot [(\alpha\rho_a)^{n+1} V_g^{n+1}] = \nabla_j \cdot [(\alpha\rho_a)^n V_g^{n+1}] \quad . \tag{2-92}$$

Liquid

$$\frac{[(1-\alpha)\rho_l]_j^{n+1} - (1-\tilde{\alpha}_j^{n+1})\tilde{\rho}_{lj}^{n+1}}{\Delta t} + \nabla_j \cdot \{[(1-\alpha)\rho_l]^{n+1} V_l^{n+1}\} = \nabla_j \cdot \{[(1-\alpha)\rho_l]^n V_l^{n+1}\}. \tag{2-93}$$

Stabilizer Energy Equations

Combined Gas

$$\frac{[(\alpha\rho_g e_g)_j^{n+1} - \tilde{\alpha}_j^{n+1}\tilde{\rho}_{gj}^{n+1}\tilde{e}_{gj}^{n+1}]}{\Delta t} + \nabla_j \cdot [(\alpha\rho_g e_g)^{n+1} V_g^{n+1}] = \nabla_j \cdot [(\alpha\rho_g e_g)^n V_g^{n+1}]. \tag{2-94}$$

Liquid

$$\frac{\left\{[(1-\alpha)\rho_l e_l]_j^{n+1} - (1-\tilde{\alpha}_j^{n+1})\tilde{\rho}_{lj}^{n+1}\tilde{e}_{lj}^{n+1}\right\}}{\Delta t} + \nabla_j \cdot \{[(1-\alpha)\rho_l e_l]^{n+1} V_l^{n+1}\}$$

$$= \nabla_j \cdot \{[(1-\alpha)\rho_l e_l]^n V_l^{n+1}\}. \tag{2-95}$$

Source terms in the SETS equations follow the definitions provided during the discussion of the semi-implicit methods. They are redefined below to clarify the use of intermediate variables.

$$\tilde{q}_{wl}^{n+1} = h_{wl}^n A_w (T_w^n - \tilde{T}_l^{n+1})/\text{vol}, \tag{2-96}$$

$$\tilde{q}_{wg}^{n+1} = h_{wg}^n A_w (T_w^n - \tilde{T}_g^{n+1})/\text{vol}, \tag{2-97}$$

and

$$\tilde{\Gamma}^{n+1} = \frac{-\left(\tilde{q}_{ig}^{n+1} + \tilde{q}_{il}^{n+1}\right)}{(h_v')^{n+1} - (h_l')^{n+1}}, \tag{2-98}$$

where

$$\tilde{q}_{ig}^{n+1} = h_{ig}^n A_i^n \frac{(\tilde{T}_{\text{sat}}^{n+1} - \tilde{T}_g^{n+1})}{\text{vol}} \tag{2-99}$$

and

$$\tilde{q}_{il}^{n+1} = h_{il}^{n} A_i^{n} \frac{(\tilde{T}_{\text{sat}}^{n+1} - \tilde{T}_l^{n+1})}{\text{vol}} \quad . \tag{2-100}$$

As mentioned in Section 2.1.4.5., an important subtlety in the SETS application is the use of thermodynamic variables in the evaluation of specific terms. The current form of the SETS solution provides only final new-time values for void fraction (α), macroscopic densities [$\alpha\rho_g$, $\alpha\rho_a$, $(1-\alpha)\rho_l$], and macroscopic energies [$\alpha\rho_g e_g$, $(1-\alpha)\rho_l e_l$]. A final call to the thermodynamics subroutine does not occur after the solution of the stabilizer mass and energy equations. As a result, when basic thermodynamic variables are needed for evaluation properties such as viscosity or heat-transfer coefficients, values obtained from the previous semi-implicit step are used.

Equations (2-70) and (2-71) do not involve any implicit coupling between cells and can be solved directly for the gas and liquid (caret) velocities at each mesh-cell interface. Equations (2-72) and (2-73) are not coupled to each other. Each of these systems is implicitly coupled in space through the momentum-convection term, and each requires the solution of a tridiagonal linear system. Equations (2-74) through (2-80), combined with the necessary thermodynamic and constitutive equations, form a coupled system of nonlinear equations. Equations (2-74) and (2-75) are solved directly to obtain V_g^{n+1} and V_l^{n+1} as linear functions of $\tilde{P}^{n+1}$. After substituting these equations for velocity into Eqs. (2-76) through (2-80), the resulting system is solved for the independent variables $\tilde{P}^{n+1}$, $\tilde{P}_a^{n+1}$, $\tilde{T}_g^{n+1}$, $\tilde{T}_l^{n+1}$, and $\tilde{\alpha}^{n+1}$ with a standard Newton iteration, including all coupling between cells. In practice, the linearized equations solved during this Newton iteration are reduced easily to a tridiagonal system involving only total pressures. The final eight stabilizer mass and energy equations [Eqs. (2-83) through (2-90)] also are simple tridiagonal linear systems because V_g^{n+1} and V_l^{n+1} are known after solving Eqs. (2-74) through (2-80).

The drag force predictor equations are set up and solved in subroutines StbVel1D, StbVelx, StbVely, and StbVelz. The stabilizer motion equations are set up in the same subroutines and are solved with calls to subroutine Solver from subroutine PREP. The basic momentum equations associated with the semi-implicit step are set up in subroutine TF1DS1 (1D) and TF3DS1 (3D). Subroutines TF1DS (1D), TFPLN (plenum), and TF3DS (3D) set up the solution of the mass and energy equations associated with the semi-implicit step. Subroutine BlockSolver (called from subroutine OUTER) controls the solution of the full basic semi-implicit equation set within a Newton iteration driven by subroutine HOUT. The stabilizer mass and energy equations are set up in subroutines STBME (1D), STBMPL (plenum), and STBME3 (3D). These equation are solved by calls to subroutine SOLVER from subroutine POST. Finally, a value of new-time void fraction (see Section 2.1.8.2.4.) is obtained from the macroscopic densities and energy densities in subroutines BKSSTB (1D), BKSPLN (plenums), and BKSTB3.

Note: **Differences from TRAC-M/F77.** In the development of TRAC-M/F90 (Version 3.0), new subroutines were created to perform the full solution of the linear systems generated by the approximations to the flow equations. These replace statements in the following TRAC-M/F77 subroutines:

- FEMOM, FEMOMX, FEMOMY, FEMOMZ, TF1DS, STBME that begin solution of the 1D portion of the linear equations, including all local coding for solution of the local tridiagonal matrix structures, and generation of terms in the network matrices. (The names FEMOM, FEMOMX, FEMOMY, and FEMOMZ were also changed to StbVel1D, StbVelx, StbVely, and StbVelz, respectively, because forward elimination is no longer done in those routines.)

- TF1DS and TF3DS for cell block reduction;

- OUT3D, POST3D, PREP3D, and VSSL2 for vessel matrix solution;

- OUTER, POST, and PREP1D for solution of the network matrix; and

- BKSMOM, TF1DS3, TF3DS3, BKSSTB, and BKSTB3 directly related to back-substitution steps in the solution of the linear equations.

The basic and stabilizer equations involve very different numbers of equations, and generate two different matrix structures. As a result two separate subroutines were created for TRAC-M/F90 for solution of global systems of linear equations. The more basic of these, Solver, operates on equations which are dominantly tridiagonal in structure (the stabilizer equations and pressure equation). Solution of the more complex linear system associated with the basic (semi-implicit) step is driven by subroutine BlockSolver. Details on TRAC-M/F90's solution procedures are given in Section 2.1.8.

2.1.5. 3D Finite-Difference Methods

In the 3D VESSEL component, the code solves the combined-gas mass equation [Eq. (2-4)] and the total mass equation [Eq. (2-7)] as basic equations, rather than the individual basic phasic mass equations solved in the 1D components. All the other basic equations and the stabilizer equations for the 3D VESSEL component are solved in the same form as the 1D components. The vector form of the motion equation separates into three orthogonal-coordinate velocity-component motion equations. We present only the combined-gas equations with the understanding that the liquid equations are treated analogously. The 3D VESSEL component can be modeled by the TRAC user in either cylindrical or Cartesian geometry. The following equations in cylindrical geometry convert to Cartesian geometry by replacing the r divisor by unity and deleting the V^2/r term in the divergence operator that models momentum convection. The r and θ dependence is replaced by x- and y-dependence. For an orthogonal, right-handed, cylindrical coordinate system, the three velocity-component forms of the combined-gas motion differential equation are as follows:

Axial Velocity (z) Component

$$\frac{\partial V_{gz}}{\partial t} + \left(V_{gr} \frac{\partial V_{gz}}{\partial r} + \frac{V_{g\theta}}{r} \frac{\partial V_{gz}}{\partial \theta} + V_{gz} \frac{\partial V_{gz}}{\partial z} \right) = -\frac{1}{\rho_g} \frac{\partial P}{\partial z} - \frac{\Gamma^+}{\alpha \rho_g} (V_{gz} - V_{\ell z})$$

$$- \frac{c_{iz}}{\alpha \rho_g} \left(V_{gz} - V_{\ell z} \right) \left| \vec{V}_g - \vec{V}_\ell \right| - \frac{c_{wgz}}{\alpha \rho_g} V_{gz} \left| \vec{V}_g \right| - g g_z \quad . \tag{2-101}$$

Radial Velocity (r) Component

$$\frac{\partial V_{gr}}{\partial t} + \left(V_{gr} \frac{\partial V_{gr}}{\partial r} + \frac{V_{g\theta}}{r} \frac{\partial V_{gr}}{\partial \theta} - \frac{V_{g\theta}^2}{r} + V_{gz} \frac{\partial V_{gr}}{\partial z} \right) = -\frac{1}{\rho_g} \frac{\partial P}{\partial r} - \frac{\Gamma^+}{\alpha \rho_g} (V_{gr} - V_{\ell r})$$

$$- \frac{c_{ir}}{\alpha \rho_g} (V_{gr} - V_{\ell r}) \left| \vec{V}_g - \vec{V}_\ell \right| - \frac{c_{wgr}}{\alpha \rho_g} V_{gr} \left| \vec{V}_g \right| - g g_r \, . \tag{2-102}$$

Azimuthal Velocity (θ) Component

$$\frac{\partial V_{g\theta}}{\partial t} + \left(V_{gr} \frac{\partial V_{g\theta}}{\partial r} + \frac{V_{g\theta}}{r} \frac{\partial V_{g\theta}}{\partial \theta} + \frac{V_{gr} V_{g\theta}}{r} + V_{gz} \frac{\partial V_{g\theta}}{\partial z} \right) = -\frac{1}{\rho_g r} \frac{\partial P}{\partial \theta} - \frac{\Gamma^+}{\alpha \rho_g} \left(V_{g\theta} - V_{\ell \theta} \right)$$

$$- \frac{c_{i\theta}}{\alpha \rho_g} (V_{g\theta} - V_{\ell \theta}) \left| \vec{V}_g - \vec{V}_\ell \right| - \frac{c_{wg\theta}}{\alpha \rho_g} V_{g\theta} \left| \vec{V}_g \right| - g \, g_\theta \quad . \tag{2-103}$$

In the last term of each equation, g is the gravitational acceleration constant and g_z, g_r, and g_θ are the directional components of the gravity vector based on the orientation of the 3D VESSEL component. By setting namelist input variable NVGRAV = 1, the TRAC user may define through input a general orientation for each VESSEL component. The NVGRAV = 0 default results in TRAC internally defining $g_z = 1$, $g_r = 0$, and $g_\theta = 0$, where the z-axis is oriented vertically upward for all VESSEL components in the system model.

TRAC uses a staggered-mesh scheme (Ref. 2-12.) similar to that used for the 1D components in which the velocities (V) are defined at the mesh-cell interfaces and the pressure (P), gas volume fraction (α), temperature (T), internal energy (e), and density (ρ) are defined at the mesh-cell centers. The scalar field equations (mass and energy) apply to a mesh cell, whereas the velocity-component motion equations apply to an interface between mesh cells in the three velocity-component directions. The wall heat transfer and the interfacial mass transfer required by the field equations are defined with a form similar to Eqs. (2-96) through (2-100).

The difference scheme for each motion equation is lengthy because of the cross-derivative terms. Therefore, to illustrate the procedure, we will describe only the combined-gas velocity-component, z-direction, finite-difference basic equation of motion for a typical mesh cell interface, together with the gas basic mass and energy equations, for a typical mesh cell. The gas velocity-component basic equations of motion in the θ and r directions along with all of the liquid basic equations are similar in form. The stabilizer motion, mass, and energy equations will not be illustrated; the reader is referred to the 1D component Eqs. (2-70) to (2-80) and (2-83) to (2-95) where time-level parameters with $\tilde{}$, $\hat{}$, n, and n+1 superscripts are changed in going from the basic equations to the stabilizer equations. The superscript n indicates a current-time quantity; the superscript $n+1$ indicates a new-time quantity. The functional dependence (r,θ,z) points to the cell center. By incrementing r or θ or z by ±1, one moves to the adjacent cell in the direction based on which coordinate is incremented and on the sign of the increment. The functional dependencies $(r-1/2,\theta,z)$ and $(r+1/2,\theta,z)$ point to the inside and outside radial faces of the cell, respectively; $(r,\theta-1/2,z)$ and $(r,\theta+1/2,z)$, the right and left azimuthal faces of the cell (based on a perspective of looking radially out of the cell), respectively; and $(r,\theta,z-1/2)$ and $(r,\theta,z+1/2)$, the bottom and top axial faces of the cell, respectively. The subscript g (for gas) is dropped unless it is needed for clarity.

The default for the TRAC 3D numerics is to evaluate the 3D stabilizer equations every time step. The user can override the default. (See TRAC input description for namelist variable NOSETS, which controls the status of internal flag NSTAB.) The TRAC 3D stabilizer equations and the basic step equations are solved when the flag NSTAB = 1. If NSTAB = 0, then the basic step equations are solved, which is equivalent to the TRAC-PF1/MOD1 3D numerics.

The finite-difference combined-gas basic equation of motion in the z-direction has the following form:

Combined-Gas Basic Equation of Motion in the z-Direction

$$V_z^{n+1}(r,\theta,z+1/2) = V_z^n(r,\theta,z+1/2)$$

$$-\Delta t \left[\frac{V_r \Delta_r V_z^{n+1}}{\Delta r} + \frac{V_\theta \Delta_\theta V_z^{n+1}}{r\Delta\theta} + \frac{1}{2}\left(\frac{A_{z+1/2}}{A_{z+1}} + \frac{A_{z+1/2}}{A_z}\right)\frac{V_z^{n+1}(r,\theta,z+1/2)}{\Delta z} \right.$$

$$\left. \left[\frac{A_{Z+1/2}}{A_{z+1}}\tilde{V}_z^{n+1}(r,\theta,Z+1/2) - \frac{A_{Z-1/2}}{A_z}\tilde{V}_z^{n+1}(r,\theta,Z-1/2)\right] \right]$$

$$
- \frac{[P(r,\theta,z+1) - P(r,\theta,z)]^{n+1}}{\rho^n(r,\theta,z+1/2)\Delta z} - \frac{c_{iz}^n(r,\theta,z+1/2)}{(\alpha,\rho)^n(r,\theta,z+1/2)}
$$

$$
\times \left\{ \left[\left| \vec{V}_g - \vec{V}_\ell \right|^n + \frac{((V_{gz} - V_{\ell z})^n(r,\theta,z+1/2))^2}{\left| \vec{V}_g - \vec{V}_\ell \right|^n} \right] (V_{gz} - V_{\ell z})^{n+1}(r,\theta,z+1/2) \right.
$$

$$
\left. - \frac{((V_{gz} - V_{\ell z})^n(r,\theta,z+1/2))^3}{\left| \vec{V}_g - \vec{V}_\ell \right|^n} \right\}
$$

$$
- \frac{\Gamma^{+n}(r,\theta,z+1/2)(V_{gz} - V_{\ell z})^{n+1}(r,\theta,z+1/2)}{(\alpha\rho)^n(r,\theta,z+1/2)} - gg_z
$$

$$
- \frac{c_{wz}^n(r,\theta,z+1/2) \left\{ \left[\left| \vec{V}_g \right|^n + \frac{(V_z^n(r,\theta,z+1/2))^2}{|\vec{V}_g|^n} \right] V_z^{n+1}(r,\theta,z+1/2) - \frac{(V_z^n(r,\theta,z+1/2))^3}{|\vec{V}_g|^n} \right\}}{(\alpha\rho)^n(r,\theta,z+1/2)} \Bigg],
$$

(2-104)

where $Z = z$ if $V_z^n(r,\theta,z+1/2) \geq 0$ and $Z = z+1$ if $V_z^n(r,\theta,z+1/2) < 0$.

Any finite-difference scheme requires certain quantities at locations where they are not defined formally; therefore, additional relations are needed. TRAC obtains the volume-averaged properties $\alpha\rho$ and ρ at the cell axial interface from a cell-length weighted average,

$$
(\alpha\rho)(r,\theta,z+1/2) = \frac{\Delta z(z)\alpha(r,\theta,z)\rho(r,\theta,z) + \Delta z(z+1)\alpha(r,\theta,z+1)\rho(r,\theta,z+1)}{\Delta z(z) + \Delta z(z+1)} \qquad (2\text{-}105)
$$

and

$$
\rho(r,\theta,z+1/2) = \frac{(\alpha\rho)(r,\theta,z+1/2)}{\alpha(r,\theta,z+1/2)} = \qquad (2\text{-}106)
$$

$$
\frac{\Delta z(z)\alpha(r,\theta,z)\rho(r,\theta,z) + \Delta z(z+1)\alpha(r,\theta,z+1)\rho(r,\theta,z+1)}{\Delta z(z)\alpha(r,\theta,z) + \Delta z(z+1)\alpha(r,\theta,z+1)}
$$

This averaging is necessary to compute pressure heads accurately. The code obtains Γ at the cell interface from its phasic velocity donor cell as follows:

The cross-derivative term $V_r\Delta_r V_z^{n+1}$ reflects a donor-cell average:

$$V_r\Delta_r V_z^{n+1} = \tilde{V}_r(r+1/2,\theta,z+1/2)\left[\tilde{V}_z(r+1,\theta,z+1/2)-\tilde{V}_z(r,\theta,z+1/2)\right]$$

$$+\tilde{V}_r(r-1/2,\theta,z+1/2)\left[\tilde{V}_z(r,\theta,z+1/2)-\tilde{V}_z(r-1,\theta,z+1/2)\right], \qquad (2\text{-}107)$$

where

$$\tilde{V}_r(r+1/2,\theta,z+1/2) = \qquad (2\text{-}108)$$

$$\min\left[\frac{SC_r(r+1/2,\theta,z+1)\tilde{V}_r(r+1/2,\theta,z+1)\Delta z(z)+SC_r(r+1/2,\theta,z)\tilde{V}_r(r+1/2,\theta,z)\Delta z(z+1)}{\Delta z(z)+\Delta z(z+1)},0\right]$$

and

$$\tilde{V}_r(r-1/2,\theta,z+1/2) = \qquad (2\text{-}109)$$

$$\max\left[\frac{SC_r(r-1/2,\theta,z+1)\tilde{V}_r(r-1/2,\theta,z+1)\Delta z(z)+SC_r(r-1/2,\theta,z)\tilde{V}_r(r-1/2,\theta,z)\Delta z(z+1)}{\Delta z(z)+\Delta z(z+1)},0\right].$$

In the above equations, "min" and "max" are the mathematical functions of minimum and maximum values of the terms inside the brackets. $SC_r(r+1/2,\theta,z)$ is the product of an orifice factor that is 0 (when an orifice plate is present at the r+1/2 interface) or 1 and the ratio of the flow area through the r + 1/2 interface to the (r,θ,z) cell flow area in the radial direction, $\mathrm{vol}(r,\theta,z)/\Delta r_{cell}$. An analogous expression holds for the $V_\theta\Delta_\theta V_z^{n+1}$ term.

Note that the V_z differences in the r and θ directions do not contain the z-direction flow-area weighting form. The SC_r and SC_θ factors make this correction for z-direction momentum convection in the r and θ directions, respectively.

In the interfacial drag terms, the magnitude of the relative velocity is defined as follows:

$$\left|\vec{V}_g-\vec{V}_\ell\right| = \{[V_{zg}(r,\theta,z+1/2)-V_{z\ell}(r,\theta,z+1/2)]^2 \qquad (2\text{-}110)$$

$$+0.25[(V_{rg}(r+1/2,\theta,z)+V_{rg}(r-1/2,\theta,z)$$

$$-V_{r\ell}(r+1/2,\theta,z)-V_{r\ell}(r+-1/2,\theta,z)]^2$$

$$+0.25[V_{\theta g}(r,\theta+1/2,z)+V_{\theta g}(r,\theta-1/2,z)$$

$$-V_{\theta\ell}(r,\theta+1/2,z)-V_{\theta\ell}(r,\theta-1/2,z)]^2\}^{1/2}.$$

The convective terms in the finite-difference relations for the scalar field equations are in conservative form. The finite-difference form of the combined-gas basic mass equation is

Combined-Gas Basic Mass Equation

$$
\begin{aligned}
(\tilde{\alpha}\tilde{\rho})^{n+1} = (\alpha\rho)^n - \left[\frac{\Delta t}{\mathrm{vol}}\right] \Big\{ & A_{z+1/2}\left\langle (\alpha\rho)^n V_z^{n+1}\right\rangle_{z+1/2} - A_{z-1/2}\left\langle (\alpha\rho)^n V_z^{n+1}\right\rangle_{z-1/2} \\
& + A_{r+1/2}\left\langle (\alpha\rho)^n V_r^{n+1}\right\rangle_{r+1/2} - A_{r-1/2}\left\langle (\alpha\rho)^n V_r^{n+1}\right\rangle_{r-1/2} \\
& + A_{\theta+1/2}\left\langle (\alpha\rho)^n V_\theta^{n+1}\right\rangle_{\theta+1/2} - A_{\theta-1/2}\left\langle (\alpha\rho)^n V_\theta^{n+1}\right\rangle_{\theta-1/2} \Big\} \\
& + \Delta t\,\tilde{\Gamma}^{n+1} \quad . \qquad \text{(2-111)}
\end{aligned}
$$

The combined-gas basic energy equation is

Combined-Gas Basic Energy Equation

$$
\begin{aligned}
(\tilde{\alpha}\tilde{\rho}\tilde{e})^{n+1} = (\alpha\rho e)^n - \left[\frac{\Delta t}{\mathrm{vol}}\right] \Big\{ & A_{z+1/2}\left\langle (\alpha\rho e)^n V_z^{n+1}\right\rangle_{z+1/2} - A_{z-1/2}\left\langle (\alpha\rho e)^n V_z^{n+1}\right\rangle_{z-1/2} \\
& + A_{r+1/2}\left\langle (\alpha\rho e)^n V_r^{n+1}\right\rangle_{r+1/2} - A_{r-1/2}\left\langle (\alpha\rho e)^n V_r^{n+1}\right\rangle_{r-1/2} \\
& + A_{\theta+1/2}\left\langle (\alpha\rho e)^n V_\theta^{n+1}\right\rangle_{\theta+1/2} - A_{\theta-1/2}\left\langle (\alpha\rho e)^n V_\theta^{n+1}\right\rangle_{\theta-1/2} \Big\} \\
& - \tilde{P}^{n+1}\left(\tilde{\alpha}^{n+1} - \alpha^n\right) \\
& - \left[\frac{\tilde{P}^{n+1}\Delta t}{\mathrm{vol}}\right] \Big[\left\langle A\alpha^n V_z^{n+1}\right\rangle_{z+1/2} - \left\langle A\alpha^n V_z^{n+1}\right\rangle_{z-1/2} \\
& \qquad + \left\langle A\alpha^n V_r^{n+1}\right\rangle_{r+1/2} - \left\langle A\alpha^n V_r^{n+1}\right\rangle_{r-1/2} \\
& \qquad + \left\langle A\alpha^n V_\theta^{n+1}\right\rangle_{\theta+1/2} - \left\langle A\alpha^n V_\theta^{n+1}\right\rangle_{\theta-1/2} \Big] \\
& + \Delta t(\tilde{q}_{wg}^{n+1} + q_{dg}^n + \tilde{q}_{ig}^{n+1} + \tilde{\Gamma}^{n+1}\tilde{h}_{sg}^{n+1}) \qquad \text{(2-112)}
\end{aligned}
$$

The differencing of the other scalar equations (the total mass and energy equations, the noncondensable-gas mass equation, and the liquid-solute mass equation) is similar. The time level of the convected mass $\alpha\rho$ and convected energy $\alpha\rho\varepsilon$ is the n+1 in the stabilizer equations. If the stabilizer mass and energy equations are not evaluated (NSTAB = 0), the tilde parameters in Eqs. (2-111) and (2-112) are defined without tildes.

All the field equations in the 3D VESSEL component can have additional source terms to allow one or more 1D component junctions to be connected to a mesh-cell interface anywhere in the 3D VESSEL component. The source terms in the mass and energy equations follow below. The subscripts 1D and 3D indicate that quantities are obtained from the 1D component-junction interface or junction cell and the 3D VESSEL-component mesh cell, respectively. The $\langle\ \rangle$ indicates the convected quantity has either the subscript 1D or 3D of the upstream donor cell based on the direction of the phase velocity at the source-connection 1D component-junction interface, illustrated by Eqs. (2-21) and (2-31). Each of these source terms is added to the downstream mesh cell's mass or energy equation and an equivalent sink term is subtracted from the upstream mesh cell's equation.

Total Basic Mass-Equation Source Term

$$\left[\frac{\Delta t}{\mathrm{vol}}\right]\{\langle(\alpha\rho_g)^n V_g^{n+1}\rangle_{1D}A_{1D} + \langle[(1-\alpha)\rho_\ell]^n V_\ell^{n+1}\rangle_{1D}A_{1D}\}\ . \tag{2-113}$$

Combined-Gas Basic Mass-Equation Source Term

$$\left[\frac{\Delta t}{\mathrm{vol}}\right]\left\{\left\langle\left(\alpha\rho_g\right)^n_{\mathrm{Donor}} V_g^{n+1}\right\rangle_{1D} A_{1D}\right\}\ . \tag{2-114}$$

Total Basic Energy Equation Source Term

$$\left[\frac{\Delta t}{\mathrm{vol}}\right]\left\{\left\langle\left[(1-\alpha)\rho_\ell e_\ell\right]^n V_\ell^{n+1}\right\rangle_{1D} A_{1D} + \left\langle\left(\alpha\rho_g e_g\right)^n V_g^{n+1}\right\rangle_{1D} A_{1D}\right.$$
$$\left. + P_{3D}\left[\left\langle\alpha^n V_g^{n+1}\right\rangle_{1D} A_{1D} + \left\langle(1-\alpha)^n V_\ell^{n+1}\right\rangle_{1D}\right]A_{1D}\right\}\ . \tag{2-115}$$

Combined-Gas Basic Energy Equation Source Term

$$\left[\frac{\Delta t}{\text{vol}}\right]\left\{\left\langle(\alpha\rho_g e_g)^n V_g^{n+1}\right\rangle_{1D} A_{1D} + P_{3D}\left\langle\alpha^n (V_g^{n+1})\right\rangle_{1D} A_{1D}\right\} \quad . \tag{2-116}$$

Noncondensable-Gas Basic Mass-Equation Source Term

$$\left[\frac{\Delta t}{\text{vol}}\right]\left\langle(\alpha\rho_a)^n V_g^{n+1}\right\rangle_{1D} A_{1D} \quad . \tag{2-117}$$

Liquid-Solute Basic Mass-Equation Source Term

$$\left[\frac{\Delta t}{\text{vol}}\right]\left\langle\left((1-\alpha)m\rho_\ell\right)^n V_\ell^{n+1}\right\rangle_{1D} A_{1D} \quad . \tag{2-118}$$

The momentum source term is complicated by the staggered differencing and by the fact that the actual 1D component may enter at an arbitrary angle. For TRAC, we assume that the 1D component attaches normal (perpendicular) to the vessel mesh-cell interface. The interface flow area A_{3D} and velocity V_{3D} are defined on the opposite side of the 3D mesh cell from the interface where the 1D component-junction source convection is made. It is that opposite mesh-cell interface from the source-convection interface that has in its motion equation the following momentum-convection source term for the combined-gas or liquid basic equation of motion when $V_{3D} \pm 1/2$ flows away from the 1D component source-convection interface into the 3D + 1 mesh cell. An S factor is applied to the 1D component so that its positive flow direction becomes the positive flow direction of the vessel.

Basic Equation-of-Motion Source Term

$$\frac{\Delta t}{2}\left(\frac{A_{3D}}{\text{vol}_{3D\pm1}/\Delta x_{3D\pm1}} + \frac{A_{3D}}{\text{vol}_{3D}/\Delta x_{3D}}\right)\frac{V_{3D}^{n+1}}{\Delta x_{3D}}\left[\frac{A_{1D}S\tilde{V}_{1D}^{n+1}}{\text{vol}_{3D}/\Delta x_{3D}}\right] \quad . \tag{2-119}$$

Each stabilizer equation of motion is solved with all vessels in the modeled system implicitly coupled in space through their 1D-component-loop-source connections. The spatial coupling between directions and the interfacial drag coupling between fluid phases, however, are explicit in that the motion equations for each direction and for each fluid phase are solved separately as a vessel matrix equation. When solving the stabilizer

equations, the time-step size normally exceeds the material Courant time-step limit and implicit coupling in space for a given velocity-component direction for all vessel components is necessary to assure a numerically stable solution. This means that each 1D component loop must have all its vessel-component source connections made to the same direction interfaces of the 3D vessel mesh cells. Different loops can be connected to different faces, however. For example, one loop may be connected to r-direction interfaces of three different vessels, another loop to z-direction interfaces of one vessel, and a third loop connected to θ-direction and y-direction interfaces of two different vessels with different geometries. The latter example is allowed because the θ- and y-directions are implicitly coupled between two VESSEL components in the vessel matrix equation by which their equations are evaluated. If the TRAC user defines any 1D component loop with source connections to different vessel-interface directions, TRAC edits a warning message during the input phase and limits the time-step size to not exceed the material Courant limit in the VESSEL components of the modeled system.

The number of independent parameter variables is limited to V_ℓ, V_g, T_ℓ, T_g, α, P, and P_a by using the thermal equations of state,

$$\rho_\ell = \rho_\ell (P, T_\ell) , \qquad \rho_v = \rho_v (P_v, T_g) , \text{ and } \qquad \rho_a = \rho_a (P_a, T_g) ; \tag{2-120}$$

the caloric equations of state,

$$e_\ell = e_\ell \left(P, T_\ell\right) , \qquad e_v = e_v \left(P_v, T_g\right) , \text{ and } \qquad e_a = e_a \left(P_a, T_g\right) ; \tag{2-121}$$

and the definitions for ρ_g, e_g, and P [Eqs. (2-14), (2-15), and (2-16)].

If hardware structure exists in the 3D mesh cells, the interface flow area (A) for fluid flow and the mesh-cell fluid volume (vol) are reduced from their geometric mesh-cell values by the user through inputting fractions of their geometric area and volume. These fractions can be input with values greater than unity, but it is recommended that the user not do so for the model to be physically valid. Thus, A should be less than or equal to the geometric mesh-cell side area and "vol" should be less than or equal to the geometric mesh-cell volume. Mesh-cell fluid volumes are constrained to be $\geq 10^{-12}$ m^3 by TRAC. When the flow area is defined to be zero, fluid flow across the mesh-cell interface is zero. This procedure allows large obstacles, such as the downcomer walls and flow channels, to be modeled within the VESSEL component.

When NSTAB = 1, the combined-gas and liquid stabilizer equations of motion are determined in subroutines StbVelx, StbVely, and StbVelz (FEMOMX, FEMOMY, and FEMOMZ in TRAC-M/F77) and solved in subroutine VSSL1 for a single vessel-component system model or in subroutine PREP3D for a multivessel-component system model. The combined-gas and liquid basic equations of motion are determined in subroutine TF3DS1 and then substituted for the velocity in determining the mass and energy basic equations in subroutine TF3DS. The reduced pressure matrix equation is solved in subroutine VSSL2 for a single vessel-component model or subroutine OUT3D

for a multivessel-component model. The pressure solution is back-substituted in subroutine TF3DS3 to determine the remainder of the basic equation solution. A Newton method iterative solution of these basic equations is performed until the pressure solution converges to within a user-defined tolerance. When NSTAB = 1, the combined-gas and liquid stabilizer mass equations are determined in subroutine STBME3 and solved in subroutine VSSL3 for a single vessel-component system model or in subroutine POST3D for a multivessel-component system model. All the different forms of the above equations are solved as vessel matrix equations by subroutine MATSOL using the capacitance matrix method described in Section 2.1.8.4.

2.1.6. Modifications to the Basic Equation Set

Because of the choice of independent parameter variables in the solution of the 1D basic equations (total pressure, air partial pressure, void fraction, combined-gas and liquid temperatures, and combined-gas and liquid velocities), the basic equation set becomes singular at void fractions of zero and one. To avoid this solution difficulty, the combined-gas mass equation is replaced with a mean mass equation at these void-fraction limits. At a void fraction of zero, the liquid mass and combined-gas energy equations are replaced with equations that set the void fraction to zero and set the combined-gas temperature equal to the saturation temperature based on the total pressure. At a void fraction of one, these same equations are replaced with equations that set the void fraction to one and the liquid temperature equal to the saturation temperature based on the partial pressure of water vapor. The same approach is used to handle this singularity in the 3D basic equations, except that here the mean mass equations are always evaluated and the combined-gas rather than the liquid mass equation is replaced when the void fraction is zero or one.

When the transition from single-phase gas or liquid to a two-phase fluid first occurs, the combined-gas and liquid mass equations are evaluated but the replacement equation for the gas energy equation is used for one more time step. This forces the second phase to initially appear at saturation conditions, which is generally a very good approximation. It drastically reduces sporadic numerical problems associated with the use of two energy equations in which the first appearance of a phase can be associated with an exceptionally bad predicted value of its temperature. Special considerations are also made during the linearization for the Newton solution of the semi-implicit equations. When an explicit mass test suggests the first appearance of a second phase, flux of the second phase is used to estimate the new-time void fraction. If air is just appearing in a cell, an initial estimate is also made of the air partial pressure. Both of these estimates are used to specify the base state for the linearization associated with the current Newton iteration.

When the pressure exceeds the critical-point pressure, the basic equations become singular. To evaluate this fluid state with minimal coding changes, the thermal properties of steam have been modified slightly. TRAC constrains the calculated steam density never to exceed 0.999 times the liquid density and thus prevents a singularity from arising. Also, at pressures above the critical point, the calculated saturation

temperature is set to a higher value than the vapor temperature to drive the fluid to be a pure liquid through phase change.

Thermodynamic properties used when evaluating the basic equations are calculated by subroutine THERMO. These properties are determined as functions of total pressure, air partial pressure, and the combined-gas and liquid temperatures. When the values of these solution parameters lie outside the database range for which the thermodynamic-property functional fits are valid, subroutine THERMO edits a warning message and constrains the parameter values to the database range limits defined in Appendix A before evaluating the thermodynamic properties. However, the solution parameter variable values are not changed.

2.1.7. Conserving Convected Momentum

The TRAC-PF1/MOD1 backward difference approach to determine the $V\nabla V$ term in the TRAC momentum equation is known to be stable numerically. For smooth area changes, however, this backward or upwind difference scheme is not accurate and does not conserve momentum. For abrupt area changes, it can be shown that the upwind difference scheme for $V\nabla V$ will result in pressure changes that include both reversible and irreversible effects. Upwind differencing is accurate for abrupt expansions and overestimates the pressure change for an abrupt contraction. (See Appendix I, Section I.1. for details.)

It has been shown that the accuracy of a central difference representation of $V\nabla V$ is quite accurate for smooth area changes and for the reversible portion of an abrupt area change. Central differencing is, in general, unconditionally unstable, however, based on linear stability analyses. An approach that was originally developed for TRAC-PF1/MOD2 to improve momentum conservation is to determine factors based on geometry that change the upwind differencing of the $V\nabla V$ so that its accuracy is consistent with central differencing. The assumption used in developing these factors is constant volumetric flow from the cell center to the cell edge. This method bas been brought over to TRAC-M.

A central difference for $V\nabla V$ for 1D flow yields

$$V\nabla V = \frac{VdV}{dx} = \frac{0.5d\left(V^2\right)}{dx} \equiv \frac{0.5\left(V_{j+1}^2 - V_j^2\right)}{\Delta x_{j+1/2}} \quad . \tag{2-122}$$

Equation (2-122) can be rewritten as

$$V\nabla V = \frac{0.5\left(V_{j+1} + V_j\right)\left(V_{j+1} - V_j\right)}{\Delta x_{j+1/2}} \quad . \tag{2-123}$$

In TRAC, velocities are calculated at cell edges, therefore cell-center velocities must be estimated from cell-edge velocities. Equation (2-123) can be written in terms of the cell-edge velocities by applying the following equations based on constant volumetric flow from cell center to the cell edge:

$$A_{j+1}V_{j+1} = A_{j+1/2}V_{j+1/2} \quad , \tag{2-124}$$

$$A_j V_j = A_{j+1/2}V_{j+1/2} \quad , \tag{2-125}$$

and

$$A_j V_j = A_{j-1/2}V_{j-1/2} \quad . \tag{2-126}$$

If Eqs. (2-124) and (2-125) are substituted into the summed portion of Eq. (2-123), and Eqs. (2-124) and (2-126) are substituted into the difference portion of Eq. (2-123), an upwind difference form that is as accurate as central differencing is obtained for $V\nabla V$.

$$V\nabla V = 0.5\,(A_{j+1/2}/A_{j+1} + A_{j+1/2}/A_j)\,V_{j+1/2}(A_{j+1/2}V_{j+1/2}/A_{j+1} - A_{j-1/2}V_{j-1/2}/A_j)/\Delta x_{j+1/2} \tag{2-127}$$

These equations assume that $V_{j+1/2} \geq 0$, but similar sets of equations can be derived for $V_{j+1/2} < 0$. In the MOD2 and TRAC-M codes, Eq. (2-127) is the approximation used in both the 1D and 3D momentum-convection terms to improve the conservation of momentum. For comparison purposes, the MOD1 representation for $V\nabla V$ is equivalent to the MOD2 and TRAC-M approximation if the cell-edge flow areas and cell-center flow areas are all equal. For the MOD1 code, $V\nabla V$ is estimated for $V_{j+1/2} \geq 0$ as

$$V\nabla V = V_{j+1/2}\left(V_{j+1/2} - V_{j-1/2}\right)/\Delta x_{j+1/2} \quad . \tag{2-128}$$

In general, TRAC, even with the corrected $V\nabla V$ term, is still solving a nonconserving momentum equation. A conserving form of the momentum equation for single-phase flow with no momentum sources or sinks can be written as

$$\frac{d(\rho V)}{dt} = \frac{d(\rho VAV)}{Adx} = 0 \tag{2-129}$$

Expanding the derivatives of Eq. (2-129) yields

$$V\left\{\frac{d(\rho)}{dt} + \frac{d(\rho V A)}{A\,dx}\right\} + \rho\left\{\frac{d(V)}{dt} + V\frac{d(V)}{dx}\right\} = 0 \quad . \tag{2-130}$$

The continuity equation for single-phase flow with no sources or sinks can be written as

$$\frac{d(\rho)}{dt} + \frac{d(\rho VA)}{Adx} = 0 \tag{2-131}$$

Therefore, Eq. (2-130) can be written as

$$\frac{d(V)}{dt} + V\frac{d(V)}{dx} = 0 \quad . \tag{2-132}$$

Equation (2-132) represents the type of nonconserving form of the momentum equation solved by the TRAC code. This derivation indicates that TRAC will conserve momentum with the nonconserving form of the momentum equation if mass is conserved on a point-by-point basis. TRAC conserves mass within each hydraulic cell and assumes that within that cell, the density and void fractions are constant. This assumption may lead to errors in conserving momentum, since the nonconserving momentum equation is solved from cell center to cell center and the geometry area ratio factors developed for Eq. (2-127) assume constant density and void fraction from cell center to cell edge.

If we assume constant volumetric flow from cell edge j–1/2 to cell edge j+1/2, Eq. (2-127) in the form of the Bernoulli equation is equivalent to

$$P_{j+1} - P_j + \frac{\rho}{2}\left[\left(\frac{A_{j+1/2}}{A_{j+1}}V_{j+1/2}\right)^2 - \left(\frac{A_{j-1/2}}{A_j}V_{j-1/2}\right)^2\right] + \rho g \Delta x_{j+1/2}\cos\theta = 0 \; . \tag{2-133}$$

Substitute the constant volumetric-flow relations $A_{j+1/2}V_{j+1/2} = A_{j+1}V_{j+1}$ and $A_{j-1/2}V_{j-1/2} = A_jV_j$ into the momentum-convection term of Eq. (2-133) to obtain the Bernoulli equation

$$P_{j+1} - P_j + \tfrac{1}{2}\rho\,[V_{j+1}^2 - V_j^2] + \rho g \Delta x_{j+1/2}\cos\theta = 0 \quad . \tag{2-134}$$

We see from the above derivation of the momentum-convection term and the assumptions made that the equation of motion for single-phase liquid (a near-incompressible fluid) to a very good approximation satisfies the conservative form of the momentum equation (and thus the Bernoulli equation). Convected momentum flux between momentum cells should be nearly conserved. Reversible form losses caused by flow-area and elevation changes should be evaluated correctly. This has been demonstrated (Ref. 2-13.) for single-phase liquid with a variable flow-area and elevation flow-channel test problem having a total of seven 1D PIPE and VESSEL components connected in series with a FILL-component velocity and BREAK-component pressure boundary condition at each end of the flow channel, respectively. Each 1D VESSEL component was evaluated in each of three Cartesian-coordinate directions in separate calculations. Wall losses in the flow channel with flow area varying from 0.1 to 0.6 m^2 were minimized by increasing the flow-channel hydraulic diameter by a factor of 100.

A plot of the MOD2-calculated Bernoulli expression $P_j / \rho_j + V_j^2 / 2 + gh_j$ versus flow-channel cell number j for four different PIPE- and VESSEL-component models is shown in Fig. 2-1., with and without flow-area ratios applied in the momentum-convection term of the liquid equation of motion. Each of the four models comprised a different combination of PIPE and/or 1D VESSEL components, yet each gave the same results. Conservation of convected momentum and an accurate evaluation of the Bernoulli equation is demonstrated by the constant value of the Bernoulli expression when flow-area ratios are applied in the momentum-convection term. Similar calculations were performed for single-phase vapor wherein MOD2 was temporarily modified to evaluate a constant vapor microscopic density (making vapor an incompressible fluid). The results determined were similar to those of liquid, which served as a check that the combined-gas equation of motion as well as the liquid equation of motion are programmed correctly for both 1D and 3D components.

For a compressible single-phase vapor, the change in its microscopic density because of fluid pressure and temperature variation over a mesh-cell distance generally is small. Approximating constant density within a fluid cell should cause only a small error in conserving convected vapor momentum flux between momentum cells.

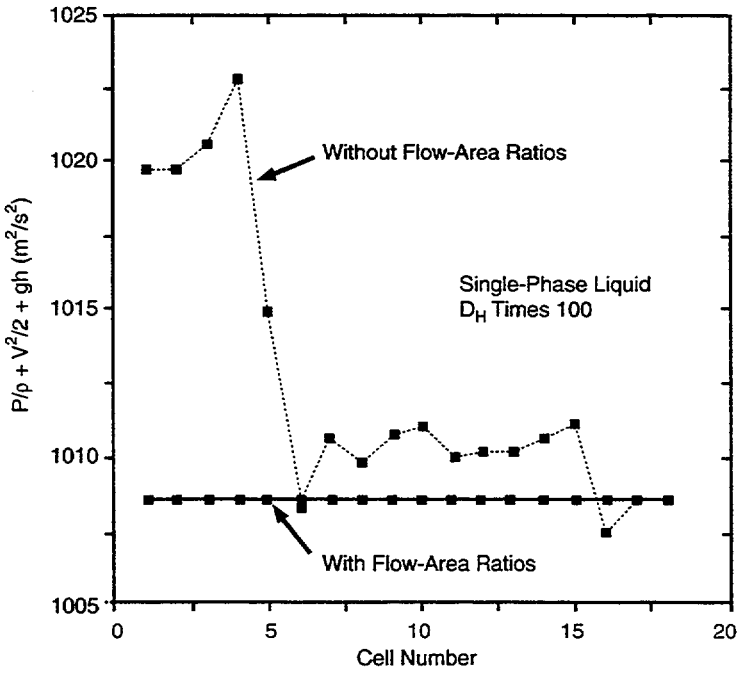

Fig. 2-1. The Bernoulli expression $P_j / \rho_j + V_j^2 / 2 + gh_j$ vs. flow-channel cell number j from a 1D flow-channel test problem having variable flow area and elevation.

A spatial variation in the fluid void fraction across a mesh cell can result in a momentum-flux conservation error because of the constant volumetric-flow assumption. The MOD2 and TRAC-M momentum equation solution has significant improvements in accuracy over the MOD1 momentum equation solution. For rapidly changing void fractions or densities within a short distance, however, MOD2 and TRAC-M still may not conserve momentum.

The ability to evaluate momentum convection with and without flow-area ratios has been provided. Each flow-area ratio is multiplied by variable ARY (Area Ratio Yes) and then summed to variable ARN (Area Ratio No) before being applied in the momentum-convection term. These two variables are initialized in module OneDDat (subroutine BLKDAT in TRAC-M/F77) to ARY=1 and ARN=0 to evaluate momentum convection with area ratios. Redefining ARY=0 and ARN=1 in module OneDDat (subroutine BLKDAT in TRAC-M/F77) sets all area ratios in the momentum-convection term to unity. This provides the TRAC user with a convenient way to compare TRAC calculations with flow-area ratios (TRAC-PF1/MOD2 and TRAC-M model) and without flow-area ratios (TRAC-PF1/MOD1 model) in the momentum-convection term.

2.1.7.1. Reversible and Irreversible Form Losses. With flow-area ratios in the momentum-convection term, TRAC approximately conserves convected momentum and evaluates only the reversible form losses of the Bernoulli equation. The TRAC user becomes responsible for input specifying all irreversible form losses due to abrupt or semi-abrupt flow-area expansions and contractions, thin-plate-orifice-type flow restrictions, and flow redirection (turning) at an elbow or tee, as discussed in Appendix I, Section I.1. Without flow-area ratios, the TRAC-PF1/MOD1-type momentum-convection term does not conserve convected momentum. That error can be shown to be the irreversible form loss of an abrupt expansion and approximately twice the irreversible form loss of an abrupt contraction. A flow-area change between mesh cells in TRAC-PF1/MOD1 calculation adds such an irreversible form loss that is appropriate for an abrupt expansion but in all other situations adds too much irreversible form loss. TRAC users who have prepared TRAC-PF1/MOD1 input-data plant models have compensated for such added irreversible form-loss error by not including other irreversible form losses at flow restrictions or at elbows and tees in order to evaluate the correct overall pressure drop through a portion or all of a flow loop. TRAC-PF1/MOD2 or TRAC-M users who inherit and convert such TRAC-PF1/MOD1 input-data files into TRAC-PF1/MOD2 (or TRAC-M) input-data files need to be aware that their plant model may have built-in compensating-error features for TRAC-PF1/MOD1 that, when evaluated by TRAC-PF1/MOD2 or TRAC-M, give wrong results. The user's response to this situation should be to never use converted TRAC-PF1/MOD1 input-data files blindly. All mesh-cell interface flow areas and mesh-cell volumes and lengths (whose ratio defines mesh-cell flow area) need to be checked against plant specifications, and all input-specified FRICs or K-factors (and those that have not been specified) need to be defined to account for their actual irreversible form losses at abrupt or semi-abrupt flow-area changes, flow restrictions, and flow turns (redirections).

TRAC assists MOD1, MOD2, and TRAC-M users by not requiring them to determine FRIC or K-factor values at abrupt expansion or contraction 1D component mesh-cell interfaces for input specification. TRAC does this internally when the user inputs the friction-factor-correlation option array NFF with a negative value at selected mesh-cell interfaces. At all such interfaces, all three versions of TRAC internally evaluate the standard K-factor formulas in Appendix I, Section I.1., for abrupt-expansion [$K = (1 - A_{min}/A_{max})^2$] and abrupt-contraction [$K = 0.5 - 0.7(A_{min}/A_{max}) + 0.2\,(A_{min}/A_{max})^2$] form losses based on mesh-cell flow areas and add them as FRICs to the input-specified FRICs or K-factors (converted to FRICs). TRAC-PF1/MOD1 also subtracts its momentum-convection term finite-difference error [$K = (1 - A_{min}/A_{max})^2$] to correctly evaluate the reversible plus irreversible form loss at interfaces where NFF < 0. Thus, all 1D mesh-cell interfaces having NFF < 0 model reversible plus irreversible abrupt-area-change form losses correctly (and in the same way) in MOD1, MOD2, and TRAC-M. This feature was extended in TRAC-PF1/MOD2 to 3D VESSEL components as well (this VESSEL extension was brought over to TRAC-M), where rather than inputting NFF < 0 (NFF is not a VESSEL-component input parameter), the MOD2 (and TRAC-M) user inputs the 3D friction-factor correlation coefficients CFZL–R < 0, CFZL–T < 0, and CFZL–Z < 0. Inputting negative values for the *X*- or *R*-, *Y*- or θ-, and *Z*-interface FRICs or K-factor results in MOD2 and TRAC-M internally evaluating an abrupt expansion or contraction (based on the fluid-phase flow direction) form loss and adding to it the absolute value of the input FRIC or K-factor. If the user does not want to add an additional input-specified FRIC or K-factor, a small negative value such as –1.0E-20 should be input.

2.1.7.2. Special Cases. The definition of flow-area ratios and irreversible form losses when evaluating momentum convection in BREAK, PLENUM, TEE, and VESSEL components needs further consideration. These special situations are handled in TRAC-PF1/MOD2 and TRAC-M in the following way.

2.1.7.2.1. BREAK Component. TRAC-PF1/MOD1 models a BREAK component with its mesh cell having either the same flow area as the adjacent-component mesh cell (IVDV = 0) or an infinitely large containment-room volume (IVDV = 1). Its input-specified VOLIN is not used. TRAC-PF1/MOD2 and TRAC-M specify this differently with more generality by defining the BREAK mesh-cell flow area by VOLIN / DXIN (which allows all possible flow-area changes to be modeled across the BREAK junction). The option parameter IVDV is no longer input. The BREAK-junction equation of motion is evaluated in the usual manner by the adjacent component's junction-interface equation of motion. Its momentum-convection term flow-area ratios are defined based on VOLIN and DXIN (from the BD array) defining the flow area of the BREAK mesh cell.

When the flow area changes between the BREAK mesh cell and the adjacent-component mesh cell, we recommend that at the junction interface in the adjacent component's input-data specification, the user set NFF < 0 if the area change is abrupt or input an appropriate FRIC or K-factor for the fluid-flow direction and the area change. It is important that the actual flow-area-change irreversible form loss be applied to provide a

dissipative term in the equation of motion to determine the correct and numerically stable solution. A BREAK component is a pressure boundary condition that locally removes a degree of freedom from the hydrodynamic solution. The equation set becomes locally stiffer and more sensitive to error growth when there is not a dissipative term.

For flow from the adjacent component into the BREAK component when the flow area is expanding, the donor-cell convection approximation's stabilizing effect is reduced in the momentum-convection term due to the flow-area ratios. Including the flow-area expansion irreversible form loss stabilizes the equation of motion by providing a dissipative term that compensates for the loss of the stabilizing effect from the donor-cell convection approximation with flow-area ratios. For flow from the BREAK component, TRAC assumes no momentum flux in the BREAK component. This has been found to be stable. This implies that, for flow into a BREAK component, TRAC is treating the BREAK pressure as a static pressure. For flow out of a BREAK component, the pressure is assumed to be a total pressure. For large BREAK-component volumes, both pressures are the same.

2.1.7.2.2. PLENUM Component. The PLENUM component is a single mesh cell with NPLJN junction interfaces connected to 1D components. The PLENUM component in TRAC is programmed to convect momentum across the PLENUM mesh cell in one coordinate direction only. The TRAC user specifies through input that the first JUNS1 junctions are on Side 1, the next JUNS2 junctions are on Side 2 (directly across the PLENUM mesh cell from Side 1), and the remaining NPLJN – JUNS1 – JUNS2 junctions are on the other sides of the plenum mesh cell. For these later junctions, we assume the PLENUM mesh cell has an infinite flow area with zero momentum flux at its center from or to each of these junctions. The PLENUM mesh-cell flow area associated with each Side 1 or Side 2 junction j is VOL/DX_j times the ratio of the junction j flow area to the sum of all junction flow areas on its side. This defines the PLENUM mesh-cell flow area which is passed through the BD array to determine the flow-area ratios for the momentum-convection term of the junction j equation of motion. Momentum is convected across the PLENUM mesh cell by assuming that junction j on Side 1 shares a common portion of the VOL/DX_j flow area with junction MIN(JUNS1+j, JUNS1+JUNS2) on Side 2 and that junction j on Side 2 shares a common portion of the VOL/DX_j flow area with junction MIN(j – JUNS1, JUNS1) on Side 1. This is a rather simple model for coupling a junction on Side 1 with a junction on Side 2 in order to convect momentum between them across the PLENUM mesh cell.

Flow-area ratios should be defined by partitioning the PLENUM mesh-cell flow area with a junction-to-side volumetric-flow ratio rather than a junction-to-side flow-area ratio, but the explicit velocity feedback from the former for large time-step size can cause numerical instability. This condition is unique to the PLENUM component because momentum convection across the PLENUM component in the stabilizer equation of motion is not coupled implicitly. When the PLENUM component was implemented in TRAC-PF1/MOD1, it was programmed in this limited form to avoid the complexity of

changing the 1D component-network solution. Assuming the momentum flux goes to zero at the center of the PLENUM mesh cell eliminates the need for such coupling. Changing TRAC-PF1/MOD2 to convect momentum across the PLENUM mesh cell should have also involved convecting that momentum with implicit coupling in the stabilizer equation of motion for the JUNS1+JUNS2 junctions. That evaluation is done implicitly for components other than the PLENUM, but it is not coupled across the PLENUM mesh cell. An acceptor-cell approximation for the momentum flux convected out of the PLENUM cell is assumed. The numerical instability of that assumption is controlled by requiring that the flow area of the PLENUM mesh cell be greater that the summed junction flow areas of each side. Through flow-area ratios in the momentum-convection term, the above requirement reduces the destabilizing effect of the acceptor-cell approximation. The PLENUM mesh-cell flow area being larger than the flow area of the junctions on each of its sides is naturally satisfied for most situations where a PLENUM component is used.

2.1.7.2.3. TEE Component. The TEE component has three interface connections to mesh cell JCELL on its primary side. The momentum-convection term in the equation of motion for each of its three interfaces needs to be modified to account for the momentum flux's directional-component contribution to/from the secondary side. In addition, the volumetric-flow fraction to/from the secondary side affects the definition of the flow-area ratios. The angle ϕ between the secondary side and the low-numbered mesh-cell end of the primary side determines which of the two primary-side interfaces is coupled to the secondary-side interface through their equation-of-motion momentum-convection term. For $\cos(\phi) > 0$ the $-\cos(\phi)\, V_J$ component of the secondary-side junction J velocity V_J convects momentum to the secondary side from momentum cell JCELL+1/2 when $V_{JCELL+1/2} < 0$; the $-\cos(\phi)\, V_{JCELL+1/2}$ component of the primary-side velocity $V_{JCELL+1/2}$ convects momentum from the primary side to momentum cell J when $V_J > 0$. For $\cos(\phi) < 0$, a similar coupling applies to momentum cell JCELL–1/2. When $\cos(\phi) = 0$ (secondary side is perpendicular to the primary side), no momentum is convected between the primary and secondary sides because the $\cos(\phi)$ velocity component is zero.

The same TEE model as that in TRAC-PF1/MOD1 is used in TRAC-PF1/MOD2 and in TRAC-M. The area-ratio logic for momentum convection is not applied at the three interfaces of TEE-cell JCELL. In addition, abrupt flow-area change (and flow-turning) irreversible form losses are not evaluated for the three interfaces of JCELL when their NFF values are negative. Input for the current TEE component should observe the following:

- Define the TEE main-tube cell-averaged flow areas, VOL(j)/DX(j) for j = JCELL–1, JCELL, and JCELL+1, to be the same as the interface flow areas, FA(j) for j = JCELL and JCELL+1. For JCELLs at a network junction, this applies also to the neighboring component. Define the TEE side-tube first cell's cell-averaged flow area, VOL(1)/DX(1) (i.e., for $j = 1$ in the side-tube input), to be the same as the internal junction interface flow area, FA(1) in the side-tube input.

- Do not use the negative-NFF option at the three JCELL interfaces of TEE components. Abrupt flow-area change and flow-turning irreversible form losses need to be defined by the user through FRIC-array input data.

A thorough discussion of the present status of the MOD2 (and TRAC-M) TEE model is given in Ref. 2-22.

To demonstrate how the TEE momentum source is implemented in the code, we will assume a positive flow, in which case the conservative form of the liquid momentum equation can be written as

$$\mathrm{vol}_j \frac{\partial\left[(1-\alpha_j)\rho_{\ell_j} V_{\ell_{j+1/2}}\right]}{\partial t} + A_{j+1/2}(1-\alpha_j)\rho_{\ell_j} V_{\ell_{j+1/2}} V_{\ell_{j+1/2}} - A_{j-1/2}(1-\alpha_{j-1})\rho_{\ell_{j-1}} V_{\ell_{j-1/2}} V_{\ell_{j-1/2}} = \text{R.H.S.} \quad , \tag{2-135}$$

where R.H.S. stands for the terms on the right-hand side of the equation. After using the chain rule to expand the time-derivative term and substituting in the finite-difference liquid mass equation, we can write the momentum equation as

$$\frac{\partial V_{\ell_{j+1/2}}}{\partial t} + \frac{A_{j-1/2}(1-\alpha_{j-1})\rho_{\ell_{j-1}}}{\mathrm{vol}_j(1-\alpha_j)\rho_{\ell_j}} V_{\ell_{j-1/2}}\left(V_{\ell_{j+1/2}} - V_{\ell_{j-1/2}}\right) = \text{R.H.S.} \tag{2-136}$$

We do not use this form of the momentum equation directly because it requires major changes to the way that the code passes boundary information between components. Applying the finite-difference mass equation again, we can eliminate $A_{j-1/2}(1-\alpha_{j-1})\rho_{\ell_{j-1}} V_{\ell_{j-1/2}}$ to produce

$$\frac{\partial V_{\ell_{j+1/2}}}{\partial t} + \frac{A_{j+1/2}}{\mathrm{vol}_j} V_{\ell_{j+1/2}}\left(V_{\ell_{j+1/2}} - V_{\ell_{j-1/2}}\right) + \frac{V_{\ell_{j+1/2}} - V_{\ell_{j-1/2}}}{(1-\alpha_j)\rho_{\ell_j}} \frac{\partial\left[\left(1-\alpha_j\right)\rho_{\ell_j}\right]}{\partial t} = \text{R.H.S.} \tag{2-137}$$

If a TEE junction is present at a 1D cell, we add the following term to the left side of Eq. (2-135):

$$-A_T(1 - \alpha_T)\rho_{\ell_T} V_T V_T \cos\phi \quad , \tag{2-138}$$

where the subscript T indicates the first cell in the side leg of the TEE or the interface between the j^{th} cell of the primary (through input, this cell is labeled JCELL) and the first cell in the side leg, depending on the type of variable, and ϕ is the angle of incidence of the TEE side leg from the direction of lower-numbered cells in the primary tube. After we convert this modified momentum equation to a form similar to Eq. (2-137), we obtain a correction to the left side of the difference equation for liquid motion in the form

$$-\frac{A_T(1-\alpha_T)\rho_{\ell_T}}{\mathrm{vol}_j(1-\alpha_j)\rho_{\ell_j}} V_T\left(V_{j-1/2}+V_T\cos\phi\right) \quad . \tag{2-139}$$

As far as time levels are concerned, we evaluate this term in a linearized implicit manner that is consistent with the rest of the 1D momentum-flux term. In the standard two-step notation, it is

$$-\frac{A_T(1-\alpha_T)\rho_{\ell_T}}{\mathrm{vol}_j(1-\alpha_j)\rho_{\ell_j}} \left[\tilde{V}_T^{n+1}\left(2\tilde{V}_T^n\cos\phi+\tilde{V}_{j-1/2}^n\right) + \tilde{V}_T^n\tilde{V}_{j-1/2}^{n+1}-\tilde{V}_T^n\left(\tilde{V}_{j-1/2}^n+\tilde{V}_T^n\cos\phi\right) \right] \quad . \tag{2-140}$$

The vapor equation uses a similar term. Subroutine ETEE generates the quantities necessary for these source terms, and subroutines StbVel1D (FEMOM in TRAC-M/F77) and TF1DS1 add the source terms to the momentum equations.

2.1.7.2.4. VESSEL Component. Using flow-area ratios to correctly donor-cell the approximate momentum flux at a mesh-cell center (based on its interface-defined velocity a half mesh-cell distance away) is done only for momentum that is convected by its own component-direction velocity. This is not done in the cross-derivative terms of the divergence operator for momentum convection as shown in Eqs. (2-104), (2-108), and (2-109).

Flow-area ratios are evaluated using the mesh-cell average flow area, $\mathrm{vol}_{i,j,k}/\Delta_d$, where $d = i, j,$ or k defines the component direction of the equation of motion. When the structure volume fraction within a 3D mesh cell is nonuniform in the d direction, the average flow area for the mesh cell can be incorrectly defined by $\mathrm{vol}_{i,j,k}/\Delta_d$. Nonphysical mesh-cell flow areas affect the pressure solution through the Bernoulli equation by not approximating the donor-cell-approximated velocity components at the mesh-cell centers correctly. Locating 3D mesh-cell interfaces on planes of structure volume-fraction discontinuity can minimize this modeling difficulty. A modeling example that is difficult to handle correctly is representing the internal structure curved surface of a pressure vessel that bisects mesh cells in the vessel lower plenum.

A source connection to a 3D VESSEL component by a 1D component uses the $\mathrm{vol}_{i,j,k}$ and Δ_d geometry parameters of the (i,j,k) mesh cell, whose d-direction interface it is connected to, to define the 3D mesh-cell flow area for evaluating the source-connection junction momentum-convection term flow-area ratios. The actual d-direction flow area in the VESSEL component that the 1D component flow is expanding or contracting into may be significantly different from $\mathrm{vol}_{i,j,k}/\Delta_d$. The sides of the mesh-cell volume $\mathrm{vol}_{i,j,k}$ that the source-connection flow expands or contracts into may not be physical-structure surfaces

that limit the flow area as in a 1D component pipe. Again the user needs to be aware of this when defining mesh-cell interface planes and source connections to 3D mesh cells. The effect that the resulting incorrect flow-area ratios has on evaluating a Bernoulli-equation solution needs to be recognized. These area ratios also affect the irreversible flow loss evaluated by TRAC when NFF < 0 at the 1D component source-connection junction.

2.1.8. A Synopsis of TRAC-M/F90 Solution Procedures

Solution procedures will be discussed at three levels. At the highest level, the general solution steps will be outlined for the two numerical methods approximating the flow equations (semi-implicit and SETS). At some point each of these numerical methods requires the solution of a system of nonlinear equations. A summary is provided of the Newton iteration used for both cases. Each iteration of the nonlinear solution and all stabilizer steps of the SETS method produce a sparse system of linear equations. This most basic aspect of the code's solution procedure is also described below.

Below are six subsections. The first subsection describes the overall solution strategy in terms of the computational flow. The next two subsections give the details of the basic solution strategy, as illustrated by a simple 1D problem and extensions to the solution strategy required for 3D flows, respectively. Section 2.1.8.4. describes the special capacitance matrix solution applied to any 3D blocks of a system matrix. The last two subsections describe the treatment of special numerical and physical situations, including water packing, critical flow, CCFL, and offtake of separated phases from horizontal pipes.

Note: **Differences from TRAC-M/F77.** Two TRAC-M/F90 development activities for Version 3.0 significantly improved the data interfaces within the code as compared to TRAC-M/F77. They also laid the groundwork for communication in a parallel execution of the main computational engine of the code. The first activity fully separated the evaluation of terms in the flow equations from the solution of the resulting system of linear equations. This provided a well defined location for equation terms, and eliminated the need for generation of this data for 1D components, before evaluation of the equations in 3D components. The second task dealt directly with the problem of inter-component data communication, requiring only one request at initialization to establish automatic information passing between components. This was implemented as a system service, with sufficient generality to permit later use by higher order and more implicit difference methods. Details on the data structures that were developed to implement the new equation solution procedures and inter-component communication are given in the TRAC-M/F90 Programmer's Manual (Ref. 2-23.).

2.1.8.1. Overall Solution Strategy. Solving the equations should be viewed from two perspectives. In the broadest view, we are solving an approximation to the partial differential equations modeling two-phase flow. In this context, time and spatial location are independent variables, and physical properties (pressure, temperature, etc.) are

dependent variables of the system. Initial and boundary conditions are available, and the solution is integrated forward in time over the spatial domain of the problem. Within this program, the time integration is driven by subroutine TRANS or subroutine STEADY (transient evolution to a steady-state configuration). The size of the next step forward in time is selected by a call to subroutine TIMSTP. Details of the solution within a given step in time are driven through calls to subroutines PREP, HOUT, and POST.

The second perspective on the solution ignores the original partial differential equations. Within a given time step, one or more systems of algebraic equations must be solved to obtain the state of the system at the end of the time step. In this context, time and spatial location are not independent variables. They are just contributions to constants within the algebraic equations. The independent variables for the algebraic equations are end-of-time-step state variables (e.g., velocity, temperature, pressure, and void fraction). This section takes this perspective, dealing with the solution of the algebraic equations defined in Section 2.1.4.

When using the semi-implicit approximation to the flow equations, subroutines PREP, HOUT, and POST cover three simple stages in the solution of the difference equations (Section 2.1.4.1.). First, all quantities dependent only on the state at the beginning of the time step are evaluated (PREP). This includes heat-transfer and friction coefficients and physical properties such as viscosity and conductivity. Next, the algebraic difference equations are solved (HOUT). Finally, end-of-step values are generated (POST) for various other variables needed for edits or to start the next time step.

For the SETS method, the situation is somewhat more complicated. One step involves equations basically identical to those of the semi-implicit method and is accomplished by the same coding driven from HOUT. However, this semi-implicit step is preceded by a solution of motion equations for "stabilizer" velocities. Given the existing flow of the program through system components, this solution was added to the "PREP" stage of the time step. In addition, stabilizer mass and energy equations are solved after the semi-implicit step. Again because of existing flow of the calculation, this solution was placed in the "POST" stage of the calculation. As a result, SETS involves the solution of flow equations at all three stages of a time step.

Each equation solution follows a similar flow within the program. First, a loop is made over all system components to evaluate terms in the equation and store these terms in a system-wide database. Next, the full system of equations is solved. Finally, another loop over all components copies the values of the independent variables from the system-wide database into the component data structure and, when necessary, evaluates dependent variables.

2.1.8.2. Basic Solution Strategy. Almost all aspects of the equation solution procedure can be illustrated using the 1D single-phase-flow model introduced in Section 2.1.4. For added clarity, examples will be presented based on some specific flow-path configurations. The solution of equations in the pure semi-implicit method is identical to the solution of the semi-implicit (or "basic") step in SETS. As a result, no

specific discussion is provided for solution when the semi-implicit method is selected (namelist variable NOSETS=1).

To illustrate the 1D portion of the solution, we will describe a specific example for flow in a closed loop (Fig. 2-2.). Cells and cell faces in Fig. 2-2. have been given absolute numbers to facilitate discussion of full system-equation coupling. In terms of component numbering, cells 1–4 in this figure can be considered cells 1–4 of PIPE 1, and cells 5–8 in the figure would be cells 1–4 of PIPE 2.

2.1.8.2.1. Solution of the 1D Stabilizer Motion Equations. The stabilizer motion equations are purely linear in the unknown stabilizer velocities. If the tilde and superscript are dropped for simplicity, the general form for this linear system for the flow loop in Fig. 2-2. is

$$\begin{pmatrix} a_{1,1} & a_{1,2} & 0 & 0 & 0 & 0 & 0 & a_{1,8} \\ a_{2,1} & a_{2,2} & a_{2,3} & 0 & 0 & 0 & 0 & 0 \\ 0 & a_{3,2} & a_{3,3} & a_{3,4} & 0 & 0 & 0 & 0 \\ 0 & 0 & a_{4,3} & a_{4,4} & a_{4,5} & 0 & 0 & 0 \\ 0 & 0 & 0 & a_{5,4} & a_{5,5} & a_{5,6} & 0 & 0 \\ 0 & 0 & 0 & 0 & a_{6,5} & a_{6,6} & a_{6,7} & 0 \\ 0 & 0 & 0 & 0 & 0 & a_{7,6} & a_{7,7} & a_{7,8} \\ a_{8,1} & 0 & 0 & 0 & 0 & 0 & a_{8,7} & a_{8,8} \end{pmatrix} \begin{pmatrix} V_1 \\ V_2 \\ V_3 \\ V_4 \\ V_5 \\ V_6 \\ V_7 \\ V_8 \end{pmatrix} = \begin{pmatrix} b_1 \\ b_2 \\ b_3 \\ b_4 \\ b_5 \\ b_6 \\ b_7 \\ b_8 \end{pmatrix}. \quad (2\text{-}141)$$

One standard linear algebra trick to solve this problem is to break it into blocks that can be more easily solved. One obvious approach would be to isolate the last row and column of the matrix as follows:

$$\left(\begin{array}{cccccccc} a_{1,1} & a_{1,2} & 0 & 0 & 0 & 0 & 0 & a_{1,8} \\ a_{2,1} & a_{2,2} & a_{2,3} & 0 & 0 & 0 & 0 & 0 \\ 0 & a_{3,2} & a_{3,3} & a_{3,4} & 0 & 0 & 0 & 0 \\ 0 & 0 & a_{4,3} & a_{4,4} & a_{4,5} & 0 & 0 & 0 \\ 0 & 0 & 0 & a_{5,4} & a_{5,5} & a_{5,6} & 0 & 0 \\ 0 & 0 & 0 & 0 & a_{6,5} & a_{6,6} & a_{6,7} & 0 \\ 0 & 0 & 0 & 0 & 0 & a_{7,6} & a_{7,7} & a_{7,8} \\ \hline a_{8,1} & 0 & 0 & 0 & 0 & 0 & a_{8,7} & a_{8,8} \end{array}\right) \begin{pmatrix} V_1 \\ V_2 \\ V_3 \\ V_4 \\ V_5 \\ V_6 \\ V_7 \\ V_8 \end{pmatrix} = \begin{pmatrix} b_1 \\ b_2 \\ b_3 \\ b_4 \\ b_5 \\ b_6 \\ b_7 \\ b_8 \end{pmatrix}. \quad (2\text{-}142)$$

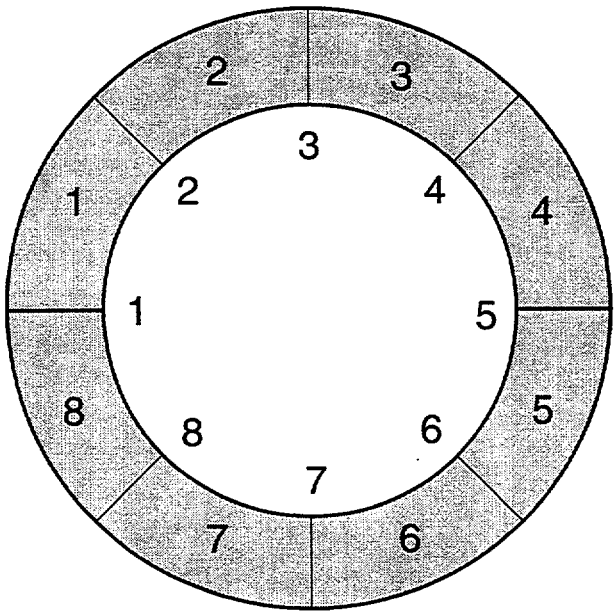

Fig. 2-2. Flow loop for an example of 1D solution.

This can then be written more clearly as the following problem:

$$\begin{pmatrix} a_{1,1} & a_{1,2} & 0 & 0 & 0 & 0 & 0 \\ a_{2,1} & a_{2,2} & a_{2,3} & 0 & 0 & 0 & 0 \\ 0 & a_{3,2} & a_{3,3} & a_{3,4} & 0 & 0 & 0 \\ 0 & 0 & a_{4,3} & a_{4,4} & a_{4,5} & 0 & 0 \\ 0 & 0 & 0 & a_{5,4} & a_{5,5} & a_{5,6} & 0 \\ 0 & 0 & 0 & 0 & a_{6,5} & a_{6,6} & a_{6,7} \\ 0 & 0 & 0 & 0 & 0 & a_{7,6} & a_{7,7} \end{pmatrix} \begin{pmatrix} V_1 \\ V_2 \\ V_3 \\ V_4 \\ V_5 \\ V_6 \\ V_7 \end{pmatrix} = \begin{pmatrix} b_1 \\ b_2 \\ b_3 \\ b_4 \\ b_5 \\ b_6 \\ b_7 \end{pmatrix} - \begin{pmatrix} a_{1,8} \\ 0 \\ 0 \\ 0 \\ 0 \\ 0 \\ a_{7,8} \end{pmatrix} V_8 \qquad (2\text{-}143)$$

and

$$a_{8,1}V_1 + a_{8,7}V_7 + a_{8,8}V_8 = b_8 \ . \qquad (2\text{-}144)$$

Equation (2-143) is solved to obtain velocities V_1 through V_7 as linear functions of V_8. The existence of two constant vectors on the right-hand side of the equation means that two solutions of a 7×7 system are required. However, use of an L-U (lower-upper) decomposition method substantially reduces the cost of the second solution. Once these solutions are available, the specific linear expressions for V_1 and V_7 as functions of V_8 are

substituted into Eq. (2-144) and a value of V_8 is obtained. Back-substitution of this value into the equations for the other velocities completes the solution.

The current version of TRAC-M is not quite as selective as the previous example in isolating submatrices for solution. When the basic matrix structure is established, all rows are scanned for the presence of those coefficients not on the main (tridiagonal) band. These rows are designated as "network equations" and variables with the same index as "network variables."

$$\left(\begin{array}{c|ccccccc} a_{1,1} & a_{1,2} & 0 & 0 & 0 & 0 & 0 & a_{1,8} \\ \hline a_{2,1} & a_{2,2} & a_{2,3} & 0 & 0 & 0 & 0 & 0 \\ 0 & a_{3,2} & a_{3,3} & a_{3,4} & 0 & 0 & 0 & 0 \\ 0 & 0 & a_{4,3} & a_{4,4} & a_{4,5} & 0 & 0 & 0 \\ 0 & 0 & 0 & a_{5,4} & a_{5,5} & a_{5,6} & 0 & 0 \\ 0 & 0 & 0 & 0 & a_{6,5} & a_{6,6} & a_{6,7} & 0 \\ 0 & 0 & 0 & 0 & 0 & a_{7,6} & a_{7,7} & a_{7,8} \\ \hline a_{8,1} & 0 & 0 & 0 & 0 & 0 & a_{8,7} & a_{8,8} \end{array}\right)\left(\begin{array}{c} V_1 \\ V_2 \\ V_3 \\ V_4 \\ V_5 \\ V_6 \\ V_7 \\ V_8 \end{array}\right) = \left(\begin{array}{c} b_1 \\ b_2 \\ b_3 \\ b_4 \\ b_5 \\ b_6 \\ b_7 \\ b_8 \end{array}\right) . \qquad (2\text{-}145)$$

Solving Eq. (2-145) is analogous to the steps outlined for Eq. (2-143). In this instance, the central tridiagonal matrix block is reduced to provide velocities V_2 through V_7 as linear functions of V_1 and V_8 (e.g., $V_j = V_{0,j} + c_{j,1} V_1 + c_{j,8} V_{8,j} = 2,7$). The resulting equations are substituted into the two isolated rows of Eq. (2-145) to obtain the following pair of network equations involving only V_1 and V_8:

$$(a_{1,1} + a_{1,2}c_{2,1})V_1 + (a_{1,2}c_{2,8} + a_{1,8})V_8 = b_1 - a_{1,2}V_{0,2} \text{ and} \qquad (2\text{-}146)$$

$$(a_{8,1} + a_{8,7}c_{7,1})V_1 + (a_{8,7}c_{7,8} + a_{8,8})V_8 = b_8 - a_{8,7}V_{0,7} . \qquad (2\text{-}147)$$

This closed system is solved for V_1 and V_8. Back-substitution of these values into the equations for V_2 through V_7 completes the solution of the system.

2.1.8.2.2. Solving the SETS Semi-Implicit Step. After the stabilizer motion equations are solved, the version of SETS implemented in TRAC-M proceeds to solve the semi-implicit (or "basic") equations for motion, mass, and energy. Apart from the use of stabilizer velocities in the momentum-transport term (and the special flux operator for two-phase flow), these equations are equivalent to the standard semi-implicit method used before TRAC-PF1 was developed. (Currently, the 3D VESSEL can be run in semi-implicit mode according to user option. Future versions of TRAC-M will allow both 1D and 3D components to be run in semi-implicit mode, according to user option.) Thus, solving the pure semi-implicit method and solving the semi-implicit step in SETS are identical.

The system solution begins by treating the new-time velocity as a dependent variable, reducing the motion equation at each cell edge to obtain the new-time velocity as a linear function of the pressure difference across that edge. In our single-phase example, Eq. (2-67) is rearranged to the form

$$V_{j+1/2}^{n+1} = \frac{V_{j+1/2}^{n} - \Delta t\left(V_{j+1/2}^{n}\nabla_{j+1/2}\tilde{V}_{j+1/2}^{n+1} - \beta V_{j+1/2}^{n}\nabla_{j+1/2}\tilde{V}_{j+1/2}^{n} + \dfrac{\tilde{P}_{j+1}^{n+1} - \tilde{P}_{j}^{n+1}}{\langle\rho\rangle_{j+1/2}^{n}\Delta x}\right)}{1 + \Delta t(2K_{j+1/2}^{n}\left|V_{j+1/2}^{n}\right| + \beta\nabla_{j+1/2}\tilde{V}_{j+1/2}^{n})} . \tag{2-148}$$

For the two-phase equations, the equivalent step requires simultaneous solution of the liquid and gas momentum equations at each face (2×2 linear system). This solution is accomplished in subroutine TF1DS1 for the 1D and in TF3DS1 for the 3D flow equations. At the same time, the following key variable is defined and stored for later use in updating velocities as

$$\left.\frac{dV}{dP}\right|_{j+1/2} = \frac{\Delta t}{\langle\rho\rangle_{j+1/2}^{n}\Delta x[1 + \Delta t(2K_{j+1/2}^{n}\left|V_{j+1/2}^{n}\right| + \beta\nabla_{j+1/2}\tilde{V}_{j+1/2}^{n})]} . \tag{2-149}$$

The mass and energy equations are nonlinear in the independent variables and must be solved with an iterative technique. Here a standard Newton iteration is applied. If the i^{th} approximation to the solution is given, the next level of approximation is written as

$$\tilde{T}_{j}^{n+1,i+1} = \tilde{T}_{j}^{n+1,i} + \delta T_{j} \text{ and}$$

$$\tilde{P}_{j}^{n+1,i+1} = \tilde{P}_{j}^{n+1,i} + \delta P_{j} . \tag{2-150}$$

The pressure definition can be substituted into Eq. (2-148) and simplified with the definition in Eq. (2-149) to give the following expression for the latest approximation to velocity as a linear function of the latest pressure changes:

$$V_{j+1/2}^{n+1,i+1} = V_{j+1/2}^{n+1,i} + \left.\frac{dV}{dP}\right|_{j+1/2}(\delta P_{j} - \delta P_{j+1}) . \tag{2-151}$$

These expressions are applied to the semi-implicit mass and energy equations [Eqs. (2-57) and (2-58)] through the direct substitutions

$$\tilde{P}_{j}^{n+1} \Rightarrow \tilde{P}^{n+1,i} + \delta P_{j} ,$$

$$\tilde{T}_{j}^{n+1} \Rightarrow \tilde{T}_{j}^{n+1,i} + \delta T_{j} , \text{ and}$$

$$V_{j+1/2}^{n+1} \Rightarrow V_{j+1/2}^{n+1,i} + \left.\frac{dV}{dP}\right|_{j+1/2} (\delta P_j - \delta P_{j+1}) \ .$$

Use of the state relationships $[\rho(P,T)]$ and $[e(P,T)]$ and a first-order Taylor series expansion produces the linearized mass equation

$$\left(\left.\frac{\partial \rho}{\partial T}\right|_j^{n+1,i} \delta T_j + \left.\frac{\partial \rho}{\partial P}\right|_j^{n+1,i} \delta P_j\right)/(\Delta t)$$

$$+ \frac{\left[\langle\rho\rangle_{j+\frac{1}{2}}^{n} \left.\frac{dV}{dP}\right|_{j+1/2} (\delta P_j - \delta P_{j+1}) - \langle\rho\rangle_{j-1/2}^{n} \left.\frac{dV}{dP}\right|_{j-1/2} (\delta P_{j-1} - \delta P_j)\right]}{\Delta x} \qquad (2\text{-}152)$$

$$= -\frac{\tilde{\rho}_j^{n+1,i} - \rho_j^n}{\Delta t} - \frac{\partial}{\partial x_j}(\rho^n V^{n+1,i})$$

and the linearized energy equation

$$\left(\left.\frac{\partial \rho}{\partial T}\right|_j^{n+1,i} \tilde{e}_j^{n+1,i} + \tilde{\rho}_j^{n+1,i} \left.\frac{\partial e}{\partial T}\right|_j^{n+1,i}\right) \delta T_j/\Delta t$$

$$+ \left(\left.\frac{\partial \rho}{\partial P}\right|_j^{n+1,i} \tilde{e}_j^{n+1,i} + \tilde{\rho}_j^{n+1,i} \left.\frac{\partial e}{\partial P}\right|_j^{n+1,i}\right) \delta P_j/\Delta t$$

$$+ \frac{\left[\langle\rho e\rangle_{j+1/2}^{n} \left.\frac{dV}{dP}\right|_{j+1/2} (\delta P_j - \delta P_{j+1}) - \langle\rho e\rangle_{j-1/2}^{n} \left.\frac{dV}{dP}\right|_{j-1/2} (\delta P_{j-1} - \delta P_j)\right]}{\Delta x}$$

$$+ \tilde{P}_j^{n+1,i} \frac{\left[\left.\frac{dV}{dP}\right|_{j+1/2} (\delta P_j - \delta P_{j+1}) - \left.\frac{dV}{dP}\right|_{j-1/2} (\delta P_{j-1} - \delta P_j)\right]}{\Delta x} + \delta \tilde{P}_j \frac{V_{j+1/2}^{n+1,i} - V_{j-1/2}^{n+1,i}}{\Delta x}$$

$$= -\frac{(\tilde{\rho}_j^{n+1,i} \tilde{e}_j^{n+1,i} - (\rho e)_j^n)}{\Delta t} - \frac{\partial}{\partial x^j}(\rho^n e^n V^{n+1,i}) - \tilde{P}_j^{n+1,i} \frac{V_{j+1/2}^{n+1,i} - V_{j-1/2}^{n+1,i}}{\Delta x} \ . \qquad (2\text{-}153)$$

For the particular block-reduction technique used to solve this system of linear equations, an auxiliary variable is defined as

$$\Delta P_{j+1/2} = \delta P_{j+1} - \delta P_j \ . \qquad (2\text{-}154)$$

This results in a set of linear equations for each cell in the form

$$\begin{pmatrix} a_{j,1,1} & a_{j,1,2} \\ a_{j,2,1} & a_{j,2,2} \end{pmatrix} \begin{pmatrix} \delta P_j \\ \delta T_j \end{pmatrix} = \begin{pmatrix} b_{j,1} \\ b_{j,2} \end{pmatrix} - \begin{pmatrix} c_{1j,1} \\ c_{1j,2} \end{pmatrix} \Delta P_{j-1/2} + \begin{pmatrix} c_{rj,1} \\ c_{rj,2} \end{pmatrix} \Delta P_{j+1/2} \,. \tag{2-155}$$

The first row in the above linear system can be considered to be the linearized mass conservation equation and the second to be the linearized energy equation. At each cell, this system is solved for the pressure and temperature variations in the form

$$\begin{pmatrix} \delta P_j \\ \delta T_i \end{pmatrix} = \begin{pmatrix} b'_{j,1} \\ b'_{j,2} \end{pmatrix} - \begin{pmatrix} c'_{1j,1} \\ c'_{1j,2} \end{pmatrix} \Delta P_{j-1/2} + \begin{pmatrix} c'_{rj,1} \\ c''_{rj,2} \end{pmatrix} \Delta P_{j+1/2} \,. \tag{2-156}$$

At this point, the b' constants represent the linearized predictions of change in pressure and temperature assuming no further velocity changes at the cell faces. The c' coefficients account for contributions due to velocity changes (driven by changes in the pressure gradient).

The solution of the basic equations is completed in two steps. First, for each block represented by Eq. (2-156), the pressure equation is isolated and Eq. (2-154) is substituted to provide a set of 10 equations in the form

$$-c_{1j,1}\delta P_{j-1} + (1 + c_{1j,1} + c_{rj,1})\delta P_j - c_{rj,1}\delta P_{j+1} = b_j \,. \tag{2-157}$$

This results in a system with the same form as the stabilizer velocity equations,

$$\begin{pmatrix} a_{1,1} & a_{1,2} & 0 & 0 & 0 & 0 & 0 & a_{1,8} \\ a_{2,1} & a_{2,2} & a_{2,3} & 0 & 0 & 0 & 0 & 0 \\ 0 & a_{3,2} & a_{3,3} & a_{3,4} & 0 & 0 & 0 & 0 \\ 0 & 0 & a_{4,3} & a_{4,4} & a_{4,5} & 0 & 0 & 0 \\ 0 & 0 & 0 & a_{5,4} & a_{5,5} & a_{5,6} & 0 & 0 \\ 0 & 0 & 0 & 0 & a_{6,5} & a_{6,6} & a_{6,7} & 0 \\ 0 & 0 & 0 & 0 & 0 & a_{7,6} & a_{7,7} & a_{7,8} \\ a_{8,1} & 0 & 0 & 0 & 0 & 0 & a_{8,7} & a_{8,8} \end{pmatrix} \begin{pmatrix} \delta P_1 \\ \delta P_2 \\ \delta P_3 \\ \delta P_4 \\ \delta P_5 \\ \delta P_6 \\ \delta P_7 \\ \delta P_8 \end{pmatrix} = \begin{pmatrix} b_1 \\ b_2 \\ b_3 \\ b_4 \\ b_5 \\ b_6 \\ b_7 \\ b_8 \end{pmatrix}, \tag{2-158}$$

which is solved with the same procedure outlined for Eq. (2-145). The resulting values of δPs are first substituted into Eq. (2-154) to obtain a set of ΔP values, which are then substituted into the second row of Eq. (2-156) to provide values for temperature changes. The variations in pressure and temperature are substituted into Eq. (2-150) to provide an improved approximation to the new-time variables. The ΔP values are also fed to Eq. (2-151) to obtain new-time velocities, which are consistent with the updated pressure field. If variations in pressure and temperature are small enough, the iteration is

terminated. If not, the linearized equations are evaluated again to generate the next approximate solution.

The iteration usually is started by setting the initial guess at the solution to the beginning of time-step values (e.g., $P_j^{n+1,0} = P_j^n$). The only exceptions occur in the full two-phase equations. When the old-time void fraction is zero but a prediction-based flux and phase change indicates appearance of gas, an explicit evaluation of the gas mass equation is used to provide an initial estimate of the new-time void fraction. When the first appearance of noncondensable gas is predicted, information from an explicit noncondensable mass equation is added to provide an estimate of the new-time partial pressure of noncondensable gas.

Use of old-time quantities to start the iteration provides an easy cure to situations in which the initial guess is beyond the convergence radius of the method. The new-time values must approach the old-time values as the time-step size approaches zero. If an iteration fails to converge, the time-step size is reduced and the solution is retried at the new-time-step size. Preemptive action is also taken to minimize convergence problems. If more than five iterations are required to converge the solution on a given time step, the size of the next step is reduced by the ratio of five divided by the last iteration count.

2.1.8.2.3. Solution of the SETS Stabilizer Mass and Energy Equations. The final step in the SETS method is the solution of the stabilizer mass and energy equations. At this point, the new-time velocities have been determined and can be treated as constants in the solution of the equations. The equations vary from the mass and energy equations of the semi-implicit step only in that the densities and energies in flux terms are now evaluated at the new time.

The mass and energy equations are linear in ρ^{n+1} and $(\rho e)^{n+1}$ respectively, with a structure that is basically tridiagonal. For the loop flow problem, the general form of the mass equation can be written as

$$\begin{pmatrix} a_{1,1} & a_{1,2} & 0 & 0 & 0 & 0 & 0 & a_{1,8} \\ a_{2,1} & a_{2,2} & a_{2,3} & 0 & 0 & 0 & 0 & 0 \\ 0 & a_{3,2} & a_{3,3} & a_{3,4} & 0 & 0 & 0 & 0 \\ 0 & 0 & a_{4,3} & a_{4,4} & a_{4,5} & 0 & 0 & 0 \\ 0 & 0 & 0 & a_{5,4} & a_{5,5} & a_{5,6} & 0 & 0 \\ 0 & 0 & 0 & 0 & a_{6,5} & a_{6,6} & a_{6,7} & 0 \\ 0 & 0 & 0 & 0 & 0 & a_{7,6} & a_{7,7} & a_{7,8} \\ a_{8,1} & 0 & 0 & 0 & 0 & 0 & a_{8,7} & a_{8,8} \end{pmatrix} \begin{pmatrix} \rho_1 \\ \rho_2 \\ \rho_3 \\ \rho_4 \\ \rho_5 \\ \rho_6 \\ \rho_7 \\ \rho_8 \end{pmatrix} = \begin{pmatrix} b_1 \\ b_2 \\ b_3 \\ b_4 \\ b_5 \\ b_6 \\ b_7 \\ b_8 \end{pmatrix}, \quad (2\text{-}159)$$

where superscripts representing new time (n+1) have been dropped. This can be recognized as identical in form to Eq. (2-145) and is solved with the same procedure.

The linear system produced by the stabilizer energy equation has the same coefficient matrix as that of the mass equation. Time is saved by storing matrix factorization steps used in the mass equation solution and by applying the results during the solution of the energy equation.

2.1.8.2.4. Final Solution for a New-Time Void Fraction. Solving the stabilizer mass and energy equations provides new-time values only for macroscopic densities $[\alpha\rho_g, \alpha\rho_a, (1-\alpha)\rho_l]$ and macroscopic energy densities $[\alpha\rho_g e_g, (1-\alpha)\rho_l e_l]$. Experience with the method has shown that when end-of-time-step values are needed in correlations for variables such as temperature or pressure, the values obtained during the solution of the semi-implicit step are adequate. However, the method is more robust if an attempt is made to obtain a better value of the new-time void fraction.

After the stabilizer solution is completed, an approximate solution is obtained in each computational volume to the following equations:

$$\begin{aligned}
&\alpha_j^{n+1}\rho_{g,j}^{n+1} = (\alpha\rho_g)_j^{n+1}, \\
&\alpha_j^{n+1}\rho_{a,j}^{n+1} = (\alpha\rho_a)_j^{n+1}, \\
&(1-\alpha_j^{n+1})\rho_{l,j}^{n+1} = [(1-\alpha)\rho_l]_j^{n+1}, \\
&\alpha_j^{n+1}\rho_{g,j}^{n+1} e_{g,j}^{n+1} = (\alpha\rho_g e_g)_j^{n+1}, \text{ and} \\
&(1-\alpha_j^{n+1})\rho_{l,j}^{n+1} e_{l,j}^{n+1} = [(1-\alpha)\rho_l e_l]_j^{n+1}.
\end{aligned} \tag{2-160}$$

where the right-hand sides are the known results from the stabilizer equations. These equations are linearized with respect to the independent variables P^{n+1}, $T_g^{n+1}, T_l^{n+1}, P_a^{n+1}$, and α^{n+1}. The starting point of the linearization is taken to be the values of the corresponding variables obtained after the last iteration of the solution to the semi-implicit step. Thus, the values of the independent variables become

$$\begin{aligned}
&T_{g,j}^{n+1} = \tilde{T}_{g,j}^{n+1} + \delta T_{g,j}, \\
&T_{l,j}^{n+1} = \tilde{T}_{l,j}^{n+1} + \delta T_{l,j}, \\
&P_j^{n+1} = \tilde{P}_j^{n+1} + \delta P_j, \\
&P_{a,j}^{n+1} = \tilde{P}_{a,j}^{n+1} + \delta P_{a,j}, \text{ and} \\
&\alpha_j^{n+1} = \tilde{\alpha}_j^{n+1} + \delta\alpha_j.
\end{aligned} \tag{2-161}$$

These are substituted into Eq. (2-160), and a first-order Taylor expansion is applied. As an example of the results, the linearized macroscopic gas energy density is

$$\left(\tilde{\alpha}_j^{n+1}\frac{\partial\tilde{\rho}_g}{\partial T}\bigg|_j^{n+1}\tilde{e}_{g,j}^{n+1}+\tilde{\alpha}_j^{n+1}\tilde{\rho}_{g,j}^{n+1}\frac{\partial\tilde{e}_g}{\partial T}\bigg|_j^{n+1}\right)\delta T_j$$

$$+\left(\alpha_j^{n+1}\frac{\partial\tilde{\rho}_g}{\partial P}\bigg|_j^{n+1}\tilde{e}_{g,j}^{n+1}+\tilde{\alpha}_j^{n+1}\tilde{\rho}_{g,j}^{n+1}\frac{\partial\tilde{e}_g}{\partial P}\bigg|_j^{n+1}\right)\delta P_j$$

$$+\tilde{\rho}_{g,j}^{n+1}\tilde{e}_{g,j}^{n+1}\delta\alpha_j$$

$$=(\alpha\rho_g e_g)_j^{n+1}-\tilde{\alpha}_j^{n+1}\tilde{\rho}_{g,j}^{n+1}\tilde{e}_{g,j}^{n+1}\ . \qquad (2\text{-}162)$$

This equation, combined with the other four linearized equations, produces a 5×5 linear system that is solved by direct Gauss elimination. Although linearized approximations to all new-time variables are available after this solution, only the void fraction is kept for use in the next time step. The other variables are discarded as a result of numerical experiments comparing various approaches. The consistent pressure field resulting from the solution of the semi-implicit step provides the best initial guess for velocities at the next time step. The tendency of temperatures in two-phase problems to follow the saturation temperature makes selection of temperatures consistent with that pressure field a good strategy for the most robust code behavior.

2.1.8.3. Considerations for 3D Solutions. When VESSELS are present, the above procedure is followed, with one key exception in each set of equations. When any VESSEL variable (velocity, δP, ρ, or ρe) occurs in a 1D equation, it is moved to the right-hand side with its coefficient and all 1D variables are solved as functions of the unknown VESSEL variables. These results are substituted as needed into the difference equations for the VESSEL to give a closed set of equations that can be solved for all vessel variables. Values for VESSEL variables are back-substituted into the 1D equations, and final values for all 1D unknowns are obtained.

Specific examples of this process are provided here for the system illustrated in Fig. 2-3. As in Fig. 2-2., cells are given "absolute" numbers rather than a combination of component number and component cell number. For this example, cells numbered 1–5 are in a pipe and cells 6–9 are in a 3D (collapsed to 2D here) VESSEL.

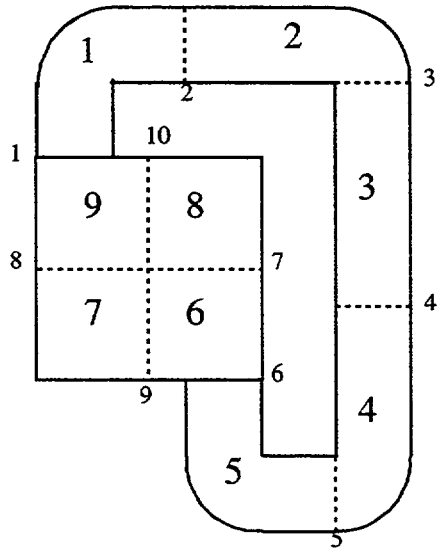

Fig. 2-3. System for 3D solution examples.

The full system of stabilizer momentum equations for the flow loop in Fig. 2-3. is represented by Eq. (2-163). The last block in the coefficient matrix is associated with the radial velocities V_9 and V_{10} and is completely isolated from equations for the axial velocities in the same "3D" region. This reflects the fundamental structure of the 3D stabilizer momentum equations. For example, the axial stabilizer momentum equations evaluate contributions from axial velocities only implicitly. Radial and azimuthal velocities appearing in momentum-transport terms are evaluated explicitly. This results in no coupling coefficients between velocity variables in the axial momentum block and those in the radial (or azimuthal) blocks. In matrix notation, we have

$$\begin{pmatrix} a_{1,1} & a_{1,2} & 0 & 0 & 0 & 0 & 0 & a_{1,8} & 0 & 0 \\ a_{2,1} & a_{2,2} & a_{2,3} & 0 & 0 & 0 & 0 & 0 & 0 & 0 \\ 0 & a_{3,2} & a_{3,3} & a_{3,4} & 0 & 0 & 0 & 0 & 0 & 0 \\ 0 & 0 & a_{4,3} & a_{4,4} & a_{4,5} & 0 & 0 & 0 & 0 & 0 \\ 0 & 0 & 0 & a_{5,4} & a_{5,5} & a_{5,6} & 0 & 0 & 0 & 0 \\ 0 & 0 & 0 & 0 & a_{6,5} & a_{6,6} & a_{6,7} & 0 & 0 & 0 \\ 0 & 0 & 0 & 0 & 0 & a_{7,6} & a_{7,7} & a_{7,8} & 0 & 0 \\ a_{8,1} & 0 & 0 & 0 & 0 & 0 & a_{8,7} & a_{8,8} & 0 & 0 \\ 0 & 0 & 0 & 0 & 0 & 0 & 0 & 0 & a_{9,9} & a_{9,10} \\ 0 & 0 & 0 & 0 & 0 & 0 & 0 & 0 & a_{10,9} & a_{10,10} \end{pmatrix} \begin{pmatrix} V_1 \\ V_2 \\ V_3 \\ V_4 \\ V_5 \\ V_6 \\ V_7 \\ V_8 \\ V_9 \\ V_{10} \end{pmatrix} = \begin{pmatrix} b_1 \\ b_2 \\ b_3 \\ b_4 \\ b_5 \\ b_6 \\ b_7 \\ b_8 \\ b_9 \\ b_{10} \end{pmatrix} . \qquad (2\text{-}163)$$

Solving the 1D portion of this system proceeds as before, isolating the 1D block as

$$\begin{bmatrix} a_{2,2} & a_{2,3} & 0 & 0 \\ a_{3,2} & a_{3,3} & a_{3,4} & 0 \\ 0 & a_{4,3} & a_{4,4} & a_{4,5} \\ 0 & 0 & a_{5,4} & a_{5,5} \end{bmatrix} \begin{bmatrix} V_2 \\ V_3 \\ V_4 \\ V_5 \end{bmatrix} = \begin{bmatrix} b_2 \\ b_3 \\ b_4 \\ b_5 \end{bmatrix} - \begin{bmatrix} a_{2,1} \\ 0 \\ 0 \\ 0 \end{bmatrix} V_1 - \begin{bmatrix} 0 \\ 0 \\ 0 \\ a_{5,6} \end{bmatrix} V_6 \, . \tag{2-164}$$

This is solved to obtain the equation

$$\begin{bmatrix} V_2 \\ V_3 \\ V_4 \\ V_5 \end{bmatrix} = \begin{bmatrix} b'_2 \\ b'_3 \\ b'_4 \\ b'_5 \end{bmatrix} + \begin{bmatrix} c'_{2,1} \\ c'_{3,1} \\ c'_{4,1} \\ c'_{5,1} \end{bmatrix} V_1 + \begin{bmatrix} c'_{2,6} \\ c'_{3,6} \\ c'_{4,6} \\ c'_{5,6} \end{bmatrix} V_6 \, , \tag{2-165}$$

and these results are substituted into the junction equations to obtain

$$(a_{1,1} + a_{1,2}c'_{2,1})V_1 + a_{1,2}c'_{2,6}V_6 = b_1 - a_{1,2}b'_2 - a_{1,8}V_8 \text{ and} \tag{2-166}$$

$$a_{6,5}c'_{5,1}V_1 + (a_{6,6} + a_{6,5}c'_{5,6})V_6 = b_6 - a_{6,5}b'_5 - a_{6,7}V_7 \, . \tag{2-167}$$

Solving the previous two equations gives junction velocities as a linear combination of "3D" velocities as

$$\begin{bmatrix} V_1 \\ V_6 \end{bmatrix} = \begin{bmatrix} b'_1 \\ b'_6 \end{bmatrix} + \begin{bmatrix} c'_{1,7} \\ c'_{6,7} \end{bmatrix} V_7 + \begin{bmatrix} c'_{1,8} \\ c'_{6,8} \end{bmatrix} V_8 \, . \tag{2-168}$$

These two expressions are substituted into the 3D axial flow equations to obtain a final closed set of equations for the 3D axial velocities (V_7 and V_8). The current method used to solve this final equation block is described in the next subsection. Once the 3D velocities are known, the 1D network junction velocities (V_1 and V_6) follow by back-substitution of vessel velocities V_7 and V_8 into Eq. (2-168), and the internal component velocities are obtained in a final stage of the back-substitution of V_1 and V_6 into Eq. (2-165).

A similar solution pattern follows for the pressure equation of the semi-implicit (basic) step and for the stabilizer mass and energy equations.

2.1.8.4. The Capacitance Matrix Method. The capacitance matrix method is applied in TRAC to provide an efficient numerical solution algorithm for solving the multidimensional vessel-matrix equations. Each vessel-matrix equation combines the

multidimensional mesh-cell or interface equations of all vessel components in the modeled system. The external or internal connectivity to the VESSEL component(s) of 1D hydro-component loops introduces nonzero elements into the vessel matrix, coupling the vessel mesh cells or interfaces at the loop source connections to the vessel(s). The vessel-matrix equations that are solved are the semi-implicit pressure vessel-matrix equation in the outer-stage solution and, if the stability-enhanced, two-step, 3D (SETS3D) method is applied in the VESSEL components (NSTAB = 1), the stabilizer motion x- or r-, y- or θ-, and z-direction vessel-matrix equations in the prep-stage solution and the stabilizer mass and energy vessel-matrix equations in the post-stage solution.

TRAC-PF1/MOD1 provided the user with a choice of solving the pressure vessel-matrix equation with a successive line over-relaxation (SLOR) iterative solution algorithm or a direct full-matrix L-U matrix-decomposition solution algorithm. The latter algorithm is more efficient for small vessel matrices of order <50 (<50 vessel mesh cells). For system models with a vessel or vessels having more mesh cells, SLOR is more efficient, but can result in mass and energy conservation error unless the iterative solution algorithm is tightly converged by performing more iterations, which requires more calculative effort.

TRAC-M applies the SETS3D method to the vessel hydrodynamic solution. TRAC-M cannot use the SLOR iterative solution algorithm to solve the stabilizer mass and energy vessel-matrix equations because these equations may lack matrix diagonal dominance (the magnitude of the sum of the off-diagonal elements in any row or column is equal to or greater than the magnitude of the diagonal element). The SLOR iterative solution algorithm requires that the matrix equation satisfy the matrix property of diagonal dominance for the solution algorithm to be numerically stable. The direct full-matrix L-U matrix-decomposition solution algorithm could be used to solve the stabilizer mass and energy equations but would require an excessive amount of calculative effort and computer memory for vessel matrices of order greater than a few hundred. The resolution to this dilemma was to replace both of these algorithms in TRAC-PF1/MOD2 with the capacitance matrix method (Ref. 2-14.), which provides an accurate and numerically stable direct L-U matrix-decomposition solution algorithm while being as efficient as the SLOR iterative solution algorithm for vessel matrices of large order. This method was brought over to TRAC-M. Because the capacitance matrix method is the best choice among all three methods, it is used to solve all forms of the vessel-matrix equations.

The capacitance matrix method is a direct L-U matrix-decomposition solution algorithm like the direct full-matrix L-U matrix-decomposition solution algorithm in TRAC-PF1/MOD1, but it does the L-U matrix decomposition on the banded portion of the vessel matrix with a more efficient banded-matrix solver routine. The banded portion of the vessel matrix includes the nonzero coupling elements between a vessel mesh cell or interface and its six adjacent (neighboring) mesh cells or interfaces in 3D geometry. Nonzero elements outside the bandwidth of the matrix that couple vessel mesh cells or interfaces to nonadjacent mesh cells or interfaces of the same vessel or a different vessel component (due to 1D hydro-component loop connectivity) will be referred to as

nonzero outlying elements. The effect that the nonzero outlying elements have on the matrix-equation solution is accounted for in the capacitance matrix method by a direct full-matrix L-U matrix decomposition of a lower-order capacitance matrix. That solution is used to modify the banded-matrix equation solution to give the desired solution of the vessel matrix with its nonzero outlying elements. The capacitance matrix method was found in a study to be more efficient than a direct full-matrix L-U matrix-decomposition solution of a vessel-matrix equation when fewer than 20% of the vessel-matrix rows have nonzero outlying elements. The test problem in that study had two VESSEL components coupled by PIPE, PUMP, and TEE components. Fig. 2-4. shows the matrix-equation solution CPU times on a Cray X-MP/48 computer versus the matrix order for different numbers of rows having nonzero outlying elements. For most system models (especially those with more than a hundred vessel mesh cells), only a few percent of the vessel-matrix rows have nonzero outlying elements. Thus, for a four-loop plant model with eight rows on nonzero outlying elements, Fig. 2-4. indicates that the capacitance matrix method is faster than a full-matrix method by factors of 2, 4, 8, and 12 for vessel matrices of order 100, 200, 300, and 400, respectively. Similar factors apply to computer memory storage for the vessel-matrix equation by the full-matrix method versus the capacitance matrix method.

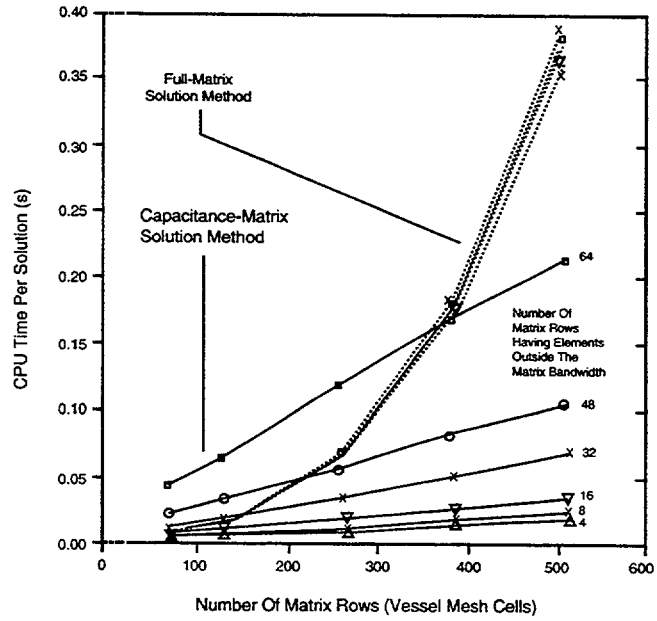

Fig. 2-4. Vessel-matrix equation solution CPU times on a Cray X-MP/48 computer vs. the order of the vessel matrix for different numbers of matrix rows having nonzero outlying elements.

We can summarize the above description of the method by noting that the capacitance matrix method is a direct two-stage procedure. In the first stage, the banded-matrix portion of the matrix equation is solved with an efficient banded-matrix solver to determine the solution for the vessel-matrix equation with zero-valued outlying elements. Then, if there are nonzero outlying elements in the vessel matrix (1D hydro-component loops that connect back to a nonadjacent vessel location generate nonzero outlying elements), the second stage evaluates a direct full-matrix L-U matrix-decomposition solution of a much lower-order capacitance-matrix equation. Doing this accounts for the effect the nonzero outlying elements have on the vessel-matrix equation solution. This results in a modification of the banded-matrix solution to determine the solution of the vessel-matrix equation with nonzero outlying elements.

The following derivation determines the working equations and presents the four-step solution procedure programmed in subroutine MATSOL of TRAC-PF1/MOD2. Given the vessel-matrix equation

$$\underline{\underline{A}} \cdot \underline{x} = \underline{b}\,, \tag{2-169}$$

where $\underline{\underline{A}}$ is a known (vessel) matrix, $\underline{x}$ is an unknown (mass density, velocity, energy, or pressure) vector, and $\underline{b}$ is a known vector, let us partition $\underline{\underline{A}}$ as follows into the sum of its banded matrix $\underline{\underline{B}}$ and a matrix product $\underline{\underline{E}} \cdot \underline{\underline{R}}$ that has only the nonzero elements lying outside the bandwidth:

$$\underline{\underline{A}} \cdot \underline{x} = (\underline{\underline{B}} + \underline{\underline{E}} \cdot \underline{\underline{R}}) \cdot \underline{x} = \underline{b}\,. \tag{2-170}$$

Consider the following example of how a simple form for $\underline{\underline{A}}$ would appear when partitioned.

$$\text{For } \underline{\underline{A}} = \begin{bmatrix} x & x & O & O & O & O \\ x & x & x & O & t & O \\ O & x & x & x & O & O \\ O & O & x & x & x & O \\ r & O & s & x & x & x \\ O & O & O & O & x & x \end{bmatrix}, \text{ a matrix of order } N, \tag{2-171}$$

$$(N \times N)$$

where r, s, t, and x are nonzero elements, $N = 6$ is the total number of rows and columns in $\underline{\underline{A}}$, and $M = 2$ is the number of rows in $\underline{\underline{A}}$ having nonzero elements outside the three-diagonal bandwidth, then define

$$\underline{\underline{A}} = \underline{\underline{B}} + \underline{\underline{E}} \cdot \underline{\underline{R}} \tag{2-172}$$

where

$$\underline{\underline{B}} = \begin{bmatrix} x & x & O & O & O & O \\ x & x & x & O & O & O \\ O & x & x & x & O & O \\ O & O & x & x & x & O \\ O & O & O & x & x & x \\ O & O & O & O & x & x \end{bmatrix} \quad , \quad \underline{\underline{E}} = \begin{bmatrix} O & O \\ O & 1 \\ O & O \\ O & O \\ 1 & O \\ O & O \end{bmatrix}$$

$(N \times N)$ $\qquad$ $(N \times M)$

$$\underline{\underline{R}} = \begin{bmatrix} r & O & s & O & O & O \\ O & O & O & O & t & O \end{bmatrix} \quad , \quad \underline{\underline{E}} \cdot \underline{\underline{R}} = \begin{bmatrix} O & O & O & O & O & O \\ O & O & O & O & t & O \\ O & O & O & O & O & O \\ O & O & O & O & O & O \\ r & O & s & O & O & O \\ O & O & O & O & O & O \end{bmatrix} . \tag{2-173}$$

$(M \times N)$ $\qquad$ $(N \times N)$

Note that the nonzero elements in $\underline{\underline{E}}$ are unity and in $\underline{\underline{R}}$ are the actual nonzero outlying elements of $\underline{\underline{A}}$. The term $\underline{\underline{A}}$ is an $\bar{N} \times N$ matrix with $\bar{M}$ rows having nonzero elements outside its bandwidth, $\underline{\underline{B}}$ is an $N \times N$ banded matrix, $\underline{\underline{E}}$ is an $N \times M$ matrix, and $\underline{\underline{R}}$ is an $M \times N$ matrix.

Multiply Eq. (2-170) by the inverse of the banded matrix, $\underline{\underline{B}}$ to get

$$(\underline{\underline{I}} + \underline{\underline{B}}^{-1} \cdot \underline{\underline{E}} \cdot \underline{\underline{R}}) \cdot \underline{x} = \underline{\underline{B}}^{-1} \cdot \underline{b} . \tag{2-174}$$

Define $\underline{\underline{R}} \cdot \underline{x} = \underline{y}$ and move its term in Eq. (2-174) to the right-hand side of the equation, giving

$$\underline{x} = \underline{\underline{B}}^{-1} \cdot \underline{b} - \underline{\underline{B}}^{-1} \underline{\underline{E}} \cdot \underline{y} . \tag{2-175}$$

Substitute Eq. (2-175) for $\underline{x}$ into Eq. (2-174) to give

$$(\underline{\underline{I}} + \underline{\underline{B}}^{-1} \cdot \underline{\underline{E}} \cdot \underline{\underline{R}}) \cdot (\underline{\underline{B}}^{-1} \cdot \underline{b} - \underline{\underline{B}}^{-1} \cdot \underline{\underline{E}} \cdot \underline{y}) = \underline{\underline{B}}^{-1} \cdot \underline{b} . \tag{2-176}$$

Expand Eq. (2-176), delete the $\underline{\underline{B}}^{-1} \cdot \underline{b}$ term from both sides of the equation, and multiply the equation by $(\underline{\underline{B}}^{-1} \cdot \underline{\underline{E}})^{-1}$ giving

$$(\underline{\underline{I}} + \underline{\underline{R}} \cdot \underline{\underline{B}}^{-1} \cdot \underline{\underline{E}}) \cdot \underline{y} = \underline{\underline{R}} \cdot \underline{\underline{B}}^{-1} \cdot \underline{b} . \tag{2-177}$$

Multiply Eq. (2-177) by the inverse of the matrix on its left-hand side to define $\underline{y}$ as follows:

$$\underline{y} = (\underline{\underline{I}} + \underline{\underline{R}} \cdot \underline{\underline{B}}^{-1} \cdot \underline{\underline{E}})^{-1} \cdot \underline{\underline{R}} \cdot \underline{\underline{B}}^{-1} \cdot \underline{b} . \tag{2-178}$$

To determine $\underline{x} = \underline{\underline{A}}^{-1} \cdot \underline{b}$, evaluate Eq. (2-178) for $\underline{y}$ and substitute $\underline{y}$ into Eq. (2-175) to evaluate $\underline{x}$.

This evaluation procedure appears lengthy until we observe that it involves the following four steps with some intermediate results used several times.

Step 1. Multiply the vector $\underline{b}$ and each of the M columns of $\underline{\underline{E}}$ by the inverse of $\underline{\underline{B}}$.

$$\underline{\hat{x}} = \underline{\underline{B}}^{-1} \cdot \underline{b} \quad \text{and} \quad \underline{\underline{\hat{E}}} = \underline{\underline{B}}^{-1} \cdot \underline{\underline{E}} \tag{2-179}$$

$$(N)(N \times N)(N)(N \times M)(N \times N)(N \times M)$$

Step 2. Multiply $\underline{\hat{x}}$ and $\underline{\underline{\hat{E}}}$ from Step 1 by $\underline{\underline{R}}$.

$$\underline{\hat{b}} = \underline{\underline{R}} \cdot \underline{\hat{x}} \quad \text{and} \quad \underline{\underline{\hat{R}}} = \underline{\underline{R}} \cdot \underline{\underline{\hat{E}}} \tag{2-180}$$

$$(M)(M \times N)(N)(M \times M)(M \times N)(N \times M)$$

Step 3. Evaluate Eq. (2-178) for $\underline{y}$ using $\underline{\hat{b}}$ and $\underline{\underline{\hat{R}}}$ from Step 2.

$$\underline{y} = (\underline{\underline{I}} + \underline{\underline{\hat{R}}})^{-1} \cdot \underline{\hat{b}} \tag{2-181}$$

$$(M)(M \times M)(M \times M)(M)$$

Step 4. Evaluate Eq. (2-175) for the desired solution vector $\underline{x}$ using $\underline{\hat{x}}$ and $\underline{\underline{\hat{E}}}$ from Step 1 and $\underline{y}$ from Step 3.

$$\underline{x} = \underline{\hat{x}} - \underline{\underline{\hat{E}}} \cdot \underline{y} \tag{2-182}$$

$$(N)(N)(N \times M)(M)$$

Computationally, Eq. (2-178) is solved by performing a single banded-matrix L-U matrix decomposition to determine $\underline{\underline{B}}^{-1}$. Then $\underline{\underline{B}}^{-1}$ is applied to the $1+M$ column vectors of $\underline{b}$ and $\underline{\underline{E}}$ by a direct forward-elimination and backward-substitution solution procedure. Equation (2-181) requires that a L-U matrix decomposition be applied to the full (nonbanded), but much smaller, capacitance matrix $\underline{\underline{I}}+\underline{\underline{\hat{R}}}$. The method becomes rapidly less efficient as the size of the capacitance matrix $\underline{\underline{I}}+\underline{\underline{\hat{R}}}$ increases. The remainder of the computation involves matrix multiplications that are performed efficiently on a vector computer.

2.1.8.5. Water Packing. The water-packing logic in the code is triggered under certain conditions (but not all conditions) when the code attempts during a time step to overfill (pack) a liquid-full finite-difference mesh cell or to overextract (stretch) liquid from a liquid-full cell. The physical analog to water-packing is a water hammer; when cold water surges down a dead-end pipe filled with steam, a large pressure spike occurs when the last steam collapses and the water fills the pipe. Because of the low compressibility of liquid water, the spike has a very short duration.

In any Eulerian finite-difference scheme, the boundary of a mesh cell behaves like the dead end of a pipe in a water hammer. This is especially true when condensation is present. Consider a 1D mesh cell with pure liquid entering from the left and pure vapor flowing in from the right to condense on the liquid. It is not possible for a standard finite-difference momentum equation to produce a liquid-mass flow out of the right cell face that exactly balances the flow in the left cell face at the instant when the cell fills with liquid. In fact, when strong condensation is present, the momentum equation generally will predict a liquid velocity into the cell on the right face. This circumstance produces a numerical dead end for the liquid. Unlike the water hammer, the final solution is not to halt the flow, but to push the liquid on through the right cell face. As with a hammer, this is accomplished with an abrupt increase in pressure.

In TRAC, we have adopted a method for mitigating water-packing that is similar in spirit to shock-fitting techniques. Logic has been installed that detects pressure excursions caused by water-packing. When they occur, it is clear that the finite-difference momentum equation is producing invalid results. Therefore, we modify the equation at those locations and times to obtain a better solution. A standard motion equation at a cell edge can be written as

$$V_{j+1/2}^{n+1} = V_{j+1/2}^{n} + a + b(P_j^{n+1} - P_{j+1}^{n+1}) \ . \qquad (2\text{-}183)$$

Additional force terms are incorporated in the term a, and b includes the time-step size and inverse of mesh length and density. If packing is detected in cell j, the equation is modified to the form

$$V_{j+1/2}^{n+1} = V_{j+1/2}^{n} + a + b(cP_j^{n+1} - P_{j+1}^{n+1}) \ . \qquad (2\text{-}184)$$

The constant c multiplying P_j^{n+1} is taken to be a large number so that only small changes in the pressure of the j^{th} cell are required to obtain the appropriate velocity for the liquid outflow. To prevent excessively large vapor velocities, the value of the coefficient b in the vapor equation is set equal to the corresponding coefficient in the liquid equation.

In a given cell of a 1D component, the code does not consider the water-packing logic if the cell void fraction is greater than 0.08, if the liquid in the cell is superheated, or if the net mass flow is out of the cell. Also, the code cannot make adjustments at a cell interface or test across that interface if the associated flow area is less than or equal to $10^{-10}m^2$. Further, TRAC does not consider adjacent cells in which the void fraction is less than 0.1. The code predicts the change in the current cell pressure to give a new pressure; if the predicted pressure change is negative, the code transfers to logic to detect stretching. If the pressure rise is greater than or equal to 0, and if this new pressure does not exceed the maximum of its current value and the adjacent-cell pressures by at least 7%, with a minimum increase of 50 kPa (one-half bar), the water-packing logic terminates. The void-fraction tests ensure that the water-packing logic will not smooth out a true water-hammer-type phenomenon in the calculation, while the pressure checks prevent the logic from being triggered too often. If, through the tests, more than one interface of a given cell permits the water-packing correction, the code applies the correction only at the interface across which the void fraction is higher. The code does not permit the water-packing correction at the interface opposite a FILL component if the velocities at both interfaces have the same sign or at the interface at which the PUMP-component source is applied. Also, the code terminates the water-packing logic for a given cell interface if choking is detected at that interface and if the interface is either the first or last interface of a component.

The stretching logic is similar, although the code looks for a pressure drop in the current cell that reduces its pressure to less than the minimum of 95% of its current value or 95% of the neighboring cells, with the additional constraint that the projected pressure must be less than the saturation pressure corresponding to the current liquid temperature minus 20.0 K. The final constraint for stretching is that the test pressure cannot be below the lower pressure limit for the equation of state (see Appendix A). For a stretch, the code does not make an adjustment at a given interface if the void fraction on the other side of the interface is less than or equal to 0.1, if the liquid velocity at the interface is into the cell in which the stretch is detected, or if the PUMP-component source is applied at the interface.

The 3D VESSEL water-packing detection logic is very similar. The VESSEL, however, permits packing to occur if the current cell void fraction is greater than 0.1, instead of the 0.08 in the 1D components. Also, in detecting a stretch, the code requires the pressure test to be 0.8 of that in the 1D components.

Subroutine TF1DS3 contains the fairly complex logic for detecting water-packing situations in the 1D components; the logic for making the necessary corrections is in

subroutines TF1DS and TF1DS1. The corresponding coding for the 3D VESSEL is in subroutine TF3DS3.

2.1.8.6. Special Cases. In this subsection, the implementations of the special flow models [critical flow, countercurrent flow limitation (CCFL), and the offtake model] are briefly summarized. Details are provided in Section 4.0. and Appendix I.

2.1.8.6.1. Critical-Flow Model. The critical-flow model is implemented as an option that the user may turn on using the INOPTS namelist data flag ICFLOW. When ICFLOW = 0, no critical-flow calculation is performed. If ICFLOW = 1 (default), critical-flow calculations are performed only for components connected to a BREAK component using the default multipliers. This option requires no additional user input. When ICFLOW = 2, critical-flow calculations are performed with user-specified multipliers at user-specified cell edges. This option requires the user to include the critical-flow multipliers CHM12, CHM22, CHM13, CHM23, CHM14, CHM24, CHM15, and CHM25 as additional INOPTS namelist data input if values other than the default are desired. Within each 1D component's array data cards, the array ICFLG must also be included to indicate the cell edges at which the critical-flow calculations will be performed.

The only difference to the solution procedure, when the critical-flow model has been turned on, occurs in the basic step. Subroutine TF1DS1 solves for the new-time velocities as a function of the new-time pressures and the derivatives of those velocities with respect to pressure. If the critical-flow model is turned on, subroutine CHOKE is called just before subroutine TF1DS1 is exited. Based on the void fraction of the flow, subroutine CHOKE calculates a second set of new-time velocities and the derivatives with respect to pressure using a choking condition. If the new-time choking velocities calculated by subroutine CHOKE are larger in magnitude than the new-time momentum-solution velocities calculated by subroutine TF1DS1, nothing is changed and the solution proceeds as if the critical-flow model had not been turned on. If, however, the choking velocities are smaller in magnitude than the momentum-solution velocities, then the calculation proceeds with the choking velocities and the derivatives being used in place of the momentum-solution quantities.

2.1.8.6.2. Countercurrent Flow Limitation (CCFL). A special model exists in the code that allows the user to invoke characteristic CCFL correlations at specific locations in the 3D VESSEL component and in the 1D components (Appendix I, Section I.3.). The CCFL correlation for a specific geometry provides the amount of liquid delivery for a given vapor upflow. The CCFL model is applied at the top edge of the chosen VESSEL cell if the vapor velocity is greater than or equal to zero. For a given vapor upflow and an upstream void fraction, the downward liquid velocity is calculated that satisfies the correlation. The old-time vapor velocity is used as input to the CCFL correlation to calculate the new-time intermediate-step liquid velocity [subroutine StbVelz (FEMOMZ in TRAC-M/F77) for 3D components and subroutine StbVel (FEMOM in TRAC-M/F77) for 1D components]. At this point, the interfacial drag coefficient is also calculated from the Bankoff correlation (see Appendix I, Section I.3.). The new-time final-value liquid velocity and the derivative of the new-time final-value liquid velocity with respect to

pressure are calculated in subroutine TF3DS1 for 1D components and subroutine TF3DS3 for 3D components from the CCFL correlation based on the new-time final-value vapor velocity.

2.1.8.6.3. TEE-Component Offtake Model. The TEE-component offtake model is implemented as an option that the user may turn on using the INOPTS namelist data flag IOFFTK. When IOFFTK = 1 (default = 0), the user is required to insert an additional line of input for each TEE component within the TRAC input deck specifying the value of the variable IENTRN. This new Card Number 15 requires IENTRN = 1 to implement the offtake model for a particular TEE. Similarly, no offtake model is implemented for any TEE for which IENTRN = 0.

Upon initialization in subroutine ITEE, TRAC checks for the appropriate geometry for all TEEs in which the offtake model has been requested by the user. For this initial model, the side tube of the tee is required to be either top, bottom, or centrally oriented from the main tube and is required to be at a 90° angle to the main tube. In addition, the TEE main-tube junction cell is required to be horizontal. Lastly in subroutine ITEE, old-old-, old-, and new-time values of the offtake void fraction (ALPOTO, ALPOT, and ALPOTN, respectively) are initialized equal to the main-tube junction-cell void fraction input by the user. It should be noted that geometry checks traditionally are performed in subroutine RTEE. The GRAVs, however, are not computed until subroutine ITEE if a user chooses to specify cell-centered elevations in his/her input deck. Therefore, the geometry checks for this particular model are located in subroutine ITEE.

The momentum-stabilizer step for a TEE component is controlled by subroutine TEE1. At the beginning of this step, all dual-time variables are updated. If the offtake model for this particular TEE has been turned on by the user through input, all offtake void fractions are also time-updated. Next, the side-tube boundary arrays are set up. In the absence of the offtake model, the variables in the boundary array at the junction (BD4) normally reflect main-tube junction-cell conditions. If the offtake model is turned on, however, it is recognized that the void fraction that exits the offtake may be significantly different than that which exists in the main-tube junction cell. Therefore, all of the variables in this BD4 array that include a void-fraction term are reset to reflect the offtake void fraction rather than the main-tube junction-cell void fraction. Old-old-time variables are reset using the old-old-time offtake void fraction, ALPOTO, whereas old-time variables are adjusted using the old-time offtake void fraction, ALPOT. Similarly, the new-time variables are reset using the new-time offtake void fraction, ALPOTN. Except for the additional time-updating and the boundary array adjustments just described, the existing logic for the momentum-stabilizer step remains unchanged by the offtake model, and the calculation proceeds as for any other TEE component.

The mass and energy basic step for a TEE component is controlled by subroutine TEE2. As in the case of the momentum-stabilizer step, adjustments are necessary when the side-tube boundary array at the TEE junction (BD4) is set up. All elements of the boundary array containing void-fraction terms are reset again to reflect the offtake void fraction rather than the main-tube junction-cell void fraction in exactly the manner

described in the previous paragraph. In addition, a phase separator flag is activated for the main tube to accomplish two things. First, when the source-term fluxes for the main-tube junction cell are being calculated (in subroutine TF1DS), the flag signals that the offtake model is turned on. The source-term fluxes then are calculated using the offtake void fraction rather than the junction-cell void fraction. Second, the phase separator flag forces XVSET for the main-tube junction cell to be zero to ensure that only known old-time quantities (namely, void fraction) are used when calculating source-term fluxes. Except for the boundary array adjustments and the slightly different treatment of the main-tube junction-cell source-term fluxes just described, the existing logic for the mass and energy basic step remains unchanged by the offtake model, and the calculation proceeds as for any other TEE component.

The mass and energy stabilizer step for a TEE component is handled by subroutine TEE3. This final step consists of an implicit solution for the macroscopic fluid densities and energies known as the stabilizer quantities in each of the fluid cells given the flow velocities across the cell edges. Because the quantities being solved for actually include the void fraction (which the offtake model is attempting to alter), a slightly different procedure must be used within this step. To incorporate the effect of the offtake model on the fluxed quantities, the new-time TEE-junction interface velocities (which are used in subroutine STBME when setting up the stabilizer solution matrix) are scaled when offtake flow exists. This scaling factor consists of the ratio of the new-time offtake void fraction to the new-time main-tube junction-cell void fraction. The velocities are altered in both their A-array locations and in the side-tube boundary array. After the solution matrix has been set up, the new-time junction interface velocities are restored to their original values. This results in the mass and energy stabilizer equations being solved for new-time conditions that reflect the offtake void fraction rather than the main-tube junction-cell void fraction. Following the successful determination of new-time conditions, subroutine OFFTKE is called to calculate a corresponding new-time offtake void fraction, ALPOTN. If the mass and energy stabilizer step is reached with conditions indicating that a back-up is in progress, however, subroutine OFFTKE is not called to calculate a new-time offtake void fraction, and ALPOTN remains equal to ALPOT.

2.2. Heat Conduction in Solid Materials

The nuclear reaction in the core of a PWR generates energy inside the fuel. That energy is transferred to the primary fluid and crosses the steam-generator tubes to the secondary fluid. The code must calculate the heat conduction in the fuel and the steam-generator tubes to simulate correctly the heat-transfer processes involved in thermal-energy transport. Also, the passive solid structures, such as piping walls, vessel walls, and the internal vessel structures, represent significant metal masses that can store or release large amounts of thermal energy depending upon the reactor coolant temperature. Therefore, the code needs to model these additional structures.

The following nomenclature applies to Section 2.2.

NOMENCLATURE

A:	area in radial direction
A^*:	area in axial direction
$\underline{\underline{A}}$:	coefficient matrix
a:	nonzero elements of $\underline{\underline{A}}$
$\underline{B}$:	equality vector
b:	elements of $\underline{B}$
c_p:	specific heat
$\underline{\underline{C}}, \underline{\underline{D}}, \underline{\underline{E}}$:	nonzero submatrices of $\underline{\underline{A}}$
f_t, f_{ss}:	stability flags
h:	convective HTC
h_{gap}:	gap conductance
k:	thermal conductivity
NR:	number of nodes that segment the radial direction
NZ:	number of nodes that segment the axial direction
$\bar{q}$:	heat flux vector
q''':	heat generation rate per unit volume
q_{total}:	total heat flux
R:	radius
R^+, R^-:	variables defined by Eqs. (2-198) and (2-199)
r:	radial coordinate
t:	time
T:	temperature
$\underline{T}$:	temperature vector
V:	cell volume
z:	axial distance
z_b:	bottom of the fuel rod
z_u:	top of the fuel rod
Δr:	radial increment
Δt:	time increment
Δx:	slab thickness
Δz:	axial increment
ρ:	density

Subscripts

g:	gas
I:	inner surface
i, j:	finite-difference indices
l:	liquid
max:	maximum
o:	outer surface
w:	wall

Superscripts

$n, n+1$:	current-time and new-time values
$+, -$:	refers to material to the right and left of the interface, respectively
$'$:	new quantities when a fine mesh is added

2.2.1. Governing Equations

Because the heat flux in a solid material is a vector quantity, the following general equation describes the heat-conduction process in an arbitrary geometry:

$$\frac{\partial(\rho c_p T)}{\partial t} + \nabla \cdot \bar{q} = q''' \ . \tag{2-185}$$

In practice, the product ρc_p is assumed to be constant for purposes of taking the time derivative.

The heat flux $\bar{q}$ can be expressed in terms of the temperature gradient by Fourier's law of conduction (Ref. 2-15.) as follows:

$$\bar{q} = -k\nabla T \ . \tag{2-186}$$

Therefore, Eq. (2-185) becomes

$$\rho c_p \frac{\partial T}{\partial t} = \nabla \cdot (k\nabla T) + q''' \ . \tag{2-187}$$

The thermal history of the reactor structure is obtained from a solution of the heat-conduction equation applied to different geometries. This section first discusses the coupling of the heat-conduction field equation in any of its many forms to the thermal-hydraulic field equations representing the fluid (see Section 2.1.2.). Following this discussion, the next two sections detail the various formulations of the heat-conduction equations to represent particular geometries typically found in reactor systems. The geometries include cylindrical walls, slabs, and core fuel rods. The first model analyzes

heat conduction within the walls of the 1D loop components, such as pipe walls. The latter two are associated with heat transfer within structural components of the vessel. They are modeled similarly in the code, differing only in the area and volume calculations used in the finite-difference equations. The calculations of slab and rod conduction are done in the same subroutines in the code. Both of these components are therefore discussed in the same section of this manual.

2.2.2. Coupling of Thermal Hydraulics with the Reactor Structure

The energy transported by convective heat transfer from any structure into the different fluid phases is modeled using Newton's law of cooling to represent the energy exchange rate between the structure and the fluid phase. These terms appear in the energy equations of the different fluid phases. Appendix F, Section F.2. discusses the logic used to determine which heat-transfer regime exists between the wall and fluid and which correlations for the wall heat-transfer coefficient (HTC) are used to represent the different regimes. The coupling algorithm (Fig. 2-5.) is semi-implicit. For each new-time step, the wall HTCs (h) of a given structure are evaluated using the surface wall temperatures (T_w) and the fluid conditions obtained for the last time step. The new-time fluid-dynamics equations are solved using these HTCs, the old-time surface temperatures, and the new-time fluid temperatures where the sum of the total energy transported into the fluid cell can be written as

$$q_{\text{total}}^{\,n+1} = h_l^n(T_w^n - T_l^{n+1}) + h_g^n(T_w^n - T_g^{n+1}) \ .$$

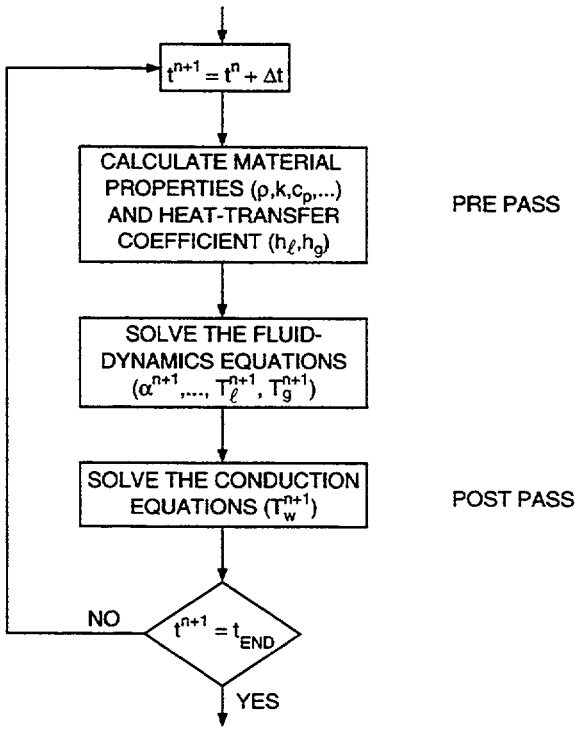

Fig. 2-5. Semi-implicit coupling between hydrodynamics and structural heat transfer.

After the fluid-dynamics equations are solved, the new-time wall temperature distributions are obtained by solution of the conduction equation for each structure modeled. This solution uses the same HTCs and the final new-time fluid temperatures.

2.2.3. Cylindrical Wall Heat Conduction

The temperature distribution within the walls of the 1D components is determined by subroutine CYLHT. A solution is obtained from a finite-difference approximation to the 1D conduction equation,

$$\rho c_p \frac{\partial T}{\partial t} = \frac{1}{r}\left[\frac{\partial}{\partial r}\left(rk\frac{\partial T}{\partial r}\right)\right] + q''' \quad . \tag{2-188}$$

The finite-difference equations are derived by applying an integral method (Ref. 2-16.) to the elemental volumes shown in Fig. 2-6. The general form of the i^{th} volume ($1 < i < N$) is

$$\frac{r_{i-1/2}k_{i-1/2}}{\Delta r_{i-1}}T_{i-1}^{n+1} - \left\{\frac{r_{i-1/2}k_{i-1/2}}{\Delta r_{i-1}} + \frac{r_{i+1/2}k_{i+1/2}}{\Delta r_i}\right. \tag{2-189}$$

$$\left. + \frac{1}{2\Delta t}\left[\left(r_i\Delta r_{i-1} - \frac{\Delta r_{i-1}^2}{4}\right)(\rho c_p)_{i-1/2} + \left(r_i\Delta r_i + \frac{\Delta r_i^2}{4}\right)(\rho c_p)_{i+1/2}\right]\right\}T_i^{n+1}$$

$$+ \frac{r_{i+1/2}k_{i+1/2}}{\Delta r_i}T_{i+1}^{n+1} = -\frac{1}{2}\left\{\left(r_i\Delta r_{i-1} - \frac{\Delta r_{i-1}^2}{4}\right)\left[\frac{(\rho c_p)_{i-1/2}}{\Delta t}T_i^n + q'''\right]\right.$$

$$\left. + \left(r_i\Delta r_i + \frac{\Delta r_i^2}{4}\right)\left[\frac{(\rho c_p)_{i+1/2}}{\Delta t}T_i^n + q'''\right]\right\}$$

where

$$f_i^n = f(t^n, r_i) \quad .$$

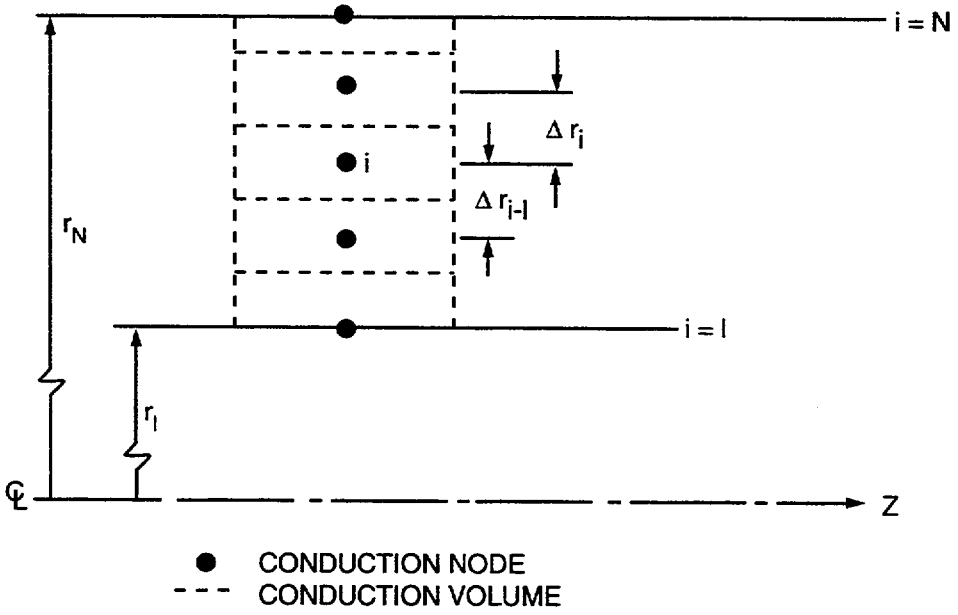

Fig. 2-6. Cylindrical wall geometry.

This formulation positions nodal points on material interfaces. Material properties are evaluated between nodes. The boundary conditions applied to the inner ($i = 1$) and outer ($i = N$) surfaces are

$$-k\frac{\partial T}{\partial r}\bigg|_{i=1,N} = \pm[h_l(T_l - T_i) + h_g(T_g - T_i)] \ . \tag{2-190}$$

For example, application of this boundary condition to the inner surface ($i = 1$) yields

$$-\left\{\frac{r_{3/2}k_{3/2}}{\Delta r_1} + \frac{1}{2}\left[r_1\Delta r_1 + \frac{\Delta r_1^2}{4}\right]\frac{(\rho c_p)_{3/2}}{\Delta t} + f_{ss}r_1(h_l + h_g)\right\}T_1^{n+1} + \frac{r_{3/2}k_{3/2}}{\Delta r_1}T_2^{n+1}$$

$$= -\frac{1}{2}\left(r_1\Delta r_1 + \frac{\Delta r_1^2}{4}\right)\left[\frac{(\rho c_p)_{3/2}}{\Delta t}T_1^n + q'''\right]$$

$$+ r_1[h_l(f_t T_1^n - T_l^{n+1}) + h_g(f_t T_1^n - T_g^{n+1})] \ . \tag{2-191}$$

The parameters f_t and f_{ss} are 0 and 1, respectively, to provide maximum stability.

The resulting linear equations are solved in a sequential fashion in the axial z-direction. For each axial position, a solution is achieved using Gaussian elimination.

A lumped-parameter solution is available to the user if the number of nodes is set equal to one. For this option the wall temperature is obtained from the equation,

$$T^{n+1} = \left\{\frac{1}{2}\left(2\Delta r + \frac{\Delta r^2}{R_I}\right)\left(\frac{\rho c_p}{\Delta t}T^n + q'''\right) + h_{l_I}(T_{l_I}^{n+1} - f_t T^n)\right.$$

$$\left. + h_{g_I}(T_{g_I}^{n+1} - f_t T^n) - \left(1 + \frac{\Delta r}{R_I}\right)[h_{l_o}(f_t T^n - T_{l_o}^{n+1}) + h_{g_o}(f_t T^n - T_{g_o}^{n+1})]\right\}$$

$$\left\{\frac{1}{2}\left(2\Delta r + \frac{\Delta r^2}{R_I}\right)\left(\frac{\rho c_p}{\Delta t}\right) + f_{ss}\left[h_{l_I} + h_{g_I} + \left(1 + \frac{\Delta r}{R_I}\right)(h_{l_o} + h_{g_o})\right]\right\}^{-1} . \qquad (2\text{-}192)$$

The subscripts I and o refer to the inner and outer radii, respectively.

2.2.4. Slab and Rod Heat Conduction

Structures that can exchange heat with the fluid in a reactor vessel include downcomer walls and support plates, modeled as slabs, and vessel rods. These elements are referred to as heat-structure components. Both nuclear and electrically heated rods or slabs can be analyzed. The effects of gap conduction, metal-water reaction, and variable material properties are included.

Only one rod within a cell may have hydro-cell coupling. This "average" rod is coupled to the fluid by Newton's law of cooling. Any number of additional user-specified rods may be included in each segment. The rod power factors (that is, relative to the average rod located within each segment) are specified by the user for these supplemental rods. The supplemental rods allow the user to include hot rods in the reactor vessel. Such rods do not affect the fluid-dynamics calculation because their contributions are already represented by average rods. They are included separately only for the purpose of determining their temperature response.

More than one slab may be located within a cell. Each slab is coupled to the fluid by Newton's law of cooling.

The user has four numerical calculation options for computing temperature distribution in slabs and rods. For thin slabs or rods of small diameter where the radial temperature profile is flat and axial conduction is negligible, the user may choose the "lumped-parameter" solution. This option gives the best calculational efficiency and should be used whenever it can be justified.

The second option is a 1D solution with implicit differencing in the radial direction and no conduction in the axial direction. This option is appropriate when steep axial profiles do not exist.

The third option is a 2D solution with implicit differencing in the radial direction and explicit differencing in the axial direction. This allows the very small radial node spacing required by the large radial power variations without severely limiting the time step. The explicit differencing in the axial direction does limit the maximum time-step size for axial spacing. In many cases, however, this maximum time-step size is much greater than that used for the fluid-dynamics calculation and is not restrictive. For those cases, the semi-implicit calculation gives good computational efficiency.

The fourth option is the fully implicit, 2D finite-difference calculation. This is the best choice for cases where the axial temperature gradient is very large, such as in the vicinity of a quench front. Then the very fine axial noding that is required would cause the time step to be severely limited if the semi-implicit calculation was used. These methods are discussed in the following sections.

2.2.4.1. The Lumped-Parameter Solution. The lumped-parameter equation for cylindrical coordinates is Eq. (2-192). If we choose $f_t = 0$ and $f_{ss} = 1$ for maximum stability, that equation reduces to

$$T^{n+1} = \left\{\frac{1}{2}\left(2\Delta r + \frac{\Delta r^2}{R_I}\right)\left(\frac{\rho c_p}{\Delta t}T^n + q'''\right) + h_{l_I}T_{l_I}^{n+1} + h_{g_I}T_{g_I}^{n+1} + \left(1 + \frac{\Delta r}{R_I}\right)[h_{l_o}T_{l_o}^{n+1} + h_{g_o}T_{g_o}^{n+1}]\right\}$$

$$\left\{\frac{1}{2}\left(2\Delta r + \frac{\Delta r^2}{R_I}\right)\left(\frac{\rho c_p}{\Delta t}\right) + \left[h_{l_I} + h_{g_I} + \left(1 + \frac{\Delta r}{R_I}\right)(h_{l_o} + h_{g_o})\right]\right\}^{-1} . \quad (2\text{-}193)$$

For a solid rod, the axial temperatures are

$$T^{n+1} = \left\{\frac{\Delta r}{2}\left[\frac{\rho c_p}{\Delta t}T^n + q'''\right] + h_{l_o}T_{l_o}^{n+1} + h_{g_o}T_{g_o}^{n+1}\right\}\left\{\frac{\Delta r \rho c_p}{2\Delta t} + h_{l_o} + h_{g_o}\right\}^{-1} . \quad (2\text{-}194)$$

The lumped-parameter equation for the temperature of a slab is

$$T^{n+1} = \left(\frac{\rho c_p \Delta x}{\Delta t}T^n + q'''\Delta x + h_{l_o}T_{l_o}^{n+1} + h_{g_o}T_{g_o}^{n+1} + h_{l_I}T_{l_I}^{n+1} + h_{g_I}T_{g_I}^{n+1}\right)$$

$$\left(\frac{\rho c_p \Delta x}{\Delta t} + h_{l_o} + h_{g_o} + h_{l_I} + h_{g_I}\right)^{-1} , \quad (2\text{-}195)$$

where Δx is the slab thickness.

2.2.4.2. The Semi-Implicit Calculation. Finite-difference equations are obtained by applying an integral method (Ref. 2-17.) to appropriate differential volumes. The noding within a rod (Fig. 2-7.) is staggered with respect to the nodes used in the fluid-dynamics calculations. This noding scheme is necessary to simplify the algorithm that generates the fine mesh required by the reflood calculations. The staggered mesh gives the further advantage of providing axial numerical smoothing.

Consider a general differential volume (that is, the volume labeled 1 in Fig. 2-7.). Using explicit differencing in the axial direction and implicit differencing in the radial direction, the finite-difference equation for this volume is

$$\left\{(\rho c_p)_{ij}\frac{T_{ij}^{n+1}-T_{ij}^{n}}{\Delta t}-q_{ij}'''\right\}\frac{1}{2}\left[\left(r_i\Delta r_i+\frac{\Delta r_i^2}{4}\right)+\left(r_i\Delta r_{i-1}-\frac{\Delta r_{i-1}^2}{4}\right)\right]\left[\frac{\Delta z_j+\Delta z_{j-1}}{2}\right]$$

$$=\left\{r_{i+1/2}k_{i+1/2,j}\left(\frac{T_{i+1,j}^{n+1}-T_{ij}^{n+1}}{\Delta r_i}\right)+r_{i-1/2}k_{i-1/2,j}\left(\frac{T_{i-1,j}^{n+1}-T_{ij}^{n+1}}{\Delta r_{i-1}}\right)\right\}$$

$$\times\left[\frac{\Delta z_j+\Delta z_{j-1}}{2}\right]+\left\{k_{i,j+1/2}\left(\frac{T_{i,j+1}^{n}-T_{ij}^{n}}{\Delta z_j}\right)+k_{i,j-1/2}\left(\frac{T_{i,j-1}^{n}-T_{ij}^{n}}{\Delta z_{j-1}}\right)\right\}$$

$$\times\frac{1}{2}\left[\left(r_i\Delta r_i+\frac{\Delta r_i^2}{4}\right)+\left(r_i\Delta r_{i-1}-\frac{\Delta r_{i-1}^2}{4}\right)\right], \qquad (2\text{-}196)$$

where $f_{ij}^{n}=f(t^{n},r_i,z_j)$. In Fig. 2-7., the locations of nodes within the volumes located at the boundaries differ. This difference should be considered when values are assigned for the relative power densities at each node.

The boundary conditions applied to the vessel rods are

- the top ($z = z_u$) and bottom ($z = z_b$) of the rods are assumed to be insulated,

$$k\frac{\partial T}{\partial z}\bigg|_{z=z_b,\,z_u}=0;$$

- the rod centerline ($r = 0$) is a line of symmetry,

$$\frac{\partial T}{\partial r}\bigg|_{r=0}=0;$$

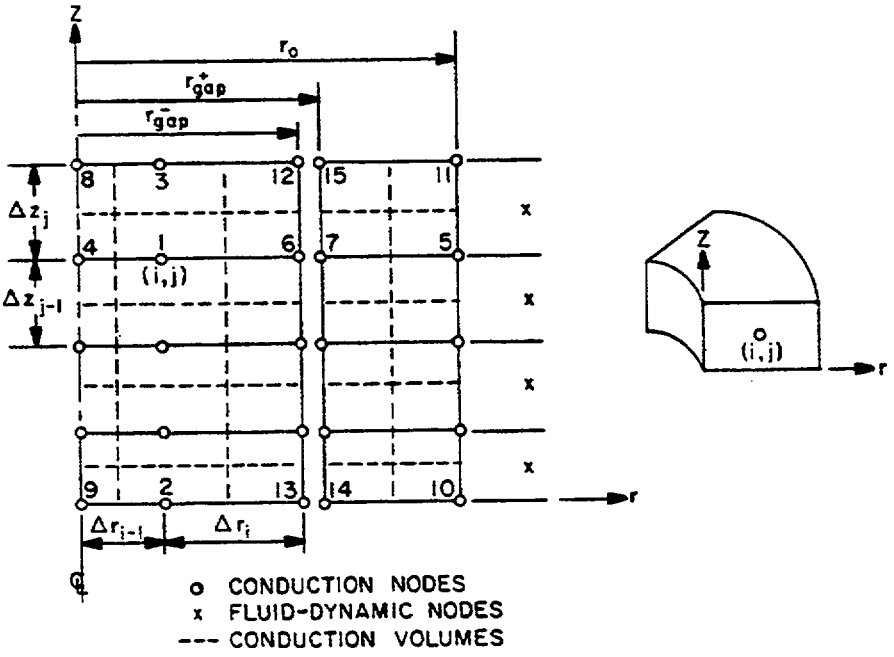

Fig. 2-7. Rod geometry.

and

- heat transfer at the inner and outer gap surfaces $(r = r_{gap}^-, r_{gap}^+)$ and at the cladding surface $(r = r_o)$ is specified using Newton's law,

$$k\frac{\partial T}{\partial r}\bigg|_{r = r_{gap}^{\pm}} = -h_{gap}^{\pm}(T_{r_{gap}^-} - T_{r_{gap}^+}) \text{ , and}$$

$$k\frac{\partial T}{\partial r}\bigg|_{r = r_0} = -h_{fluid}(T_{r_0} - T_{fluid}) \text{ ,}$$

where $h_{gap}^+ = h_{gap}^-(r_{gap}^-/r_{gap}^+)$ to conserve energy.

All properties (that is, ρ, c_p, and k) required by the difference equations are stored at the node locations. Linear interpolation is used to obtain properties between nodes (that is, at cell surfaces). A node located at the interface between two dissimilar materials requires two sets of properties. Consider the differential volume provided in Fig. 2-8. Application of an integral technique to this volume results in the differential equation (after dividing through by the volume),

$$\overline{(\rho c_p)}_{ij}\left(\frac{T_{ij}^{n+1}-T_{ij}^{n}}{\Delta t}\right)-q_{ij}^{'''}=\left\{r_{i+1/2}k_{i+1/2,j}\left(\frac{T_{i+1j}^{n+1}-T_{ij}^{n+1}}{\Delta r_i}\right)+r_{i-1/2}k_{i-1/2,j}\right.$$

$$\left.\times\left(\frac{T_{i-1,j}^{n+1}-T_{ij}^{n+1}}{\Delta r_{i-1}}\right)\right\}\times\left[\frac{\left(r_i\Delta r_i+\frac{\Delta r_i^2}{4}\right)+\left(r_i\Delta r_{i-1}+\frac{\Delta r_{i-1}^2}{4}\right)}{2}\right]^{-1}$$

$$+\left\{\bar{k}_{i,j+1/2}\left(\frac{T_{i,j+1}^{n}-T_{ij}^{n}}{\Delta z_j}\right)+\bar{k}_{i,j-1/2}\left(\frac{T_{i,j+1}^{n}-T_{ij}^{n}}{\Delta z_{j-1}}\right)\right\}\left[\frac{\Delta z_j+\Delta z_{j-1}}{2}\right]^{-1}, \qquad (2\text{-}197)$$

where

$$\overline{(\rho c_p)}_{ij}\equiv\frac{\left[(\rho c_p)_{i^+,j}^{R^+}(\rho c_p)_{i^-,j}^{R^-}\right]}{R^+ + R^-}$$

and

$$\bar{k}_{i,j+1/2}\equiv\frac{[k_{i^+,j+1/2}R^+ + k_{i^-,j+1/2}R^-]}{[R^+ + R^-]}\,.$$

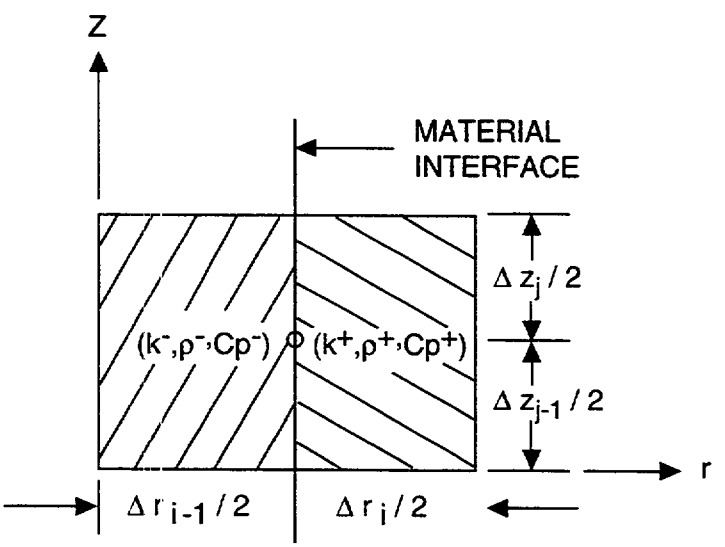

Fig. 2-8. Node located at the interface between two dissimilar materials.

In the above equations,

$$R^{+} \equiv \left(r_i + \frac{\Delta r_i}{4}\right)\frac{\Delta r_i}{2} \tag{2-198}$$

and

$$R^{-} \equiv \left(r_i - \frac{\Delta r_{i-1}}{4}\right)\frac{\Delta r_{i-1}}{2} \quad . \tag{2-199}$$

The superscripts + and – refer to the material to the right and left of the interface.

The semi-implicit finite-difference formulation for the slab is identical to that of the rod except for the obvious geometric differences.

2.2.4.3. The Fully Implicit Calculation. With the cell noding shown in Fig. 2-7., the fully implicit finite-difference equation for 2D heat conduction is (Ref. 2-18.)

$$\begin{aligned}
&(\rho c_p)_{i,j}((T_{i,j}^{n+1} - T_{i,j}^{n}) / \Delta t)V_{i,j} \\
&\quad = q_{ij}'''V_{ij} + k_{i+1/2,j}((T_{i+1,j}^{n+1} - T_{i,j}^{n+1}) / \Delta r_i)A_{i+1/2} \\
&\quad + k_{i-1/2,j}((T_{i-1,j}^{n+1} - T_{i,j}^{n+1}) / \Delta r_{i-1})A_{i-1/2} \\
&\quad + k_{i,j+1/2}((T_{i,j+1}^{n+1} - T_{i,j}^{n+1}) / \Delta z_j)A_i^{*} \\
&\quad + k_{i,j-1/2}((T_{i,j-1}^{n+1} - T_{i,j}^{n+1}) / \Delta z_{j-1})A_i^{*} \quad ,
\end{aligned} \tag{2-200}$$

where V = cell volume, A = area in radial direction, A^* = area in axial direction, and Δr = cell length in radial or x direction.

Note that this equation applies to both the slab and rod geometries, providing the areas and volumes of the cells are calculated correctly. Equation (2-200) can be written (Ref. 2-18.) as

$$a_{1,i,j}T_{i-1,j}^{n+1} + a_{2,i,j}T_{i,j}^{n+1} + a_{3,i,j}T_{i+1,j}^{n+1} + a_{4,i,j}T_{i,j-1}^{n+1} + a_{5,i,j}T_{i,j+1}^{n+1} = b_{i,j} \ , \tag{2-201}$$

where

$$a_{1,i,j} = -k_{i-1/2,j}A_{i-1/2} / \Delta r_{i-1} \ ,$$

$$a_{2,i,j} = \left(\rho c_p\right)_{i,j} V_{i,j} / \Delta t$$
$$+k_{i+1/2,j} A_{i+1/2} / \Delta r_i + k_{i-1/2,j} A_{i-1/2} / \Delta r_{i-1}$$
$$+k_{i,j+1/2,j} A_i^* / \Delta z_j + k_{i,j-1/2,j} A_i^* / \Delta z_{j-1} \quad ,$$

$$a_{3,i,j} = -k_{i+1/2,j} A_{i+1/2} / \Delta r_i \quad ,$$

$$a_{4,i,j} = -k_{i,j-1/2} A_i^* / \Delta z_{j-1} \quad ,$$

$$a_{5,i,j} = -k_{i,j+1/2} A_i^* / \Delta z_j \quad , \text{ and}$$

$$b_{i,j} = \left\{q'''_{i,j} + (\rho c_p)_{i,j} T^n_{i,j} / \Delta t\right\} V_{i,j} \quad . \tag{2-202}$$

Equation (2-201) is rewritten in matrix notation as

$$\underline{\underline{A}} \cdot \underline{T} = \underline{B} \tag{2-203}$$

or

$$\begin{pmatrix} \underline{\underline{D}}(1) & \underline{\underline{E}}(1) & & & & \\ \underline{\underline{C}}(2) & \underline{\underline{D}}(2) & \underline{\underline{E}}(2) & & & 0 \\ & \underline{\underline{C}}(3) & \underline{\underline{D}}(3) & \underline{\underline{E}}(3) & & \\ & & \ddots & & & \\ 0 & & & & & \\ & & \underline{\underline{C}}(NZ-1) & \underline{\underline{D}}(NZ-1) & \underline{\underline{E}}(NZ-1) & \\ & & & \underline{\underline{C}}(NZ) & \underline{\underline{D}}(NZ) & \end{pmatrix} \begin{pmatrix} \underline{T}(1) \\ \underline{T}(2) \\ \underline{T}(3) \\ \vdots \\ \vdots \\ \underline{T}(NZ-1) \\ \underline{T}(NZ) \end{pmatrix} = \begin{pmatrix} \underline{B}(1) \\ \underline{B}(2) \\ \underline{B}(3) \\ \vdots \\ \vdots \\ \underline{B}(NZ-1) \\ \underline{B}(NZ) \end{pmatrix} \quad , \tag{2-204}$$

where

$$\underline{T}^{(j)} = \begin{pmatrix} T_{1,j} \\ T_{2,j} \\ \vdots \\ T_{NR,j} \end{pmatrix} \quad (j = 1, NZ), \underline{B}^{(j)} = \begin{pmatrix} b_{1,j} \\ b_{2,j} \\ \vdots \\ b_{NR,j} \end{pmatrix} \quad (j = 1, NZ) \quad , \tag{2-205}$$

$$\underline{\underline{C}}^{(j)} = \begin{pmatrix} a_{4,1,j} & & & 0 \\ & a_{4,2,j} & & \\ & & \ddots & \\ 0 & & & a_{4,NR,j} \end{pmatrix} \quad (j = 2, NZ) \quad , \tag{2-206}$$

$$\underline{\underline{D}}^{(j)} = \begin{pmatrix} a_{2,1,j} & a_{3,1,j} & & & \\ a_{1,2,j} & a_{2,2,j} & a_{3,2,j} & & 0 \\ & a_{1,3,j} & a_{2,3,j} & a_{3,3,j} & \\ & & \ddots & & \\ & 0 & & a_{1,NR,j} & a_{2,NR,j} \end{pmatrix} \quad (j=1,NZ) \quad \text{, and} \tag{2-207}$$

$$\underline{\underline{E}}^{(j)} = \begin{pmatrix} a_{5,1,j} & & & 0 \\ & a_{5,2,j} & & \\ & & \ddots & \\ 0 & & & a_{5,NR,j} \end{pmatrix} \quad (j=1,NZ-1) \quad . \tag{2-208}$$

Matrix $\underline{\underline{A}}$ is a symmetrical banded matrix. To solve for the temperatures, matrix $\underline{\underline{A}}$ is inverted by a modified Cholesky method. Then the temperatures are computed from

$$\underline{T} = \underline{\underline{A}}^{-1}\underline{B} \quad . \tag{2-209}$$

2.2.4.4. Fine-Mesh Algorithm. The reflood phase of a postulated LOCA is characterized by a sequence of heat-transfer and two-phase-flow regimes advancing rapidly through the vessel core. A correctly predicted thermal response from the fuel/heater rods during reflood requires a numerical technique that can model the quenching phenomena associated with the quench-front motion.

The leading edge of the quenching region is characterized by large variations of temperatures and heat fluxes within small axial distances ($\Delta z \sim 1$ mm) (Ref. 2-19.). The front advancement is controlled by two heat-removal mechanisms, the first being axial conduction from the post-CHF region ahead of the quenched region to the nucleate-boiling region behind the advancing film. The rod conduction model contains the necessary physics to analyze such phenomena. The second is the precursory rod cooling associated with heat transfer to the slugs and droplets entrained in the vapor field downstream of the quench front. The convective heat transfer discussed in Appendix F, Section F.2., contains the physics necessary to describe this phenomenon.

To model the inherently nonstationary, Lagrangian quench-front motion and to resolve the related thermal gradients, a fine-mesh rezoning technique (Ref. 2-20.) is used during the reflood conduction calculations. The axial gradients encountered within the quenching region are resolved by the insertion of rows of transitory nodes (Fig. 2-9.). These nodes are added whenever the temperature difference between adjacent nodes exceeds a user-specified value (T_{max}). The number of rows inserted within each fluid level is specified by the user. The rows are uniformly spaced (that is, Δz is constant) within each fluid level. The temperature values at the supplemental nodes are determined from a three-point Lagrangian interpolation technique. The nodes added in this fashion remain during the entire reflood phase. The temperatures assigned to the nodes are required to conserve energy (Fig. 2-10.),

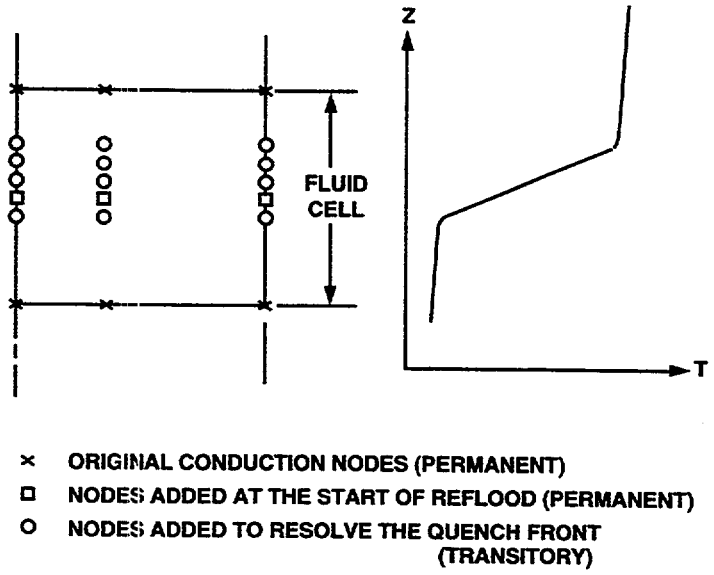

Fig. 2-9. Fine-mesh rezoning.

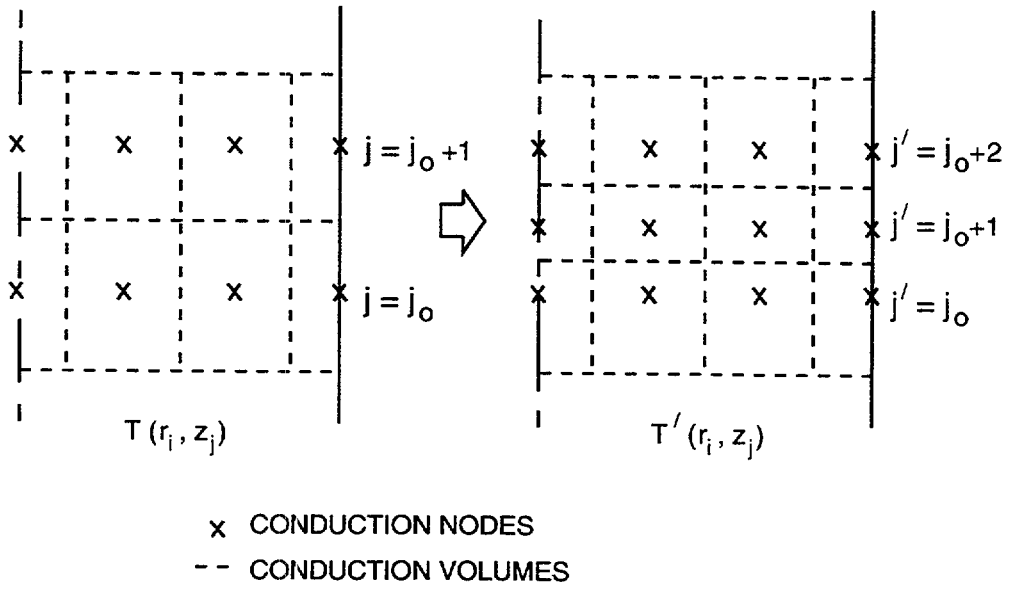

Fig. 2-10. Insertion of conduction nodes during reflood.

$$\sum_{j=j_o}^{j_o+2} \rho'_{ij} c'_{p_{ij}} T'_{ij} V'_{ij} = \sum_{j=j_o}^{j_o+1} \rho_{ij} c_{p_{ij}} T_{ij} V_{ij}, \quad \text{where } i = 1, \ldots, \text{nodes.} \tag{2-210}$$

The primed quantities denote rod properties after the nodes have been added. The values of ρ', c_p', and T' at the original node locations are set equal to their original values. After the quench front has progressed beyond the location of the inserted rows and the surface temperature difference falls below a prescribed value (ΔT_{min}), the transitory nodes are eliminated. Temperatures at nodes axially adjacent to those deleted retain their original values. For small ΔT_{min}, this results in a negligible effect on the total rod energy.

Two values for ΔT_{max} are specified by the user. The first and smaller value is applied to the part of the quenching region that is in a nucleate- or transition-boiling regime. The largest wall heat fluxes occur in these heat-transfer regimes. The second ΔT_{max} value is applied to all other heat-transfer regimes. The specified values for the ΔT_{max} are the bases of the ΔT_{min} values, which are computed internally.

The above algorithm can analyze multiple quench fronts simultaneously. Both quenching and dryout are modeled automatically.

During the reflood phase, a number of surface conduction nodes are located within each fluid cell. Therefore, it is necessary to calculate an effective wall temperature and HTC for the fluid-dynamics computations. These values are obtained by ensuring the conservation of total energy transferred to the fluid within each cell. Values applied to the liquid phase that satisfy this criterion are

$$\bar{h}_\ell \equiv \frac{\sum_j h_{\ell_j} A_j}{\sum_j A_j}$$

and

$$\bar{T}_{w_\ell} \equiv \frac{\sum_j h_{\ell_j} A_j T_j}{\sum_j h_{\ell_j} A_j},$$

where the sum is taken over all surface nodes in each fluid cell. Similar values are used in the vapor phase.

It already has been noted that, for a given time step (Δt), a minimum spacing (Δz) between rows of conduction nodes exists because of the explicit axial differencing. For reflood calculations, this axial spacing can be violated, resulting in stability problems. To avoid such problems, the time step is limited internally by a diffusion number. The user also can specify minimum spacing (Δz_{min}) beyond which supplemental rows of conduction nodes will not be added. This additional advantage can prevent excessively large computer costs.

Computing costs are reduced further by calculating material properties only at those nodes located at the edges of the fluid cells. Linear interpolation is used to obtain the properties at any additional locations required by the reflood calculations. The HTCs, however, are obtained directly from the boiling curve for all rod surface nodes.

2.2.4.5. Fuel-Cladding Gap Conductance. Two options are available in TRAC for the fuel-cladding gap conductance. If the input variable NFCI is equal to 0, a constant input value for the gap conductance is used throughout the entire calculation. If the input variable NFCI is equal to 1, the input value for the gap conductance becomes the initial value, and a thermal-expansion model is used to calculate the transient gap conductance. Section 4.5. and Appendix L, Section L.1., give additional details on TRAC's gap conductance model.

2.2.4.6. Metal-Water Reaction. TRAC calculates an additional heat source q'''_{mw} to account for zircaloy's exothermic reaction with steam. Details on this model are given in Section 4.8. and in Appendix L, Section L.2.

2.3. Reactor-Core Power Model

The primary energy source for a nuclear-reactor power plant is the reactor core. A full description of TRAC's reactor-core power model is given in Appendix M. Here we give only a brief overview. Complete input specifications for the core power model and examples of its use are given in the TRAC-M/F90 User's Manual (Ref. 2-24.).

TRAC allows the user to model the power generation in the reactor core in several ways: constant power, power specified from a table, and point-reactor kinetics with reactivity feedback. The latter cases can be run with the reactor core at a constant, user-specified trip power until a user-specified trip occurs. The core model defines the local, volumetric heat-generation rate q''' in the heat-conduction equation [Eq. (2-185)]. Subroutine RHTSTR reads the necessary input for the core description for the heat-structure components. Subroutine HTSTR1 performs the reactivity-feedback calculation in subroutine RFDBK and the point-reactor-kinetics calculation in subroutine RKIN. There is an overview of TRAC's decay-heat and sensitivity feedback models in Section 4.6.; full details are given in Appendix M.

There are several user-specified tables involved in the complete description of the reactor-core power model. In this section (or in Appendix M), we will not belabor the description of these tables and how the code obtains necessary values from them.

In particular, we will not describe signal variables, control blocks, and rate-factor tables other than briefly to define them here. Signal variables are predefined parameters, such as time, pressure, coolant levels, etc., that the code calculates and that the user can select as independent variables for tables, trips, and control blocks. Control blocks are predefined mathematical functions and logic switches, which the user can string together to model plant systems, such as control systems, or to calculate quantities not normally available from the code (and which in turn may be used to control component behavior), such as pressure drops across multiple components, liquid mass in one or more cells, etc. With the signal variables and the control blocks, the user can define the necessary independent variables for the tables. The rate-factor table is a means to vary the rate of change of the independent variable of a component-action table. That is, the rate-factor table provides a multiplier to the independent variable of a table that alters its magnitude before the code performs the table lookup. For more information, on TRAC's control procedure and component-control tables, see Section 2.4., Appendix M, and the TRAC-M/F90 User's Manual (Ref. 2-24.).

2.4. Control Procedure

A detailed description of TRAC's control procedure is given in Appendix N. Here we give a general overview. Complete input specifications for TRAC's control procedure and examples of its use are given in the TRAC-M User's Manual (Ref. 2-24.).

Simulation of PWR-plant operation involves defining its mode of operation. This requires specifying a control procedure to adjust hardware according to the state of the system and its operating plan. In that procedure one needs to model manual control by operators, automatic control by regulating hardware, and abnormal-hardware behavior. This involves specifying logic for initiating adjustable-hardware action when certain conditions occur. For example, when the coolant pressure rises above or falls below a specified level, a valve is to be opened or closed, respectively. Abnormal hardware behavior might be opening a valve to model a pipe break occurrence. The control procedure can consist of many such instructions that together direct and limit the mode of operation.

To be able to define a control procedure, one needs to understand how it fits into the TRAC model for the overall PWR-plant system. The most basic part of that model is the component description of the physical hardware (pipes, pumps, reactor core, etc.) and the mass, momentum, and energy state of the system (density, velocity, pressure, temperature, etc.). This will be referred to as the PWR physical-system model. To apply the control procedure to it, selected system parameters have their values monitored. These values are input to the control procedure along with the control procedure specifications. Evaluating the control procedure results in controllable-component hardware actions being adjusted within the PWR physical-system model. This process, diagrammed in Fig. 2-11., is evaluated at the beginning of each time step on the basis of the beginning of the time-step system state. The control procedure determines what adjustments of hardware are needed. The mode of operation of the system is thus directed as well as constrained by the control procedure.

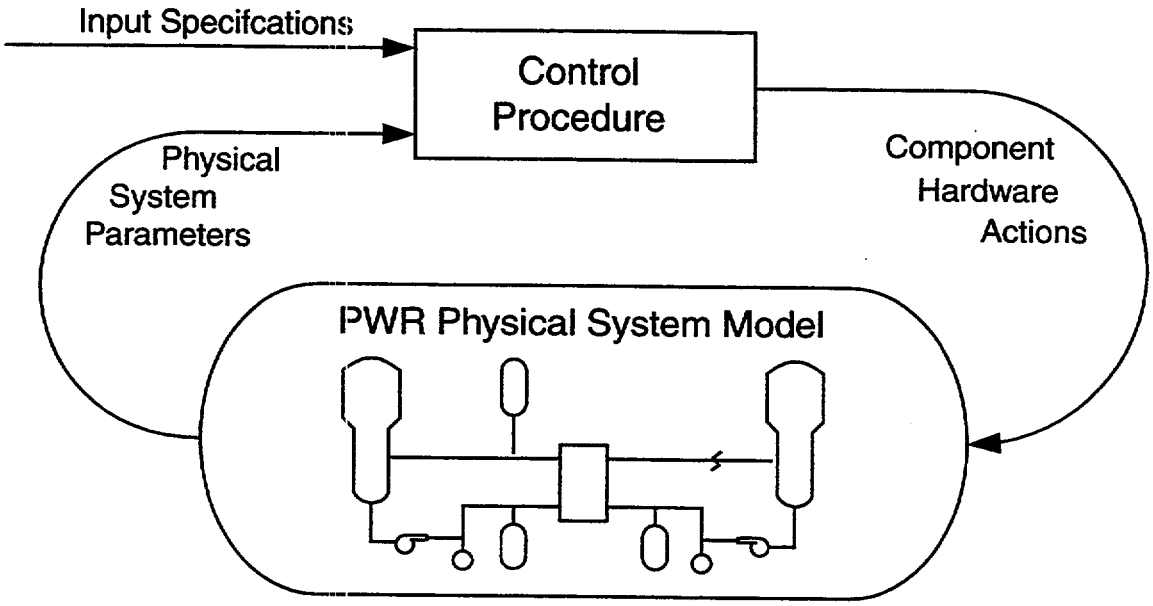

Fig. 2-11. TRAC simulation model of a PWR power plant control system.

Hardware actions that can be adjusted by the control procedure are listed in Table 2-1. The TRAC components to which they are applied are shown along with the variable-name internal letters for defining the action. In addition, the control procedure also implements the use of special time-step data, the editing of restart data dumps, and the termination of the calculation. These are the adjustable features in the TRAC model over which the user can specify control.

All information for defining the control procedure is specified in the input data for application to the general control model. Preparing the input data involves first defining the PWR physical-system model. Each hardware component is modeled by its corresponding TRAC component by specifying appropriate values for the component input parameters. For any of the components in Table 2-1., modeling one of its hardware actions is done as part of preparing the component input data. Implementing a hardware action involves specifying tabular data and associated control parameters for a component action table. Appendix N discusses the detailed form of a general component-action table, including all of its associated control parameters.

TABLE 2-1.
Adjustable Component Hardware
Actions by the Control Procedure

Actions	Components	Variable -Name Letters
Pressure boundary condition and fluid state	BREAK	B
Velocity or mass-flow boundary condition and fluid state	FILL	F
Reactor-core programmed reactivity or power	HEAT STRUCTURE	RPW
Reactor-core axial power shape	HEAT STRUCTURE	ZPW
Energy deposition in the coolant	PIPE, TEE, TURBINE	POW or PW
Energy generation in the wall	PIPE, PUMP, TEE, VALVE	QP3 or QP
Pump rotational speed	PUMP	PMP or OMG
Turbine power demand	TURBINE	TRB or POP
Valve flow-area fraction or relative stem position	VALVE	V

REFERENCES

2-1. Gunol Kocamustafaogullari, "Thermo-Fluid Dynamics of Separated Two-Phase Flow," Ph.D. thesis, Georgia Institute of Technology (December 1971).

2-2. M. Ishii, *Thermo-Fluid Dynamic Theory of Two-Phase Flow* (Collection de la Direction des Etudes et Recherches D'Electricite de France, Eyrolles, Paris, 1975).

2-3. A. E. Bergles, J. S. Collier, J. M. Delhaye, G. F. Hewitt, and F. Mayinger, *Two-Phase Flow and Heat Transfer in the Power and Process Industries* (Hemisphere Publishing Corp., New York; McGraw-Hill Book Co., New York, 1981).

2-4. F. L. Addessio, "A Review of the Development of Two-Fluid Models," Los Alamos National Laboratory report LA-8852 (NUREG/CR-2146) (August 1981).

2-5. H. Bruce Stewart and Burton Wendroff, "Two-Phase Flow: Models and Methods," *Journal of Computational Physics* 56, 363-409 (1984).

2-6. H. Bruce Stewart, "Stability of Two-Phase Flow Calculation Using Two-Fluid Models," *Journal of Computational Physics* 33, 259-270 (1979).

2-7. F. H. Harlow and A. A. Amsden, "A numerical fluid dynamics calculation method for all flow speeds," J. Comput. Phys. 8 (1971) 197-213.

2-8. D. R. Liles and W. H. Reed, "A semi-implicit method for two-phase fluid dynamics," J. Comput. Phys. 26 (1978) 390-407.

2-9. J. H. Mahaffy, "A stability enhancing two-step method for one-dimensional two-phase flow," Los Alamos Scientific Laboratory Report LA-7951-MS, US Nuclear Regulatory Commission Report NUREG/CR-0971 (1979).

2-10. J. H. Mahaffy, "A stability-enhancing two-step method for fluid flow calculations," J. Comput. Phys. 46 (1982) 329-341.

2-11. J. H. Mahaffy, "Numerics of Codes: Stability, Diffusion, Convergence," Nuclear Engineering and Design, Vol. 145, pp. 131-145 (1993)

2-12. Francis H. Harlow and Anthony A. Amsden, "A Numerical Fluid Dynamics Calculation Method for All Flow Speeds," *Journal of Computational Physics* 8, 197-213 (1971).

2-13. R. G. Steinke and J. W. Spore, "Conserving Convected Momentum in the TRAC Motion Equation," The 18th Biennial CUBE Symposium (Albuquerque, New Mexico, November 1988), p. 116.

2-14. R. G. Steinke and J. F. Dearing, "Capacitance Matrix Method in TRAC and MEL-PROG," American Nuclear Society Topical Meeting on Advances in Nuclear Engineering Computation & Radiation Shielding (Santa Fe, New Mexico, April 1989), Vol. 2, Paper 76.

2-15. G. B. Wallis, *One Dimensional Two-Phase Flow* (McGraw-Hill, Inc., New York, 1969).

2-16. Frank P. Incropera and David P. DeWitt, *Fundamentals of Heat Transfer* (John Wiley & Sons, New York, 1981).

2-17. P. J. Roache, *Computational Fluid Dynamics* (Hermosa Publishers, Albuquerque, New Mexico, 1972).

2-18. H. Akimoto, Y. Abe, and Y. Murao, "Implementation of an Implicit Method into Heat Conduction Calculation of TRAC-PF1/MOD2 Code," JAERI-memo 01-008 (February 1989).

2-19. G. Yadigaroglu, "The Reflooding Phase of the LOCA in PWRs. Part I: Core Heat Transfer and Fluid Flow," *Nuclear Safety* 19 (1978).

2-20. Reactor Safety Research Program, "Quarterly Report for the Period July 1–September 30, 1978," Battelle Pacific Northwest Laboratories report PNL-2653-3 (NUREG/CR-0546) (1978).

2-21. K. E. Carlson, R. A. Riemke, S. Z. Rouhani, R. W. Shumway, and W. L. Weaver, "RELAP5/MOD3 Code Manual, Volume 1: Code Structure, System Models, and Solution Methods (Draft)," Idaho National Engineering Laboratory report EGG-2596 (NUREG/CR-5535) (June 1990).

2-22. R. G. Steinke, "TRAC-P and Bernoulli-Equation Momentum-Convection Terms for the TEE-Component Internal-Junction Cell Interfaces," Los Alamos National Laboratory report LA-UR-96-3111 (August 1996).

2-23. B. T. Adams, J. F. Dearing, P. T. Giguere, R C. Johns, S. J. Jolly-Woodruff, J. Mahaffy, C. Murray, J. W. Spore, and R. G. Steinke, "TRAC-M/FORTRAN 90 (Version 3.0) Programmer's Manual," Los Alamos National Laboratory document LA-UR-00-803 (February 2000).

2-24. R. G. Steinke, V. Martinez, N. M. Schnurr, J. W. Spore, and J. V. Valdez, "TRAC-M Fortran 90 (Version 3.0) User's Manual," Los Alamos National Laboratory document LA-UR-00-835 (February 2000).